ISSN Print: 2518-4245
ISSN Online: 2518-4253
Vol. 56(2), June 2019

PROCEEDINGS
OF THE PAKISTAN ACADEMY OF SCIENCES:
A. Physical and Computational Sciences

PAKISTAN ACADEMY OF SCIENCES
ISLAMABAD, PAKISTAN

PAKISTAN ACADEMY OF SCIENCES

Founded 1953

President: M. Qasim Jan
Secretary General: M. Aslam Baig
Treasurer: G. A. Miana

Proceedings of the Pakistan Academy of Sciences, published since 1964, is quarterly journal of the Academy. It publishes original research papers and reviews in basic and applied sciences. All papers are peer reviewed. Authors are not required to be Fellows or Members of the Academy, or citizens of Pakistan.

Annual Subscription: **Pakistan:** Institutions, Rupees 2000/- ; Individuals, Rupees 1000/-
Other Countries: US$ 100.00 (includes air-lifted overseas delivery)

HEC Recognized, Category Y; PM&DC Recognized

Published by **Pakistan Academy of Sciences**, 3 Constitution Avenue, G-5/2, Islamabad, Pakistan
Tel: 92-5 1-920 7140 & 921 5478; **Fax:** 92-51-920 6770; **Website: www.paspk.org**

Printed at **PanGraphics (Pvt) Ltd.,** No. 1, I & T Centre, G-7/l, Islamabad, Pakistan
Tel: 92-51-220 2272, 220 2449 Fax: 92-51-220 2450 E-mail: pangraph@gmail.com

PROCEEDINGS
OF THE PAKISTAN ACADEMY OF SCIENCES:
A. Physical and Computational Sciences

CONTENTS

Volume 56, No. 2, June 2019 **Page**

Research Articles

Submission of Manuscripts: Manuscripts may be submitted as E-mail attachment at editor@paspk.org. Authors must consult the ***Instructions for Authors*** at the end of this issue or at the Website: www.paspk.org

Proceedings of the Pakistan Academy of Sciences:
A. Physical and Computational Sciences 56 (2): 1–6 (2019)

ISSN: 2518-4245 (print), 2518-4253 (online)

Pakistan Academy of Sciences

Research Article

The Reve's Puzzle with Relaxation of The Divine Rule

Abdullah-Al-Kafi Majumdar

Ritsumeikan Asia-Pacific University, 1–1 Jumonjibaru, Beppu 874-8577, Japan

Abstract: This paper considers a variant of the Reve's puzzle with $n\ (\geq 1)$ discs which admits of $r\ (\geq 1)$ number of violations of the "divine rule". Denoting by $S_4(n, r)$ the minimum number of moves required to solve the new variant, we give a scheme to find the optimality equation satisfied by $S_4(n, r)$. We then find an explicit form of the optimal value function $S_4(n, r)$.

Keywords: Tower of Hanoi, Divine rule, Sinner's tower, Reve's puzzle.

1. INTRODUCTION

The Tower of Hanoi puzzle with three pegs and *8* discs of varying sizes, invented by the French Number theorist Lucas [1], is well known. An immediate generalization of the Tower of Hanoi problem is the 4-peg variant, which appears as the Reve's puzzle in Dudeney [2]. In general form, the Reve's puzzle is as follows : There are $n\ (\geq 1)$ discs $d_1, d_2, \ldots, d_n$ of varying sizes, and 4 pegs, S, P_1, P_2 and D. Initially, the discs' rest on the source peg, S, in a tower in increasing order, with the largest disc at the bottom, the second largest disc above it, and so on, with the smallest disc at the top. The problem is to shift the tower from the peg S to the destination peg, D, in minimum number of moves, where each move can transfer only the topmost disc from one peg to another under the "divine rule" that no disc is ever placed on top of a smaller one.

The Tower of Hanoi as well as the 4-peg generalization has seen many variations, some of which have been reviewed by Majumdar [3]. Recently, Chen, Tian and Wang [4] have introduced a new variant of the Tower of Hanoi problem which allows $r\ (\geq 1)$ violations of the "divine rule". In the new variant, the problem is to shift the tower of n discs from the peg S to the peg D in minimum number of moves, where for (at most) r moves, some disc may be placed directly on top of a smaller one. Denoting by $S_3(n, r)$ the minimum number of moves required to solve the new variant, $S_3(n, r)$ is given in the following lemma, due to Chen, Tian and Wang [4].

Lemma 1.1 : For any $n \geq 1, r \geq 1,$

$$S_3(n, r) = \begin{cases} 2n-1, & \text{if } 1 \leq n \leq r+2 \\ 4n-2r-5, & \text{if } r+2 \leq n \leq 2r+3 \\ 2^{n-2r}+6r-1, & \text{if } n \geq 2r+3 \end{cases}$$

This paper generalizes the problem of Chen, Tian and Wang [4] to the Reve's puzzle. The problem that we consider here may be stated as follows: Given a tower of $n\ (\geq 1)$ discs on the peg S, the objective is to transfer it to the peg D in minimum number of moves, where the "divine rule" may be violated (at most) r times. Chen, Tian and Wang [4] call their variant as the sinner's tower. Then, the variant we consider may be called the sinner's tower with one Devil peg.

Denoting by $S_4(n, r)$ the minimum number of moves required to solve the Reve's puzzle with $n\ (\geq 1)$ discs and $r\ (\geq 1)$ relaxations of the "divine rule", we find an explicit form of $S_4(n, r)$. This is done in Section 3. In Section 2, we give some background material. In the final Section 4, some observations are made. We also give an open problem, where r number of relaxation of the "divine rule" is allowed.

Received: July 2017; Accepted: June 2019
* Corresponding Author: Abdullah Al Kafi Majumdar <majumdar@apu.ac.jp> <aakmajumdar@gmail.com>

2. PRELIMINARY RESULTS

Let $M_4(n)$ denote the minimum number of moves required to solve the Reve's puzzle with $n\ (\geq 1)$ discs. Then, the dynamic programming equation satisfied by $M_4(n)$ is (see, for example, Roth [5], Wood [6], Hinz [7], Chu and Johnson baugh [8], and Majumdar [9, 10]):

$$M_4(n) = \min_{1 \leq k \leq n-1} \{ 2M_4(K)+2^{n-k} -1 \},\ n \geq 4, \qquad (2.1a)$$

With

$$M_4(0) = 0;\ M_4(n) = 2n - 1 \text{ for all } 1 \leq n \leq 3. \qquad (2.1b)$$

Lemma 2.1: Exactly one of the following two relationships hold:

(1) $M_4(n + 2) - M_4(n + 1) = M_4(n + 1) - M_4(n)$,

(2) $M_4(n + 2) - M_4(n + 1) = 2\{M_4(n + 1) - M_4(n)\}$.

The following two corollaries are the consequences of Lemma 2.1.

Corollary 2.1:

$M_4(n + 1) - M_4(n) = 2$ *if and only if* $n = 1, 2$.

Proof: It is easy to show the "if" part of the lemma. Now, since for any $n \geq 3$,

$$M_4(n + 1) - M_4(n) \geq M_4(4) - M_4(3) = 4 > 2 = M_4(3) - M_4(2),$$

The result follows, by virtue of Lemma 2.1.

Corollary 2.2:

For $n \geq 2r + 3$, $M_4(n - r) - M_4(n - 2r) \geq 4r$.

Proof: Since

$$M_4(n-r) - M_4(n-2r) = \sum_{i=0}^{r-1} \left[M_4(n-r-i) - M_4(n-r-i-1) \right]$$

$\geq r\,[M_4(n - 2r + 1) - M_4(n - 2r)]$,

we see that, for $n \geq 2r + 3$,

$M_4(n - r) - M(n - 2r) \geq r[M_4(4) - M_4(3)] = 4r$.

The solution of the optimality equation (2.1) is given below for future reference (for a proof, the reader is referred to Majumdar [9, 10]).

Theorem 2.1: Let

$$\frac{s(s+1)}{2} < n < \frac{(s+1)(s+2)}{2}$$

for some $s \in \{1, 2, ...\}$.

Then,

$$(1)\ M_4\left(\frac{s(s+1)}{2}\right) = 2^s(s-1) + 1,$$

attained at the unique points $k = \frac{s(s-1)}{2}$.

$$(2)\ M_4(n) = 2^s\left\{ n - \frac{s(s-1)}{2} - 1 \right\} + 1,$$

attained at the two points $k = n - s - 1,\ n - s$.

***Lemma 2.2*:** Let the function $F(k)$ be defined as follows:

$$F(k) = M_4(k) - 2k,\ k \geq 0.$$

Then,

(1) $F(k)$ is strictly increasing in $k \geq 2$,

(2) $F(k)$ attains its minimum (with the minimum value – 1) at the points $k = 1, 2, 3$.

Proof: Since

$$F(k + 1) - F(k) = [M_4(k + 1) - M_4(k)] - 2,$$

part (1) follows immediately by virtue of Corollary 2.1.

Then, part (2) is an easy exercise, and is left for the reader.

Let us consider the following optimization problem:

$$\text{Min } \{2M_4(k) + 6\ell + 2m + 1\} \qquad (2.2)$$

such that

$$k + 2\ell + m = n - 1$$
$$\ell + m - 1 = r$$
$$0 \leq k \leq n - 1,\ \ell \geq 0,\ m \geq 0$$

Lemma 2.3: The optimization problem (2.2) is equivalent to the

$$\text{Min } 2\{M_4(k) - 2k\} + 4n - 2r - 5 \qquad (2.3)$$

such that

$$k = n - 2r + m - 3$$
$$\ell + m = r + 1$$
$$0 \le k \le n - 1,\ \ell \ge 0,\ m \ge 0$$

with the minimum value

$$\begin{cases} 4n - 2r - 7, & \text{if } r + 4 \le n \le 2r + 6 \\ 2M_4(n - 2r - 3) + 6r + 7, & \text{if } n \ge 2r + 7 \end{cases} \qquad (2.4)$$

Proof : From the two equality constraints in (2.2), we get after eliminating ℓ,

$$k = n - 2r + m - 3. \qquad (2.5)$$

Using the constraint conditions $\ell + m = r + 1$ and (2.5), we may re-write the objective function in (2.2) as follows:

$$2M_4(k) + 6\ell + 2m + 1 = 2M_4(k) + 6(r - m + 1) + 2m + 1$$

$$= 2M_4(k) + 6r - 4(k - n + 2r + 3) + 7$$

$$= 2M_4(k) - 4k + 4n - 2r - 5.$$

Now, if $r + 4 \le n \le 2r + 6$, then from (2.5), $m - r + 1 \le k \le m + 3$, and we may choose $m \in \{0, 1, ..., r + 1\}$ such that $k \in \{1, 2, 3\}$. Then, for any such k, $F(k)$ of Lemma 2.2 attains the minimum value – 1, and hence, the objective function in (2.3) has the minimum value $4n - 2r - 7$. On the other hand, if $n \ge 2r + 7$ (so that $k \ge m + 4$), part (2) of Lemma 2.3 asserts that the objective function in (2.3) is strictly increasing in k, and hence, it attains its minimum at $k = n - 2r - 3$. Then, after simplifying, we get (2.4).

Thus, the lemma is established.
It may be mentioned here that, when $r+4 \le n \le 2r+6$, by properly choosing m, we may have $k \in \{1, 2, 3\}$. For example, in the extreme case $n = r + 4$, choosing $m = r$ in (2.5), we get $k = 1$. Another extreme case is $n = 2r + 6$, where $m = 0$ gives $k = 3$.

3. THE PROBLEM & ITS SOLUTION

Formally, the problem that we consider is as follows: There are four pegs, S, P_1, P_2 and D. Initially, there is a tower of $n\ (\ge 1)$ discs (of varying sizes) on the source peg S, in small-on-large ordering. The objective is to move this tower to the destination peg D, using the auxiliary pegs P_1 and P_2, in minimum number of moves, where each move shifts the topmost disc from one peg to another, and for (at most) $r\ (\ge 1)$ moves, some disc may be placed directly on top of a smaller one.

Let $S_4(n, r)$ be the minimum number of moves required to solve the above problem. The following theorem gives an explicit form of $S_4(n, r)$.

Theorem 3.1: For $n \ge 1,\ r \ge 1$,

$$S_4(n, r) = \begin{cases} 2n - 1, & \text{if } 1 \le n \le r + 3 \\ 4n - 2r - 7, & \text{if } r + 4 \le n \le 2r + 6 \\ M_4(n - 2r) + 6r, & \text{if } n \ge 2r + 7 \end{cases}$$

Proof : The proof is trivial if $1 \le n \le 3$.
So, let $4 \le n \le r + 3$. In this case, the transfer of the tower from the peg S to the peg D may be affected as follows :

- ✔ Scheme 1

1. Move the topmost $n - 3\ (\le r)$ discs from the peg S to the peg P_1, one by one, in an "inverted tower" (thereby violating the "divine rule" at most $r - 1$ times).

2. Shift the next two largest discs on the peg S to the peg P_2 in an "inverted tower", which violates the "divine rule" once.

3. Transfer the largest disc d_n from the peg S to the peg D.

4. Move the discs on the peg P_2 to the peg D.

5. Finally, shift the discs on the peg P_1, one by one, to the peg D, to complete the tower on the peg D.

The total number of violations of the "divine rule" is (at most) r, and the total number of moves involved is

$$2\{(n-3)+2\}+1 = 2n-1.$$

Next, let $r+4 \le n \le 2r+6$. In this case, we follow the scheme below :

✔ Scheme 2

1. Move the top most k (≥ 0) discs, $d_1, d_2, \ldots, d_k$, from the source peg S to some auxiliary peg, say, P_1, in a tower in $M_4(k)$ moves.
2. Consider the next 2ℓ $(\ell \ge 1)$ discs on the peg S. With these 2ℓ discs, form ℓ pairs of discs (d_i, d_{i+1}). For each pair (d_i, d_{i+1}), d_i is first moved to the peg D, next d_{i+1} is shifted to the peg P_2, and then d_i is moved again (from the peg D) to the peg P_2. Note that, in this step, the first pair does not violate the "divine rule", but each of the next $\ell - 1$ pairs violate the "divine rule" once. This step requires 3ℓ moves, and the "divine rule" is violated $\ell - 1$ times (so that ℓ satisfies the condition that $1 \le \ell \le r+1$).
3. Move the next m (≥ 0) largest discs (from the peg S) to the peg P_2, one by one, in an "inverted tower", in m moves, violating the "divine rule" m times.
4. Transfer the largest disc d_n (from the peg S) to the peg D.
5. The m discs in the "inverted tower" on P_2 are shifted, one by one, to D.
6. For each of the ℓ pairs of discs (d_i, d_{i+1}) on the peg P_2, di is moved to the peg S, next d_{i+1} is shifted to the peg D, and then di is moved again (from S) to D.
7. Finally, move the k discs from the peg P_1 to the peg D, in a tower.

The total number of moves involved in the above 7 steps is:

$$2\{M_4(k) + 3\ell + m\} + 1 = 2M_4(k) + 6\ell + 2m + 1,$$

and the total number of violations of the "divine rule" is $\ell + m - 1$, where the numbers k $(0 \le k \le n-1)$, ℓ $(1 \le \ell \le r+1)$, and m $(0 \le m \le r)$ are to be determined so as to minimize the total number of moves. Thus, the above scheme leads to the optimization problem (2.2), or, equivalently, (2.3). Now, for $r+4 \le n \le 2r+6$, the result follows from Lemma 2.3.

Finally, let $n \ge 2r+7$. We consider the following scheme to transfer the tower from the peg S to the peg D.

✔ Scheme 3

1. Move the topmost k (≥ 1) discs, $d_1, d_2, \ldots, d_k$, from the peg S to some auxiliary peg P_1, say, using the four pegs available, in (minimum) $M_4(k)$ moves.
2. Shift the remaining $n-k$ discs on the peg S to the peg D, using the three pegs available, in (minimum) $S_3(n-k, r)$ moves.
3. Finally, transfer the tower of k discs from the peg P_1 to the peg D, again in (minimum) $M_4(k)$ moves, to complete the tower on the destination peg D.

The total number of moves involved is, using Lemma 1.1,

$$2M_4(k) + S_3(n-k, r) = 2M_4(k) + 2^{n-k-2r} + 6r - 1,$$

and k is to be determined such that the total number of moves is minimum. Thus, in this scheme, the minimum number of moves required is:

$$\min_{1 \le k \le n-2r} [2M_4(k) + 2^{n-2r-k} + 6r - 1] = M_4(n-2r) + 6r,$$

where we have used (2.1a).

Letting

$$n = 2r + 7 + t,\ t \ge 0,$$

the (minimum) number of moves under Scheme 2 is, by virtue of Lemma 2.3, $2M_4(t+4) + 6r + 7$, while, the (minimum) number of moves is $M_4(t+7) + 6r$ under Scheme 3. Since $M_4(6)$ in (2.1) is attained at the (unique) point $k = 3$ and $M_4(10)$ is attained at the (unique) point $k = 6$, it follows that:

$$M_4(t+7) < 2M_4(t+4) + 7 \text{ for all } t \ge 3.$$

It is an easy exercise to verify, using Theorem 2.1, that

$$M_4(t+7) = 2M_4(t+4) + 7 \text{ for all } 0 \le t \le 2$$

.

All these complete the proof of the theorem.

Remark 3.1. In addition to Scheme 2 and Scheme 3 above, there is another one to shift the tower from

the peg S to the peg D, namely, the following one:

1. Move the topmost $k\ (\geq 0)$ discs from the peg S to the peg P_1, say, in (minimum) $M_4(k)$ moves.
2. Shift the next r largest discs $d_{k+1}, d_{k+2}, \ldots, d_{k+r}$ from the peg S to the peg P_1, in an "inverted tower" (violating the "divine rule" r times).
3. Transfer the tower of $n-k-r$ discs from the peg S to the peg D, (using the three available pegs) in (minimum) $2^{n-k-r}-1$ moves.
4. Move the discs $d_{k+r}, d_{k+r-1}, \ldots, d_{k+1}$, in this order, one by one, from P_1 to D.
5. Finally, shift the tower (of k discs) on the peg P_1 to the peg D.

The minimum number of moves required under this scheme is

$$\min_{1 \leq k \leq n-r} [2\{M_4(k) + r\} + 2^{n-r-k} - 1] = M_4(n-r)+2r.$$

However, note that, by Corollary 2.2, $M_4(n-2r) + 6r \leq M_4(n-r) + 2r$ for all $n \geq 2r+3$, so that this scheme is worse than Scheme 3.

It may be mentioned here that, by symmetry, Step 2 and Step 3 in Scheme 2 may be interchanged; in this case, $0 \leq \ell \leq r$, and $1 \leq m \leq r+1$, and Step 5 and Step 6 are to be interchanged as well.

4. CONCLUSION

From the proof of Theorem 3.1, we observe that, when $n = r+3$ (so that $k = m - r \geq 0$), we have the "saturated case" of "inverted tower" in the sense that all the topmost $n-1$ discs are placed in "inverted tower" on the auxiliary peg (S) just before the largest disc is moved (from the peg S) to the peg D. Again, when $n = 2r+6$ (so that $k = m+3 \geq 3$), we have the "saturated case" in Step 2 in Scheme 2 in the sense that all the r number of violations of the "divine rule" is used up in this step. This shows that, for $n \geq 2r+7$, for each increase in n, we have to increase the number of discs in Step 1 accordingly.

From Theorem 3.1, we observe further that, for $n \geq 2r+7$, the function $S_4(n, r)$ involves $M_4(n-2r)$, and so for any $r \geq 1$ fixed, we may appeal to Theorem 2.1 to find the expression of $S_4(n, r)$. It is indeed interesting to find that the new variant has a closed-form solution, given in Theorem 3.1, and further that the optimal value function can be expressed in terms of the optimal value function of the original Reve's puzzle.

To see how the relaxation of the "divine rule" affects the original optimal value function, we consider the case when $r = 1$. From Theorem 3.1, we see that

$$S_4(n,1) = \begin{cases} 2n-1, & \text{if } 1 \leq n \leq 4 \\ 4n-9, & \text{if } 5 \leq n \leq 8 \end{cases}$$

and for $n \geq 8$,

$$S_4(n, 1) = M_4(n-2) + 6.$$

Let

$$n - 2 = \frac{s(s+1)}{2} + R \text{ for some integer } s \geq 3,$$

where $0 \leq R \leq s$. Then, by Theorem 2.1,

$$M_4\left(\frac{s(s+1)}{2} + R\right) = 2^s\left\{\frac{s(s+1)}{2} + R - \frac{s(s-1)}{2} - 1\right\} + 1$$

$$= 2^s(s + R - 1) + 1.$$

Therefore,

$$S_4(n,1) = S_4\left(\frac{s(s+1)}{2} + R + 2,\ 1\right) = 2^s(s+R-1)+7. \quad (4.1)$$

Since

$$M_4(n) = 2^s(s + R + 1) + 1, \quad (4.2)$$

from (4.1) and (4.2), we see that, the relaxation of the "divine rule" once, the number of moves decreases approximately by an additive factor of 2^{s+1}. It may be mentioned here that, in some cases, there are multiple optimal strategies. For example, when $n = 2r+4$, an alternative scheme is the following :

1. Move the disc d_1 from the source peg S to some auxiliary peg, say, P_1.
2. Consider the next $2(r+1)$ discs on the peg S. With these discs, form $r+1$ pairs of discs (d_i, d_{i+1}). For each pair (d_i, d_{i+1}), d_i is first moved to the peg D, next d_{i+1} is shifted to the peg P_2, and then d_i is moved again (from the peg D) to the peg P_2. Note that, in this step, the first pair does not violate the "divine rule", but each of the next r pairs violates the "divine rule" once. This step requires $3(r+1)$ moves,

Table 1. Values of $S_4(n, r)$ *for,* $n = 1(1)10$, $r = 0(1)6$

r / n	0	1	2	3	4	5	6
1	1	1	1	1	1	1	1
2	3	3	3	3	3	3	3
3	5	5	5	5	5	5	5
4	9	7	7	7	7	7	7
5	13	11	9	9	9	9	9
6	17	15	13	11	11	11	11
7	25	19	17	15	13	13	13
8	33	23	21	19	17	15	15
9	41	31	25	23	21	19	17
10	49	39	29	27	25	23	21

and the "divine rule" is violated $r - 2$ times.

3. Transfer the largest disc d_n (from the peg S) to the peg D.

4. For each of the $(r + 1)$ pairs of discs (d_i, d_{i+1}) on the peg P_2, d_i is moved to the peg S, next d_{i+1} is shifted to the peg D, and then d_i is moved again (from S) to D.

5. Finally, move the disc from the peg P_1 to the peg D.

The scheme requires:

$$2[1 + 3(r + 1)] + 1 = 6r + 9$$

number of moves.

It is an interesting problem to look for all the alternative optimal schemes. It may be noted here that, for $n \geq 2r + 10$, Scheme *3* is the only optimal policy. Chen, Tian and Wang [4] have posed the Tower of Hanoi problem with an evildoer disc. Another problem of interest is the following generalization:

Reve's Puzzle with r Evildoers: In the Reve's puzzle, any r of the $n \geq 1$ discs may be an evildoer, where an evildoer disc can be placed directly on top of a smaller disc any number of times.

Denoting by $E(n, r)$ the minimum number of moves required to solve the above problem, it is found that

$$E(n, 1) = S_4(n, 1) \text{ for } 1 \leq n \leq 17,$$

but $E(18, 1) = 155$, if the disc D_{16} is taken as the evildoer. It remains open to find an expression of $E(n, r)$. For small values of n and r, the values of $S_4(n, r)$ can be calculated easily. Table 1 gives the values of $S_4(n, r)$ for $n = 1(1)10$, $r = 0(1)6$. For $r \geq 7$, the number of moves is $2n - 1$, $1 \leq n \leq 10$.

6. REFERENCES

1. Claus. N, La Tour d Hanoi, *Jeu de Calcul*. Sci. Nat,1(8): 127-128 (1883).
2. Dudeney, H.E. (1958) *The Canterbury Puzzles*. Dover, 4th Edition.
3. Majumdar, A.A.K. *The Classical Tower of Hanoi Problem and Its Generalizations*, Other Generalizations. Lambert Academic Publishing, U.S.A. (2) (2013).
4. Chen, X., B. Tian, & L. Wang, Santa Claus' Towers of Hanoi, *Graphs and Combinatorics,* 23: 153-167 (2013).
5. Roth. T, The Tower of Brahma Revisited. *J. Recreational Mathematics,* 7(2): 116 -119 (1974).
6. Wood. D, The Towers of Brahma and Hanoi Revisited, *Journal of Recreational Mathematics,* 14: 17-24 (1981).
7. Hinz, A.M, An Iterative Algorithm for Tower of Hanoi Problem with Four Pegs. *Computing*, 42:133-140 (1881).
8. Chu. X. P, & R. Johnsonbaugh, The Four-Peg Tower of Hanoi Puzzle. *SIGCSE Bulletin,* 23(3): 2-4 (1991).
9. Majumdar, A.A.K, The Generalized Four-Peg Tower of Hanoi Problem. *Optimization,* 29:349-360(1994).
10. Majumdar, A.A.K, *The Classical Tower of Hanoi Problem and Its Generalizations, Multi-Peg Generalizations*. Lambert Academic Publishing, U.S.A (1) (2012).

Proceedings of the Pakistan Academy of Sciences:
A. Physical and Computational Sciences 56 (2): 7–16 (2019)

ISSN: 2518-4245 (print), 2518-4253 (online)

Pakistan Academy of Sciences

Research Article

SU(3) Symmetry Breaking Decays of Charmonia

Khadija Saeed[1*], Aneela Amin[1], Farzana Younas[1], Amir Khalid[1], Muhammad Qamar Saeed[2], and Ghalib ul Islam[3]

[1]Centre for High Energy Physics (CHEP) University of the Punjab, Lahore, 54590, Pakistan
[2]Government Dyal Sing College Lahore, Pakistan
[3]Department of Physics, The University of Lahore, Pakistan

Abstract: SU (3) symmetry breaking in several Charmonia decays was studied using the data from world's leading High Energy Physics laboratories. The charm factory BESIII was the main source of information. Branching fraction with different number of events of J/ψ, ψ (2S) → $\Lambda\bar{\Lambda}$, $\Sigma\bar{\Sigma}$, $\Xi\,\bar{\Xi}$ were computed. The total number of events for J/ψ from 1.32×10^6 to 1310.6×10^6 and that of ψ (2S) from 3.96×10^{106} to 448.1×10^{106} were studied. The corresponding branching fractions and value of decay constant α for above mentioned channels became more precise with increase of the number of events. The results of their comparison have been elaborated and are compiled in tabular form. All the data is collected year wise from the date of arise of this phenomenon (1984) to present. It has been observed from the study that with the passage of time and increased number of events gives more precise values of branching fraction and decay constant α.

1. INTRODUCTION

After the discovery of J/ψ and other Charmonia states, different experiments have been conducted to study different Baryonic decay channels. Baryon anti baryon channel has attracted the interest of both theoretical and experimental experts as it provides a test of predictive power of QCD. Also at low and intermediate energy states, the decays of J/ψ are used to study the strong interactions [1]. The observations of two body intermediate states are common in J/ψ Baryonic decays. The nature of J/ψ, in case of flavor symmetry breaking can be seen by comparing the decay rates of baryonic states with theoretical models [1]. In this work we have collected information about three baryon anti baryon channels i.e., J/ψ→$\Lambda\bar{\Lambda}$, $\Sigma\bar{\Sigma}$, $\Xi\,\bar{\Xi}$ from different laboratories. It is shown that number of data samples have been increased for both J/ψ and ψ(2S) from 1.32×10^6 to 1310.6×10^6 and 3.96×10^6 to 448.1×10^6 respectively. The corresponding branching fractions and α value are also tabulated. The comparison shows that the values of branching fraction and α-decay became more precise with the increase in number of events.

2. SU(3) SYMMETRY BREAKING IN BARYON- ANTI BARYON CHANNEL

The decay which are allowed by SU(3) symmetry breaking are

$$J/\psi \rightarrow B_1\overline{B_1}\ , B_8\,\overline{B_8}\ , B_{10}\,\overline{B_{10}} \qquad [1]$$

SU(3) symmetry can be broken in several ways, SU(3) symmetry breaking is observed in octet rather than singlet state, e.g; in one photon process

$$c\bar{c} \ \rightarrow\ \gamma 1 \ \bigotimes\ 8 \rightarrow Bi\ Bj \qquad [2]$$

Where, i≠j. This decay process is only possible when octet component contribute in direct product $8\bigotimes\overline{10}$. In Baryonic decay one of the three gluons is replaced by photon present in electromagnetic decay.

$$J/\psi \ \rightarrow \gamma \rightarrow B_{10}\,\overline{B_{10}} \qquad [3]$$

$$c\bar{c} \ \rightarrow\ gg\,\gamma \ \rightarrow B_{10}\,\overline{B_{10}} \qquad [4]$$

Equation (3) ref. [2] and equation (4) ref. [3] are representation of direct electromagnetic decay. The difference in the masses of strange and light quarks

Received: August 2017; Accepted: June 2019
* Corresponding Author: Khadija Saeed <rikza.saeed03@gmail.com>

is another mechanism for the SU (3) symmetry breaking. The difference in coupling α and β may cause the occurring of decay chain.

$$c\bar{c} \rightarrow (\mu\bar{\mu} + d\bar{d} + s\bar{s})1 \rightarrow \alpha(\mu\bar{\mu} + d\bar{d})1 \oplus 8 + \beta(s\bar{s})1 \oplus 8 \rightarrow B_{10}\bar{B}_8 \quad [5]$$

The intermediate states q are responsible for the third mechanism of SU (3) symmetry breaking [4].There are three parts of effective lagrangian of SU(3) parameterization; One is SU(3) symmetric. Second shows the effect of SU(3) breaking. Third include the effects of iso-spin breaking [1]. For octet baryon there are two types of invariant coupling of SU(3) , symmetric part and the anti symmetric one. Effective Lagrangian is

$L_{int1} = atr(\bar{B}B)$

$L_{int2} = \varepsilon tr(T^3{}_3\bar{B}B)$

$L_{int3} = \varepsilon tr(T^3{}_3[\bar{B}B])$

$L_{int4} = a\gamma 1\ tr(Q[\bar{B}B])$

$L_{int5} = a\gamma 2\ tr(Q[\bar{B}B])$

Here Q represents the electric charge matrix and SU(3) breaking effects are represented by $T^3{}_3$. More parameters are introduced by two types of SU(3) combination in case of $J/\psi \rightarrow B_8\bar{B}_8$ as compared to $J/\psi \rightarrow V_9\bar{P}_8$ [1].

3. EXPERIMENTAL SETUP AT BESIII

The charmonium factory Beijing Electron Spectrometer (BES) was established in 1989. BESII was the upgraded version of BES, established in 1996. BEPCII and BESIII, upgradation of BESII, was established in 2003. BEPC achieved maximum luminosity of $10^{31}cm^{-2}s^{-1}$ before shutting down. It was a single storage ring made to operate in single bunch mode. BEPCII is a single mode double ring collider achieving a luminosity of $\sim 1 \times 10^{33}cm^{-2}s^{-1}$ which is 100 times larger than BEPC and center of mass energy up to 2×1.89 GeV. BEPCII is used to operate in τ charm region and also used as high flux synchrotron radiation light source. The advanced design of BESIII has ability to take full advantage of high luminosity provided by BEPCII [5].The conventional 0.4 T magnet of original BES detector has been replaced by 1 T Supper Conducting Solenoid Material (SCSM) in BESIII. SCSM is present outside the Electromagnetic Calorimeter having length 3.52 m and radius 1.482 m.

Beryllium Beam Pipe are surrounded by Multilayer Drift Chamber (MDC) and MDC is surrounded by two layers of time of flight TOF system. After TOF system the electromagnetic calorimeter EMC is located. Resistive plates chamber (RPCs) are mounted above SSM, layers of these plates form Muon Identifier (MU). Spectrometer covers a solid angle $4\Omega/4\pi = 0.93$ and a polar angle of $21^0 < \theta < 159^0$ range [5].

Main Drift Chamber (MDC) is used to detect particles of relatively low momentum with good dE/dx and momentum resolution. Its outer radius is 810 mm and inner radius is 56 mm. In order to avoid multiple scattering a mixture of He – C_3H_8 60:40 is used in MDC. It is also used to reduce the background events. At the outer shell of MDC the Time of Fight (TOF) is present. It consists of two layers of staggered scintillating bars. 88 scintillation bars of 5 cm thickness are present in each layer. Time resolution of this TOF system is ~ 100 ps. The solid angle range of its endcaps is $0.85<\cos\theta<0.95$ and that of barrel TOF is $\cos\theta<0.95$ [5].

Electromagnetic Calorimeter (EMC) is located outside the TOF system. It is composed of 6240 CSI(T1) crystals. It is used to trigger signal and to measure the photons of energy above 20 MeV and momentum above 200 MeV. The length of the crystal is 28 cm and its inner radius is 94 cm. The angular coverage of its two endcaps is $21.3^0 < \theta < 34.5^0$ and $145.4^0 < \theta < 158.7^0$ ($0.85 < |\cos\theta| < 0.95$) and that of barrel EMC is $144.7^0 < \theta < 33.5^0$ ($|\cos\theta| < 0.83$). The main function of Muon Identifier is to identify and separate the muons from hadrons and other charge particles by detecting the hit pattern of muons. For this purpose muon identifier consist of 9 layers of RPCs and 9 layers of steel plates having thickness of 41 cm. The muon identifier is effective for 0.4 GeV/c momentum of muons [5]. The comparison of BESII and BESIII detector is shown in Table 1.

Table 1. Comparison between different parameters of BESII and BESIII

Parameters	Sub system	BESIII	BESII
MDC	Single wire σrϕ(μm)	130	250
	σp/p(1GeV/c)	0.5 percent	2.4 percent
	σ(dE/dx)	6 percent	8.5 percent
EMC	σE /E(1GeV)	2.5 percent	20 percent
	Position resolution (1 GeV)	0.6 cm	3 cm
TOF	στ (ps) Barral	100	180
	στ (ps) End cap	110	350
Muon	No. of layers barral/endcaps	9/8	3
	Cut of momentum MeV/c	0.4	0.5
	Solenoid magnet field T	1.0	0.4
	4Ω/4π	93 percent	83 percent

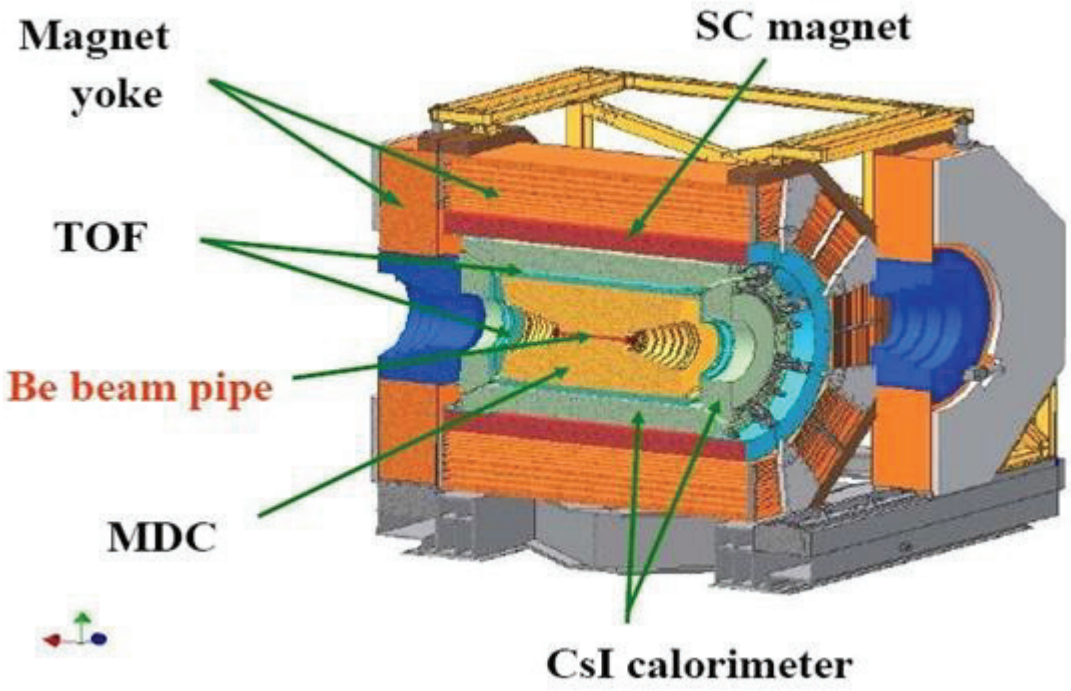

Fig. 1. Schematic diagram showing BESIII detector

4. OBSERVATION OF SU (3) SYMMETRY BREAKING DECAYS OF CHARMONIA

4.1 Observation of $\Lambda\bar{\Lambda}$ Channel

The study of Charmonia decays into baryon anti baryon is a field of interest for physicists as it provides a lot of information about the properties of baryon anti-baryon pairs. Annihilation of $c\bar{c}$ quark pair is responsible for the production of J/ψ, ψ(2S) charmonia states [6]. For the channel $e^+e^- \rightarrow \psi \rightarrow B\bar{B}$, the angular distribution is given by,

$$\text{Angular distribution} = \frac{dN}{dcos\theta}(1 + \alpha cos^2\theta) \quad [6]$$

Here θ is the angle between the beam direction and the outgoing baryon and α is the constant providing the known decay modes of $J/\psi \rightarrow B\bar{B}$ have

been computed using first order PQCD [7]. The MC observation of $J/\psi \rightarrow \Lambda\bar{\Lambda}$ is studied using Monte Carlo event generator KKMC [8], where the known decay modes of J/ψ are generated using EVTGEN [9]. In MDC charge tracks are reconstructed using track induce signals. Tracks at10 cm distance from interaction point in perpendicular direction of beam, and 20 cm along the direction of beam are selected. The angular distribution of these tracks must be $|\cos\theta < 0.93|$ in MDC. As $\Lambda \rightarrow p\,\pi^-$ and $\bar{\Lambda} \rightarrow \bar{p}\,\pi^+$ so events having four charge tracks with zero net charge should be selected. Hence all the events with positive and negative charges are considered and only those events are selected in which at least one $(p\pi^-)$ $(p\pi^+)$ tracks are present. For events containing more than one $(p\ \pi^-)(p\ \pi^+)$ tracks, the one having least value of $(M_{p\pi^-} - M_{\Lambda})^2 + (M_{\bar{p}\pi^+} + M_{\bar{\Lambda}})^2$ is selected. If the momentum of any candidate event is less than 0.3 GeV, it is rejected, as detection efficiencies of MC and data sample are different [6]. Photon candidate events are reconstructed by the energy cluster depositing at EMC. The events to be selected as photons must have a minimum energy of 25 MeV in barrel region $|\cos\theta < 0.80|$ and a minimum of 50 MeV in end cap region $(0.86| < \cos\theta| < 0.92)$. To avoid showers from other charged tracks a candidate photon must be 10 cm away from its nearest pion or proton and 300 away from anti proton track. A 4C kinematics fit

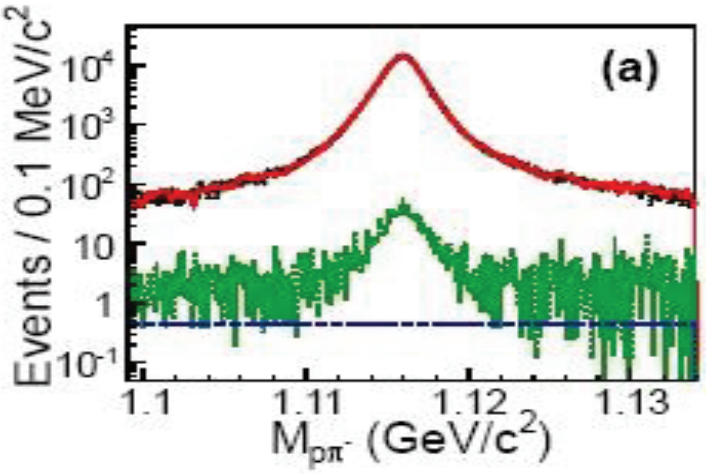

Fig. 2. The distribution of $M_{p\pi^-}$-for $J/\psi \rightarrow \Lambda\bar{\Lambda}$. Real data is represented by dots with error bars, and the red solid curve shows the fit results, background estimated by MC samples are represented by green histograms and the remaining background are represented by blue dotted line.

Table 2. Observation of decay channel $J/\psi \rightarrow \Lambda\bar{\Lambda}$

Decay Channel	No. of Events × 10^6	Branching Fraction (Br)	α	Laboratories	Year
$J/\psi \rightarrow \Lambda\bar{\Lambda}$ [9]	1.32	$(1.58\pm0.08\pm0.19)\times10^{-3}$	0.72±0.36	MarkII	1984
$J/\psi \rightarrow \Lambda\bar{\Lambda}$ [10]	7.8	$(1.08\pm0.06\pm0.24)\times 10^{-3}$	1.52±0.33±0.13	BES	1998
$J/\psi \rightarrow \Lambda\bar{\Lambda}$ [11]	386	$(2.00+0.33-0.29 \pm0.34\pm0.08)\times 10^{-3}$	(-0.63±0.46±0.27)	Belle	2005
$J/\psi \rightarrow \Lambda\bar{\Lambda}$ [12]	58	$(2.03\pm0.03\pm0.15)\times 10^{-3}$	0.65±0.11±0.03	BESII	2005
$J/\psi \rightarrow \Lambda\bar{\Lambda}$ [13]	386	$(2.00+0.34-0.29 \pm0.34\pm0.08)\times 10^{-3}$	-0.44±0.51±0.31	Belle	2006
$J/\psi \rightarrow \Lambda\bar{\Lambda}$ [14]		$(1.92\pm0.21)\times 10^{-3}$		BABAR	2007
$J/\psi \rightarrow \Lambda\bar{\Lambda}$ [15]	58	$(2.03\pm0.03\pm0.11)\times 10^{-3}$	0.65±0.11±0.03	BESIII	2008
$J/\psi \rightarrow \Lambda\bar{\Lambda}$ [2]		$(1.92\pm0.21)\times 10^{-3}$		BESIII	2009
$J/\psi \rightarrow \Lambda\bar{\Lambda}$ [6]	1310.6	$(19.43\pm0.03\pm0.33)\times10^{-4}$	0.469±0.026±0.008	BESIII	2017

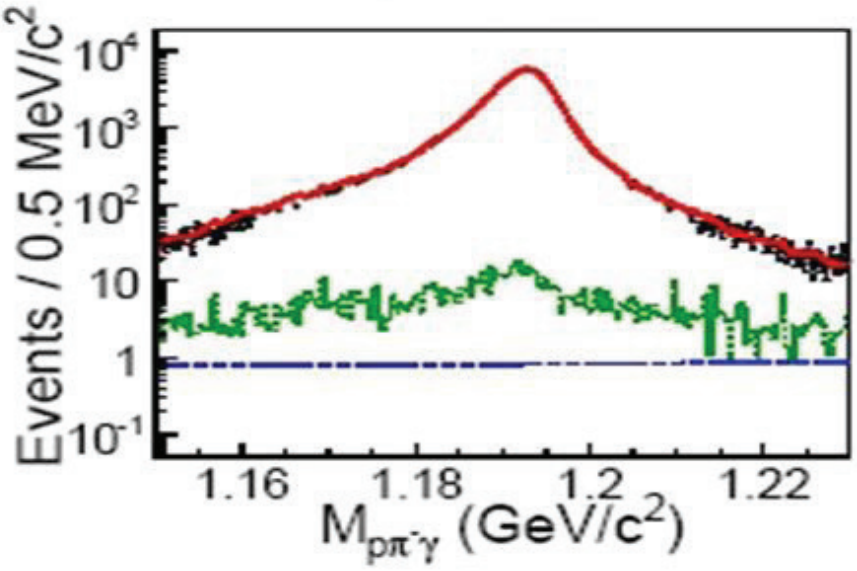

Fig. 3. The distribution of Mγpπ- for J/ψ → Σ0 $\bar{\Sigma}^0$. Real data is represented by dots with error bars and red solid curve shows the fit results , background estimated by MC samples are represented by green histograms and the remaining background are represented by blue

Table 3. Observation of decay channel ψ (2S) →Λ$\bar{\Lambda}$

Decay Channel	No. of Events × 10^6	Branching Fraction (Br)	α	Laboratories	Year
ψ(2S) →Λ$\bar{\Lambda}$ [16]	3.95	(18.1±2.0±2.7)x 10^{-5}	0.67±0.21	BES	2001
ψ(2S) →Λ$\bar{\Lambda}$ [17]	3.08	(3.28±0.23±0.25) × 10^{-3}	< 2.0 90%CL	CLEO	2005
ψ(2S) →Λ$\bar{\Lambda}$ [18]	14	(3.39±0.20±0.32) × 10^{-4}		BESIII	2007
ψ(2S) →Λ$\bar{\Lambda}$ [14]		(6.0±1.5) × 10^{-4}		BABAR	2007
ψ(2S) →Λ$\bar{\Lambda}$ [6]	1310.6	(3.97±0.02±0.12) × 10^{-4}	0.82±0.08±0.02	BESIII	2017

for energy momentum conservation is also applied to select photon candidate, and photon candidate having minimum χ^2 is selected [6].

The invariant mass of ΛΛ̄ must lie in the range [3.05, 3.15] (GeV) in order to suppress backgrounds. The dominant background remaining after event selection in analysis of J/ψ → ΛΛ̄ are J/ψ → $\Lambda\bar{\Sigma}^0$ + c.c, J/ψ → γη_c , (η_c → ΛΛ̄) and J/ψ → γ Ks Ks. The backgrounds containing ΛΛ̄ are expected to produce peak around Λ region in the invariant mass distribution of $M_{p\pi^-}$ with low background. Signal yields are determined by performing the likely hood fits. The difference in mass resolution of MC and data samples is described by fitting with Gaussian function. The branching fraction is given by the formula,

$$B(J/\psi \rightarrow B\bar{B}) = \frac{N_{obs}}{N_{\psi} \cdot \varepsilon B_i} \qquad [7]$$

Here signal events minus peaking background is equalto, detection efficiency is represented by ε. The observation of ΛΛ̄ channel in different labs is presented in tables below. Table 2 shows that the branching fraction and value of α for J/ψ → ΛΛ̄ was first observed in Mark II in 1984, using 1.32×10^6 events and the resulting branching fraction and α values are $(1.58 \pm 0.08 \pm 0.19) \times 10^{-3}$ and 0.72 ± 0.36. After that in 1998 BES shows the results for the study of same channel using 7.8×10^6 events and the observed branching fraction and α values are $(1.08 \pm 0.06 \pm 0.24) \times 10^{-3}$ and $(0.52 \pm 0.33 \pm 0.13)$.

Table 4. Observation of Decay channel $J/\psi \rightarrow \Sigma\bar{\Sigma}$

Decay Channel	No. of Events × 10^6	Branching Fraction (Br)	α	Laboratories	year
$\psi \rightarrow \Sigma^0\bar{\Sigma}^0$ [9]	1.32	$(1.58\pm0.16\pm2.5)\times10^{-3}$	0.7 ± 1.1	MarkII	1984
$\psi \rightarrow \Sigma(1385)\bar{\Sigma}^+(1385)$[9]	1.32	$(0.86\pm0.18\pm0.22)\times10^{-3}$		MarkII	1984
$\psi \rightarrow \Sigma^+(1385)\bar{\Sigma}^-(1385)$ [9]	1.32	$(1.03\pm0.24\pm0.25)\times10^{-3}$		MarkII	1984
$\psi \rightarrow \Sigma^+(1385)\bar{\Sigma}^-$ [9]	1.32	$(0.31\pm0.11\pm0.11)\times10^{-3}$		MarkII	1984
$J/\psi \rightarrow \Sigma^0\bar{\Sigma}^0$ [12]	58	$(1.33\pm0.04\pm0.11)\times10^{-3}$	$\bar{0}.24\pm0.19\pm0.07$	BESII	2005
$J/\psi \rightarrow \Sigma^0\bar{\Sigma}^0$ [20]	58	$(1.33\pm0.04\pm0.11)\times10^{-3}$	$\bar{0}.24\pm0.19\pm0.07$	BESII	2006
$J/\psi \rightarrow \Sigma^0\bar{\Sigma}^0$ [18]	14	$(2.35\pm0.36\pm0.32)\times10^{-3}$		BESIII	2007
$J/\psi \rightarrow \Sigma^0\bar{\Sigma}^0$ [14]		$(1.16\pm0.26)\times10^{-3}$		BABAR	2007
$J/\psi \rightarrow \Sigma^0\bar{\Sigma}^0$ [21]	58	$(1.40\pm0.03\pm0.07)\times10^{-3}$	-0.22±0.17	BESIII	2008
$J/\psi \rightarrow \Sigma^+\bar{\Sigma}^-$ [15]	58	$(1.50\pm0.10\pm0.22)\times10^{-3}$		BESIII	2008
$J/\psi \rightarrow \Sigma^+\bar{\Sigma}^-$[22]		$(1.5\pm0.24)\times10^{-3}$		BESIII	2009
$J/\psi \rightarrow \Sigma^0\bar{\Sigma}^0$ [2]		$(1.29\pm0.09)\times10^{-5}$		BESIII	2009
$J/\psi \rightarrow \Sigma^0\bar{\Lambda} + \bar{\Sigma}^0\Lambda$ [2]		<0.15		BESIII	2009
$J/\psi \rightarrow \Lambda\bar{\Sigma}^0 + c.c$ [23]	225	$(1.37\pm0.12\pm0.11)\times10^{-5}$		BESIII	2012
$J/\psi \rightarrow \Lambda\bar{\Sigma}^0 + c.c$ [23]	225	$(1.46\pm0.12\pm0.11)\times10^{-5}$		BESIII	2012
$J/\psi \rightarrow \Sigma^0(1385)\,\bar{\Sigma}^0(1385)$ [27]	1310.6	$(10.71\pm0.09)\times10^{-5}$	-0.64±0.03	BESIII	2016
$J/\psi \rightarrow \Sigma^0\bar{\Sigma}^0$ [5]	1310.6	$(11.64\pm0.04\pm0.23)\times10^{-4}$	-(0.449±0.026)	BESIII	2017

Table 5. Observation of Decay channel $\psi(2S) \rightarrow \Sigma\bar{\Sigma}$

Decay Channel	No. of Events ×10^6	Branching Fraction (Br)	α	Labs	year
$\psi(2S) \rightarrow \Sigma(1385)\,\bar{\Sigma}^+$[9]	1.32	$(0.31\pm0.11\pm0.11) \times 10^{-3}$		Mark II	1984
$\psi(2S) \rightarrow \Sigma^0\bar{\Sigma}^0$[16]	3.95	$(1.2\pm4\pm4) \times 10^{-3}$		BESII	2001
$\psi(2S) \rightarrow \Sigma^+\bar{\Sigma}^-$[16]	3.95	$(11\pm3\pm3) \times 10^{-5}$		BESII	2001
$\psi(2S) \rightarrow \Sigma^+\bar{\Sigma}^+$[17]	3.08	$(2.57\pm0.44\pm0.88) \times 10^{-4}$		CLEO	2005
$\psi(2S) \rightarrow \Sigma^0\bar{\Sigma}^0$[17]	3.08	$(2.63\pm0.35\pm0.21) \times 10^{-4}$		CLEO	2005
$\psi(3686) \rightarrow \Sigma^0(1385)\,\bar{\Sigma}^0(1385)$ [24]	1310.6	$(0.78\pm0.06)\times10^{-4}$	0.59±0.25	BESIII	2016
$\psi(3686) \rightarrow \Sigma^0\bar{\Sigma}^0$[6]	1310.6	$(2.44\pm0.03\pm0.11) \times 10^{-4}$	0.71±0.11±0.04	BESIII	2017

In 2005 BES has been improved to BESII, with this up gradation data events have been increased to 58×10^6 and the corresponding branching fraction and α also improved and became more precise, and there values are mentioned in the Table 2.

After 2007, BESII was again upgraded to BESIII, Its design and manufacturing parameters are improved in BESIII and are discussed in Table 1. As a result of this the branching fraction and α values are improved to be $(2.03\pm0.03\pm0.11)\times10^{-3}$ and $(0.65\pm0.11\pm0.03)$. Now in 2017 data events of BESIII are recorded to be 1310.6×10^6, with this increase in data samples the branching fraction and α value are measured more precisely. Similarly this channel has also been studied in other laboratories

Table 6. Observation of Decay Channel $J/\psi \rightarrow \Sigma\bar{\Sigma}$

Decay Channel	No. of Events	Branching Fraction	Laboratories	year
$\psi \rightarrow \Xi^-\bar{\Xi}^+$ [9]	1.32×10^6	$(1.14\pm0.08\pm0.20)\times10^{-3}$	MarkII	1984
$J/\psi \rightarrow \Xi^0\bar{\Xi}^0$ [15]	58×10^6	$(1.20\pm0.12\pm0.21)\times10^{-3}$	BESII	2008
$J/\psi \rightarrow \Xi^0\bar{\Xi}^0$ [2]		$(1.2\pm0.24)\times10^{-3}$	BESIII	2009
$J/\psi \rightarrow \Xi^-\bar{\Xi}^+$ [2]		$(0.9\pm0.2)\times10^{-3}$	BESIII	2009
$J/\psi \rightarrow \Xi^0\bar{\Xi}^0$ [24]	1310.6×10^6	$(11.65\pm0.04)\times10^{-4}$	BESIII	2016

Table 7. Observation of Decay Channel $\psi(2S) \rightarrow \Sigma\bar{\Sigma}$

Decay Channel	No. of Events	Branching Fraction	Laboratories	Year
$\psi(2S) \rightarrow \Xi^-\bar{\Xi}^+$ [16]	3.95×10^6	$(9.4\pm2.7\pm1.5)\times10^{-5}$	BESII	2001
$\psi(2S) \rightarrow \Xi^{*0}\bar{\Xi}^{*0}$ [16]	3.95×10^6	$(<8.1)\text{x}10^{-5}$	BESII	2001
$\psi \rightarrow \Xi^-\bar{\Xi}^+$ [17]	3.08×10^6	$(2.38\pm0.30\pm0.12)\times10^{-4}$	CLEO	2005
$\psi \rightarrow \Xi^0\bar{\Xi}^0$ [17]	3.08×10^6	$(2.75\pm0.64\pm0.61)\times10^{-4}$	CLEO	2005
$\psi \rightarrow \Xi^0(1530)\bar{\Xi}^0(1530)$ [17]	3.08×10^6	$0.72\pm0.10(<3.2)\times10^{-4}$	CLEO	2005
$\psi \rightarrow \Xi^-\bar{\Xi}^+$ [18]	14×10^6	$(3.03\pm0.40\pm0.32)\times10^{-3}$	BESII	2007
$\psi(3686) \rightarrow \Xi^{*0}\bar{\Xi}^{*0}$ [24]	1310.6×10^6	$(2.73\pm0.03)\times10^{-4}$	BESIII	2016

i.e. Belle and BABAR; their details are also mentioned in Table 2. Resonances of J/ψ i.e ψ(2S) $\rightarrow\Lambda\bar{\Lambda}$ was observed at BES in 2001 3.95×10^6 events and observed branching fraction and α-values are $(18.1 \pm 2.0 \pm 2.7) \times 10^{-5}$ and (0.67 ± 0.21). Later in 2007 the similar decay channel were studied at BESIII, its branching fraction is shown in Table 3. In 2017 using a huge data sample of 1310.6×10^6 at BESIII the currently measured branching fraction and α values are $(3.97 \pm 0.02 \pm 0.12) \times 10^{-4}$ and $(0.82 \pm 0.08 \pm 0.02)$, respectively.

4.2 Observation of $\Sigma\,\bar{\Sigma}$ Channel

In the analysis of $J/\psi \rightarrow \Sigma^0\bar{\Sigma}^0$ process the candidate events for Σ^0 can be reconstructed using decay $\Sigma^0 \rightarrow p\pi^-\gamma$ and candidate events for $\bar{\Sigma}^0$ are obtained using decay $\rightarrow\bar{p}\pi^+\gamma$ [5]. The events have at least two charge tracks in the range $|\cos\theta| < 0.93$ are selected in MDC. For particle identfication two parameters dE/dx and TOF are used. Energy deposits in EMC are used to identify photons. The minimum energy required for end cap showers ($0.86< |\cos\theta| <0.92$) is 50 MeV and for barrel showers ($|\cos\theta| <0.80$) is 25 MeV. Pairs of photons having invariant mass in the range $0.115\ \text{GeV/c}^2 < M_{\gamma\gamma} < 0.115\ \text{GeV/c}^2$ are reconstructed to obtain candidate events of π^0. By applying all the fitting requirements on γγ mass distribution the invariant mass distribution for π^0 is determined to be 4.2 MeV/c^2 [22]. In this case background comes from both ηc and J/ψ decay channels. For $J/\psi\rightarrow\Sigma^0\bar{\Sigma}^0$ the dominant backgrounds are $J/\psi \rightarrow \gamma\eta_c$ with $\eta_c \rightarrow \Lambda\bar{\Sigma}^0$, $J/\psi \rightarrow \Sigma^0\bar{\Sigma}^0$ and $J/\psi\rightarrow \Lambda\Sigma^{0+}$c.c. The background containing Σ^0 are expected to have a peak at invariant mass distribution of $\gamma p\pi^-$ and can be estimated with the help of MC sample [5].

Fig. 3 shows the invariant mass distribution $M_{p\pi}$, clear peak of Σ^0 are seen with low background. Signal yield is determined using maximum likelihood fits. In the fit, to resolve the difference between mass resolution of MC samples and data, MC simulation fitted with Gaussian function is used [5]. The observation of $\Sigma\,\bar{\Sigma}$ channel in different laboratories in previous years is listed in Tables 4 and 5. The channel $J/\psi \rightarrow \Sigma^0\bar{\Sigma}^0$, $\Sigma^+(1385)\,\bar{\Sigma}^-(1385)$, $\Sigma^+(1385)\,\bar{\Sigma}^-$, has been studied in MarkII in 1984 with 1.32×10^6 events, and their measured branching fraction has also been listed in the Table 4. The channel $J/\psi \rightarrow \Sigma^0\bar{\Sigma}^0$ has been studied in three laboratories BESII, BESIII and BABAR from

the year 2005 to 2017, and number of events in these labs has drastically increased. As a result of this branching fraction changed from (1.33 ± 0.04 ± 0.11) × 10^{-3} to (11.64 ± 0.04 ± 0.23) × 10^{-4} and corresponding α values have changed from (-0.24 ± 0.19 ± 0.07) to -(0.449 ± 0.026). BESII studied two channels ψ(2S)→ $\Sigma^+\bar{\Sigma}^-$, $\Sigma^0\bar{\Sigma}^0$ with number of events 3.95×10^6 in 2001 at that time measured branching fraction of these two channels is listed in Table 5, which was improved in 2005-06. Recently in 2016-17 ψ(2S) → $\Sigma^0\bar{\Sigma}^0$ channel has been studied in BESIII with events 1310.6×10^6. The channels ψ(2S) → $\Sigma^+\bar{\Sigma}^-$ and ψ(2S) → $\Sigma^-\bar{\Sigma}^+$ has still not been measured in BESIII, the more precise branching fraction can be calculated using increased data samples of BESIII.

4.3 Observation of $\Xi\bar{\Xi}$ Channel

Large samples of BESIII detector are also used to study J/ψ, ψ(3686) → Ξ $\bar{\Xi}$. One Baryon tag technique is used to study this process in order to avoid systematic uncertainties and to achieve higher efficiency. Remaining Candidate events for Ξ $\bar{\Xi}$ are reconstructed from $\Lambda\pi^0$ decays and Λ further decays to pπ− and $\pi^0 \rightarrow \gamma\gamma$. So in process there are $p\pi^-$ and $\bar{p}\pi^+$ charged tracks and two neutral track γγ. Photon tracks are reconstructed in EMC showers. To increase the energy resolution and reconstruction efficiency the energy depositing near TOF counter is also included. Photon candidates having energy of 50MeV in EMC cap region 0.86<|cosθ|<0.92 and energy of 25MeV in EMC barrel region |cosθ|<0.8 are required. Events containing more than one γ tracks are selected by applying1c kinematic fit in order to reconstruct π^0 candidate events [24]. Ξ^0 charge tracks are reconstructed by applying vertex fit at $p\pi^-$ within range of MDC covering angle cosθ<0.93 where polar angle with respect to beam is represented by θ. Events having χ^2<500 are considered. Flight time predicts by the final state particles is used to apply secondary vertex fit on those reconstructed tracks. Candidate events $p\pi^-$ with invariant mass closed to that of Λ are selected.

Candidates are reconstructed using recoiling mass against Σ^0[24]. $\pi^0\Lambda P^2_{\pi 0\Lambda}$

$$M^{recoil}_{\pi^0\Lambda} = \sqrt{(E_{CM} - E_{\pi^0\Lambda})2 - P^2_{\pi^0\Lambda}} \quad [8]$$

Whereand $E_{\pi^0\Lambda}$ are momentum and energy of $\Lambda\pi^0$ events respectively. MC samples of J/ψ events are used to the background channels. Background channel of J/ψ → Ξ $\bar{\Xi}$ channel are mainly J/ψ → $\Xi^-\bar{\Xi}^+$, $\gamma\eta_c$ ($\gamma\Xi^0\bar{\Xi}^0$, $\gamma\Xi^0\bar{\Xi}^0$), Σ^0(1385) and $\Xi^0\bar{\Xi}^0$. Peaking background for ψ(1385) → Σ^0 Σ^0 is from Σ^0 Σ^0 [24]. The branching fraction can be calculated using:

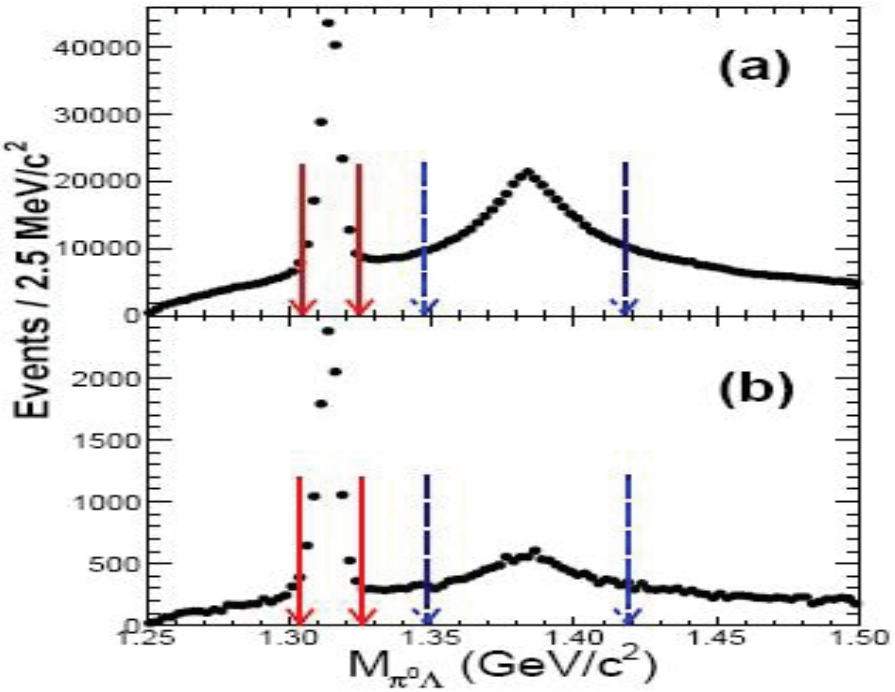

Fig. 4. (a) Shows scatter plot for M($\bar{p}\pi^+\pi^+$) and M($p\pi^-\pi^-$). **(b)** shows the invariant mass distribution of $p\pi^-$ and $\bar{p}\pi^+$

$$B[\psi \to X\bar{X}] = \frac{N_{obs}}{N_{\psi}.\varepsilon \mathrm{B}(\mathrm{X} \to \Lambda\pi^0).\mathrm{B}(\Lambda \to \mathrm{P}\pi^0).\mathrm{B}(\pi^0 \to \gamma\gamma)}$$

This channel has only been studied in BES laboratory. At first in 2008 at BESII with 58×10^6 J/ψ events the corresponding Branching fraction is $(1.20\pm0.12\pm0.21)\times10^{-3}$. After upgradation of BESII to BESIII it has been observed in 2009 and 2016. In 2016 the $(11.65\pm0.04)\times10^{-4}$ branching fraction was measured with events (1310.6×10^6). Data of channel J/ψ →Ξ $\bar{\Xi}$ has been collected from year 2001 to 2016 and summarized in Table 6. From these channels BESII lab studied two channels J/ψ→$\Xi^0\bar{\Xi}^0$, J/ψ →$\Sigma\bar{\Sigma}$ with events (3.95×10^6) during 2007. The same channel was again studied with 14×10^6 and the measured branching fraction was $(3.03\pm0.40\pm0.32)\times10^{-3}$, which is more precise. The channel ψ (3686)→$\Xi^0\bar{\Xi}^0$ has been observed with 1310.6×10^6 events in BESIII and its branching fraction is $(2.73\pm0.03)\times10^{-4}$ as shown in Table 7. Other channels like J/ψ→$\Xi^-\bar{\Xi}^+$,$\Xi^0\bar{\Xi}^0$, J/ψ →Σ^0(1530) $\bar{\Sigma}^0$ (1530) should be studied with the present data of BESIII, precision in branching fraction can be more enhanced.

5. SUMMARY

SU(3) symmetry breaking has been observed in J/ψ, ψ(2S) → $B\overline{B_1}$, $B\overline{B_8}$, $B\overline{B_{10}}$. We collected data samples from various laboratories having different number of events. From the processing of these data events branching fraction and decay constant (α) values have been studied. The sources of information are High Energy Physics laboratories like MarkI, MarkII, Belle, Cleo and BESIII. In these labs the data events for J/ψ and ψ(2*S*) varying from1.32×10^6 to 1310.6×10^6 and 3.96×10^6 to1310.6×10^6 respectively have been reported from 1984 to date ,the corresponding branching fraction and values of α have also been given. The study shows that for J/ψ, ψ(2S) → $\Lambda\bar{\Lambda}$ the values of decay constant(α) varied from 0.72 to 0.82 and corresponding branching fraction changes from $1.58\text{x }10^{-3}$ to $3.97\text{x}10^{-4}$. Also for J/ψ, ψ(2S) → $\Sigma\bar{\Sigma}$ the value of α varied from 0.7 to 0.71 and corresponding branching fraction changes form $1.58\text{ x }10^{-3}$ to $2.44\text{ x}10^{-4}$. Similarly for J/ψ → $\Xi\bar{\Xi}$ branching fraction varied from $1.14\text{x }10^{-3}$ to $2.44\text{ x}10^{-4}$.

In this work we have considered only three channels J/ψ, ψ(2S) → $\Lambda\bar{\Lambda}$, $\Sigma\bar{\Sigma}$, $\Xi\bar{\Xi}$ which shows SU(3) symmetry breaking. The comparison shows the dependence of branching fraction on number of events. The increased number of data samples provides highly precise results. The data is shown in tabulated form which shows the trends in improvement of values of branching fraction and α with increased data events. We can conclude that the improved number of events provides more precise branching fraction and α value. These more precise results will enhance d the understanding of dynamics of J/ψ and ψ(2S).

6. ACKNOWLEDGEMENTS

We are grateful to Higher Education Commission of Pakistan for their financial support under Indigenous PhD Fellowship Program, PhaseVI, and BESIII for providing data and large scale scientific facility. We are also thankful to Dr. Talib Hussain and Dr. Abrar Ahamad Zafar for their guidance.

7. REFERENCES

1 Zhi, M. Y., Zheng Han- Qing and Zhu Young-Sheng Large SU(3) Symmetry Breaking in J/ψ → BB Decays*.*Commun.Theor.Physics. Beijing, China 37:319-322 (2002).*

2 Wei, D.H. The SU(3) symmetry breaking in J/ψ decays. Journal of Physics G: Nuclear and Particle Physics J. *Phys.G: Nuclear. Particle. Physics36.115006: 6 (2009).*

3 Hu, M. X. Baryonic Decays. Rong-Gang Ping*; http:// (bes.ihep.ac.cn/bes3/phy_book/book/phy/ BaryonicDecays.pdf).*

4 Genz, H.,M. Malvetti, S. Tatur. Remark on an Su (3) f-violoting decay of ψ. *Physical. Review.D 31: 1751(1985).*

5 Ablikim, M., Z.H. An, J.Z. Bai.et al. Design and construction of the BESIII detector.*Nuclear Instruments and Methods in Physics Research Section A: Accelerators, Spectrometers, Detectors and Associated Equipment 614(3): 345-399(2010).*

6 Ablikim, M., M.N.Achasov. etal. Study of J/ψ and ψ (3686) decay to $\Lambda\bar{\Lambda}$ and $\Sigma^0\bar{\Sigma^0}$ final states.*arXiv: 1701.07191v1 [hep-ex] (2017).*

7 Claudson, M., S. L. Glashow & M. B. Wise. Isospin violation in J/ψ→ baryon + antibaryon. *Physical Review.D 25: 1345 (1985).*

8 Jadach, S., B. F.L. Ward. Event generators at BESIII. *Physical Review. D 63: 113009 (2001).*

9 Eaton, M. W. et al. Decays of the ψ(3097) to Baryon-Anti-baryon final states.*Physical Review D 29(5): 804 (1984).*

10 Bai, J. Z. et al. Decays of the J/ψ to $\Lambda\bar{\Lambda}$, $\Lambda\bar{\Lambda}\gamma$ and $\Lambda\bar{\Lambda}\pi 0$ final states. *Physics Letters B 424: 213218(1998).*

11 Abe, K. et al. Study of Charmonium Decays into Baryon-Antibaryon Pairs. *arXiv:hep- ex/0509020 (1) (2005).*

12 Ablikim, M., J.Z. et al. Study of the J/ψ decays to $\Lambda\bar{\Lambda}$ and $\Sigma^0\Sigma^0$. *Physics Letters B 632: 181186(2006).*

13 Wu, C.H., M.Z. et al. Study of J/ψ→p$\bar{p}$, $\Lambda\bar{\Lambda}$ and observation of $\eta_c \rightarrow \Lambda$ at Belle. *arXiv:hep- ex/0606022 (1) (2006).*

14 Aubert, B., M.B. et al. Study of $e^+e^- \rightarrow \Lambda\bar{\Lambda}, \Lambda\Sigma^0, \Sigma^0\Sigma^0$ using initial state radiation with BABAR.*10.1103/ PhysicalReview D. 76: 092006 (2007).*

15 Ablikim, M., J. Z. et al. First measurements of J/ψ decays into $\Sigma^+\bar{\Sigma}^-$ and $\Xi^0\bar{\Xi}^0$. *arXiv:0810.1896 (2) [hep-ex] (2008).*

16 Bai, J. Z. et al. Measurement of ψ(2S) decays to baryon pairs. *10.1103/PhysicalReview D. 63: 032002 (2001).*

17 Pedlar, T. K. et al. Branching-fraction measurements of ψ(2S) decay to baryon-antibaryon final states.*10.1103/PhysicalReview D 72: 051108 (2005).*

18 Ablikim, M., J.Z. et al. Measurements of ψ(2S) decays to octet baryonantibaryon pairs. *Physics Letters B 648: 149155 (2007).*

19 Ablikim, M., M.N. et al. Observation of ηcdecay into $\Sigma^+\bar{\Sigma}^-$ and $\Xi^-\bar{\Xi}^+$ final states. *arXiv:1210.2831 (2) [hep-ex](2012).*

20 Ablikim, M. et al. BES Collaboration, Measurements of ψ(2S) decays to octet baryon antibaryon pairs. *Physics Letter B 632: 181 (2006).*

21 M. Ablikim, J.Z. et al. Study of the J/ ψ decays to $\Lambda\bar{\Lambda}$ and $\Sigma^+\bar{\Sigma}^-$, 0arXiv:hep-ex/0506020 (1) (2005).

22 Ablikim, M. et al. J/ψ decays into $\Sigma^+\Sigma^-$ and $\Xi^-\bar{\Xi}^+$. *Physical Review D 78: 092005. (2008).*

23 Ablikim, M., M. N. Achasov5.et al. First observation of the isospin violating decay J/ψ→$\Lambda\Sigma^0$ + c.c. *arXiv:1207.1201 (3) [hep-ex](2012).*

24 Ablikim, M., M.N. et al. Study of J/ψ and ψ(3686) → Σ^0(1385) (1385) and $\Xi^-\bar{\Xi}^+$ *arXiv:1612.08664 (1) [hep-ex] (2016).*

Proceedings of the Pakistan Academy of Sciences:
A. Physical and Computational Sciences 56 (2): 17–28 (2019)

ISSN: 2518-4245 (print), 2518-4253 (online)

Pakistan Academy of Sciences

Research Article

Mathematical Modeling of Damaging Earthquakes in Pakistan

Asghar Ali[1*], Rashida Hussain[2], Javeed Shahid[2], and Faria Hamid[2]

[1]Department of Mathematics, Mirpur University of Science and Technology (MUST), Mirpur-10250 (AJK), Pakistan
[2]Department of Disaster Management University of Baluchistan Quetta, Pakistan

Abstract: Earthquakes are totally unpremeditated events and cannot be fully anticipated in advance. However, by analyzing historical knowledge and formulating mathematical models will offer researchers with an additional legitimate estimate of future losses. Earthquakes are the most deadly disaster in the world. The purpose of present study is to estimate the earthquake casualties and resulted damage costs for possible future earthquakes in Pakistan. On the basis of examination new mathematical models have been developed for estimation of earthquake casualties and related damage costs through multiple linear regression using matrices with correlation coefficient $\alpha = 0.01$. This study considers twenty-two most damaging earthquake that hit different regions of Pakistan from 1909 to 2017. The resulting models were multiple linear regression models explaining earthquake casualties and a total cost of damage through five independent variables magnitude, intensity, and depth of focus, location of epicenter and interval of earthquake.

Keywords: Mathematical Model, Earthquake, Depth of focus, Epicenter.

1. INTRODUCTION

The Islamic Republic of Pakistan has faced much in its 70-year life, in terms of man- made as well as natural disasters. Pakistan faces a severe threat from natural disasters such as flood, Tsunami, Storm, and Earthquakes. However, the worst disaster among them for Pakistan may be the Earthquake. Pakistan is one of the most seismically active countries in world, being crossed by several major faults. Historically Pakistan is indeed situated near extremely active fault line that could put risk to more than one hundred seventy million individual living in the country.

Pakistan geologically overlaps with the Indian and the Eurasian tectonic plates wherever its Sindh and Punjab provinces lie on the north-western corner of the Indian plate while Baluchistan and most of the Khyber-Pakhtunkhwa lie within the Eurasian plate which mainly comprises the Iranian plateau, some parts of the Middle East and the Central Asia [2]. The northern areas and Azad Kashmir lie mainly in Central Asia along the edge of the Indian plate and hence are prone to violent earthquakes where the two tectonic plates collide [2].

We limit this study only to the destructive earthquakes with magnitude 5 and higher. Data on casualties and cost of destructions due to these earthquakes were collected from State Disaster Management authority Muzaffarabad [10]. The information about the characteristics of the earthquakes was gathered from Pakistan Disaster Management authority Islamabad [11]. We considered the zone where the epicenter was located. Pakistan Meteorological Department (PMD) presently has a network of eleven seismic stations. By using recorded data, the seismicity and zoning maps of Pakistan have been developed by PMD [12]. Following different zones defined by PMD were considered in present study:

- ✔ Zone 1 - Kohistan-Kashmir
- ✔ Zone 2 - Quetta-Sibi
- ✔ Zone 3 - Southern Baluchistan
- ✔ Zone 4 - Hindu Kosh
- ✔ Zone 5 - Makran Coast

Received: January 2019; Accepted: June 2019
* Corresponding Author: : Asghar Ali <drali@must.edu.pk>

- Zone 6 - Runn of Kuchch
- Zone 7 - Sind-Punjab
- Zone 8 - Upper Punjab-NWFP
- Zone 9 - Western Baluchistan
- Zone 10 - Indian Kashmir
- Zone 11 - North Western Afghanistan-Tajikistan Border Region

The main objective of the study was to formulate such mathematical models which could estimate earthquake casualties and destruction cost. These models will be of great worth in formulating new programs for mitigation of earthquake hazards. According to the target of the study we try to find answers to the following questions:

- Question 1. To what extent are the major earthquake that strikes Pakistan be characterized in terms of intensity, magnitude, depth of focus, location of the epicenter and span?
- Question 2. How much destruction can earthquakes produce in terms of death, injuries, families affected and cost of destruction?
- Question 3. Which mathematical models can be formulated through regression analysis using matrices that approximately describe the earthquake casualties and cost of destruction due to destructive earthquakes?
- Question 4. How much significant are the developed mathematical models to assess the possible destructions due to an earthquake event?

1.1. Literature Review

Earthquake destruction depends upon various factors such as magnitude, intensity, interval, depth of focus etc. Mostly, earthquake destruction depends upon area where it occurs, if it hit a populated area then there will be more destruction than one that hits an un-populated area. The death tolls in earthquake depend on three main factors [1]: structural collapses, nonstructural cause and follow on disaster. According to a research study in 2016 [2], Pakistan and adjoining regions are divided into 14 seismogenic zones. Seismicity of each zone is studied considering also the major cities in the respective zone and type of infrastructure which is mainly responsible for earthquake disaster rather than earth- quake itself. There are four assumptions for multiple linear regressions [4], which are needed to be satisfied for truth worthy results. These assumptions are linearity, reliability of measurement, homoscedasticity, and normality. Linear regression is one of the fundamental models in statistics used to determine the relationship between dependent and independent variables [5]. An extension of this model, namely multiple linear regressions, is used to represent the relationship between a dependent variable and several independent variables. This study is based on multiple linear regression models using matrix notation and analyzing the model using a script approach with MATLAB.

The analysis of local network of earthquake in Pakistan is referred from the PMD (Pakistan Metrological Department) [6] covers a period of 1905 to 2007 and its comparison is done with the Global Catalog of National Earthquake Information Center (NEIC). Pakistan and adjoining region lying between longitude 60^o E to 78^o E and latitude 20^o N to 45^o N is selected for the study. From the NEIC catalog, a sub-catalog is obtained for Pakistan and surrounding region, it contains 8635 events from 1963 to 2004. Finally, to get a rather homogeneous catalog for the region, the two catalogs were merged by considering different data properties and different data analysis techniques prepared by different data collection agencies. The results of this study can be employed for the earthquake prediction research.

Rizwan et al. [7], analyzed available previous seismic data in terms of maximum annual recorded intensity of earthquakes on Richter scale at various locations of Pakistan with a view to know future earthquakes intensity and return periods required for making decision regarding the design of lifeline systems and other structures.

In 2014, Urrutia et al. [8] formulated mathematical models that could estimate the earthquake casualties and destruction costs through regression analysis using matrices. Author considered 30 earthquakes that hit Philippines from inclusive year 1968-2012. The proposed mathematical models with predictors intensity x_1, magnitude x_2, depth x_3, epicenter x_4 and duration x_5 and dependent variables deaths y_1, injured y_2, cost of damage y_3, families affected y_4, as follows:

$$\ln \hat{y}_1 = -13.405 - 0.001x_1 + 2.214x_2 - 0.013x_3 + 0.374x_4 - 0.001x_5$$

$$\ln \hat{y}_2 = -13.426 + 0.360x_1 + 1.899x_2 + 0.015x_3 + 0.444x_4 - 0.001x_5$$
$$\ln \hat{y}_3 = -16.905 + 0.083x_1 + 2.577x_2 - 0.043x_3 + 0.630x_4 + 0.002x_5$$
$$\ln \hat{y}_4 = -17.075 + 0.234x_1 + 2.520x_2 - 0.033x_3 + 0.383x_4 + 0.001x_5$$

Allison, Nicole, and Waters in 2016 [9] presented multiple linear regression models that explained total destruction resulting from an earthquake through four independent variables: whether or not a tsunami occurred (tsunami − dummy), whether or not the earthquake occurred in a developed nation (developed − dummy), intensity (intensity) and number of injuries (total − injuries)

$$Y = -19971 + 5335.98x_1 + 4203.51x_2 + 2333.30x_3 + 0.21428x_4$$

Where coefficient is in millions of dollars in 2015.

Multiple regression for one of the models that predicts death is the combination of magnitude, ln (magnitude) and epicenter with highest R2=0.563 and that is given below:

$$\hat{y}1 = 59578.966 + 11182.497x_2 - 71139.37\ln(x_2) + 167.795x_4$$

The model for predicting injuries with highest $R_2 = 0.685$ is the combination of magnitude and ln (epicenter) with ln(injured) are:

$$\ln(\hat{y}2) = 16.697 + 2.664x_2 + 1.241\ln(x_4)$$

Model that predicts cost of destruction is the combination of ln (intensity) and epicenter with highest $R_2 = 0.611$ is:

$$\ln(\hat{y}3) = -18.787 + 9.477\ln(x_2) + 0.719x_4$$

Timothy [13] represents the development of mathematical model for the estimation of required maintenance for a homogenous facilities portfolio using multiple linear regressions. The study shows how a facilities manager can take historical facility attribute data from a maintenance work-order system and develop a prediction equation by using multiple regression analysis for predicting required maintenance. The derived prediction equations results were compared with those of three popular models discussed in the research. The prediction equations results strongly correlated with all three of the models. Present study has reviewed these models and applied to collected data of earthquake that occurred in Pakistan from 1909 to 2017.

2. MATERIALS AND METHODS

2.1 Data Collection

The first step in this study was to persuade variables that may be included to develop the model. Different variables as shown in block diagram Fig.1 were used to formulate mathematical models that will evaluate the casualties and total cost of destruction. All 22 earthquakes with magnitude 5 or more occurred in Pakistan between 1909 and 2017 were examined. Data about most destructive earthquake that used in this research are presented in Table 1 & 2.

2.1.1. Relation between dependent and independent variables

The relationship between the dependent and independent variables is obtained by using Pearson's

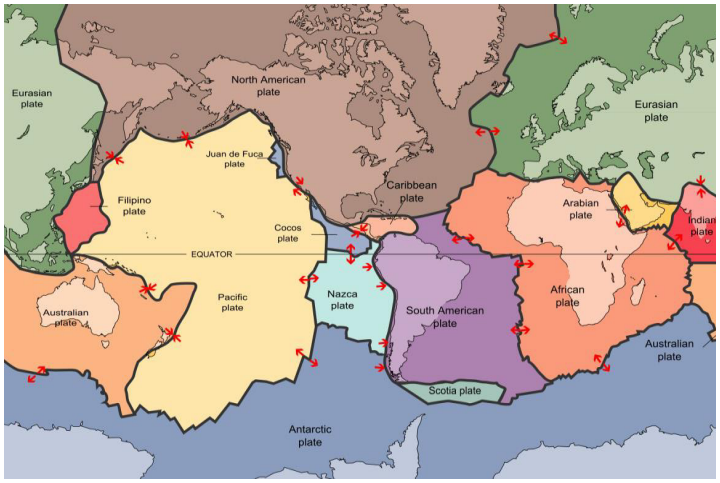

Fig. 1. Tectonic Plates

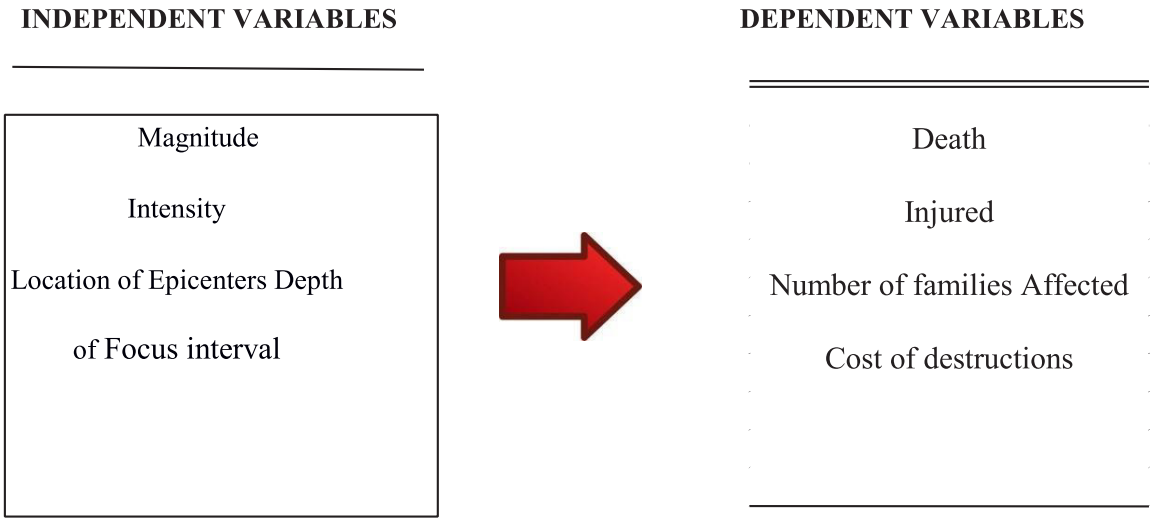

Fig. 2. Block Diagram

Table 1. Data for independent variables

No	Year of earthquake occurrence	Magnitude (x1i)	Intensity (x2i)	Interval (x3i)	Epicenter (x4i)	Depth (x5i)
1	1909	7.1	9	25	3	60
2	1935	7.7	10	180	2	17
3	1945	8	10	60	5	25
4	1966	6.7	7	35	3	10
5	1966	6.1	6.9	25	1	250
6	1971	6.8	7	20	7	230
7	1974	6.6	7	30	4	180
8	1974	7.4	6	22	4	22
9	1990	6.2	6	34	3	7250
10	1995	7.5	5.2	31	5	33
11	1997	6.9	7	30	3	33
12	2001	7.7	10	120	6	22
13	2002	5.8	5	37	10	33
14	2002	5.5	75	28	10	31
15	2004	5.5	5	27	1	10
16	2005	7.6	8	45	8	26
17	2008	7	6	25	2	15
18	2011	5	7	25	3	54
19	2011	7.4	7	20	6	300
20	2013	7.7	7	35	6	83
21	2013	5.6	7	15	3	15
22	2016	6.30	5	60	11	204.40

Table 2. Data for Casualties

No	Year of earthquake occurrence	Deaths (y1)	Injuries (y2)	Affected Families (y3)	Total cost of estruction (y4) (in rupees)
1	1909	100	72	2500	250,000
2	1935	60,000	4000	6000	600000000
3	1945	2000	3000	3000	200000000
4	1966	12	150	4860	486000000
5	1966	12	15	1300	130000000
6	1971	100	12	1000	1000,000,00
7	1974	4	10	1	100,000
8	1974	5300	1700	4400	440000000
9	1990	11	40	10	1000,000
10	1995	4	6	12	1200,000
11	1997	100	57	500	50000000
12	2001	2030	166800	400,000	796320000000
13	2002	17	30	1500	150000,000
14	2002	23	60	15	1500,000
15	2004	24	40	1	100,000
16	2005	87,351	75266	314474	387100000000
17	2008	216	370	100	10000,000
18	2011	4	5	200	20000000
19	2011	4	5	200	20000000
20	2013	34	80	10,000	1000,000,000
21	2013	800	700	1000	1000,000,000
22	2016	4	100	3	5600,000

Table 3. Pearson's coefficient of correlation

Intensity, Parameter	Magnitude	Depth of focus	Location of epicenters	Time interval	Coefficients of correlation
Death(y1)	0.378	0.339	-0.226	0.060	0.491*
Injured(y2)	0.469*	0.325	-0.205	0.160	0.452*
Affected Families(y3)	0.441*	0.341	-0.214	0.206	0.338
Total destruction Cost(y4)	0.453*	0.314	-0.197	0.168	0.431*

Table 4. Pearson's coefficient of correlation

Parameters	ln(death)	ln(injuries)	ln(families)	ln(total destruction)
Intensity	0.607**	0.580**	0.653**	0.565**
Magnitude	0.508*	0.500*	0.489*	0.443*
Depth	-0.483*	-0.498*	-0.316	-0.160
Epicenter	-0.086	0.073	0.082	0.246
Time interval	0.536*	0.576**	0.355	0.394

coefficient of correlation, as shown in the Table 3. Data shows that the magnitude of considered earthquakes is not significantly correlated with any of the dependent variables. Unlike the magnitude, the intensity of considered earthquakes is significantly correlated with injuries, number of affected families and total cost of destruction at 0.05 levels. The coefficient of correlation for depth and location of epicenter are not significantly correlated with any of the dependent variables but time interval is significantly correlated with death, injuries and total cost of destruction. This also shows that all the dependent variables correlate with one or two independent variables. Since all assumption for the multiple linear regressions does not meet, therefore to formulate the mathematical models that could estimate the causalities and destruction costs the dependent variables were transformed.

Table 4 shows that the transformed variable death is significantly correlated with magnitude, intensity and time interval. The transformed variable injuries are significantly correlated with intensity, and magnitude. The transformed variable affected families are significantly correlated with intensity and magnitude. The transformed variable total cost of destruction is significantly correlated with intensity and magnitude. After transformation all the assumption for the multiple linear regression analysis were satisfied. The assumption for normality is tested by using (P-P) plot, the homoscedasticity was checked by plotting the predicted values and residuals on a scatter plot, and the multi-collinearity was tested by the variance inflation factor (VIF) value.

2.1.2. Multiple linear regression by using matrices

Multiple linear regression analysis is used to investigate the relationship between dependent and independent variables when the number of variables exceed by two. The knowledge of matrix theory can facilitate the mathematical manipulation considerably. Relationship between k independent variable x_1, x_2..., x_k and n observations y_1, y_2, ..., y_n, each of which can be expressed by equation.

$$y_i = \beta 0 + \beta 1x1i + \beta 2x2i + ... + \beta kxki + \epsilon .$$

Where β determines the contribution of independent variable X's and ϵ is random error. This model essentially represents n equations describing how the response values are generated in the scientific process. Using matrix notation, we can write the following equation:

$$y = X\beta + \epsilon ,$$

$$y = \begin{bmatrix} y_1 \\ y_2 \\ \vdots \\ y_n \end{bmatrix}, X = \begin{bmatrix} 1 & x_{11} & x_{21} & \dots & x_{k1} \\ 1 & x_{12} & x_{22} & \dots & x_{k2} \\ \vdots & \vdots & \vdots & & \vdots \\ 1 & x_{1n} & x_{2n} & \dots & x_{kn} \end{bmatrix}, \beta = \begin{bmatrix} \beta_0 \\ \beta_1 \\ \vdots \\ \beta_k \end{bmatrix}, \epsilon = \begin{bmatrix} \epsilon_1 \\ \epsilon_2 \\ \vdots \\ \epsilon_n \end{bmatrix}$$

Then the least squares method for estimation of β, involves finding b. The criterion is to minimize a sum of squares of residuals, which can be written as:

$$SSE = \epsilon\epsilon'$$
$$SSE = (y - b)'(y - X)$$

is minimized. This minimization process is involves for solving b

$$\begin{aligned} SSE &= (y - Xb)'(y - X) \\ &= (y' - b'X')(y - Xb) \\ &= y'y - y'Xb - b'X'y + b'X'Xb \end{aligned}$$

by using identity

$$b'X'y = y'Xb$$
$$\begin{aligned} SSE &= y'y - b'y'X - b'X'y + b'X'Xb \\ &= y'y - 2`X'y + b'X'Xb \end{aligned}$$

$$\frac{\partial}{\partial b}(SSE) = 0$$

$$\frac{\partial}{\partial b}(SSE) = 0 - 2X'y + 2b'X'y$$

$$bX'X - X'y = 0$$
$$X'Xb = X'y$$

On the assumption that the inverse matrix exists, the equations have a unique solution, which is the vector of ordinary least-squares estimates. The result reduces to the solution of b in:

$$(X'X)b = X'y$$

Notice the nature of the X matrix. Apart from the

initial element, the ith row represents the x-values that give rise to the response y_1. Writing:

$$A = XX' = \begin{bmatrix} n & \sum_{i=1}^{n} x_{1i} & \sum_{i=1}^{n} x_{2i} & \cdots & \sum_{i=1}^{n} x_{ki} \\ \sum_{i=1}^{n} x_{1i} & \sum_{i=1}^{n} x_{1i} & {}^{2}\sum_{i=1}^{n} x_{1i}\ x_{2i} & \cdots & \sum_{i=1}^{n} x_{1i}\ x_{ki} \\ \cdot & \cdot & \cdot & \cdots & \\ \cdot & \cdot & \cdot & \cdots & \\ \cdot & \cdot & \cdot & \cdots & \\ \sum_{i=1}^{n} x_{ki} & \sum_{i=1}^{n} x_{ki}x_{1i} & \sum_{i=1}^{n} x_{ki}\ x_{2i} & \cdots & \sum_{i=1}^{n} x_{ki}{}^{2} \end{bmatrix}$$

$$g = X'y = \begin{bmatrix} g_0 = \sum_{i=1}^{n} y_i \\ g_1 = \sum_{i=1}^{n} x_{1i}\ y_i \\ \cdot \\ \cdot \\ \cdot \\ g_k = \sum_{i=1}^{n} x_{ki}\ y_i \end{bmatrix}$$

allows the normal equation to be put in the matrix form

$$Ab = g$$

If the matrix A is non-singular, we write the solution for the regression coefficient as

$$b = A^{-1}g = (X`X)^{-1}x'y$$

Thus, we can obtain the prediction equation or regression equation by solving a set of k + 1 equation in a like numbers of unknowns. This involves the inversion of the *k + 1* by *k + 1* matrix *X`X* [14]

2.1.3. Mathematical model for estimation of death

By using the relation

$$b = X'y(X'X)^{-1}$$

and following matrix was obtained:

$$\begin{bmatrix} b_0 \\ b_1 \\ b_2 \\ b_3 \\ b_4 \\ b_5 \end{bmatrix} = \begin{bmatrix} 99.05 \\ 749.88 \\ 694.909 \\ 5531.56 \\ 473.83 \\ 549.69 \end{bmatrix} \begin{bmatrix} 22 & 153.1 & 147.6 & 1903.3 & 109 & 929 \\ 153.1 & 119.65 & 1044.29 & 12733.6 & 733.9 & 7234.7 \\ 147.6 & 1044.29 & 1008.2 & 12651.62 & 736.1 & 6527.7 \\ 1903.4 & 12733.6 & 12651.62 & 362920.36 & 10073.4 & 62945 \\ 109 & 733.7 & 736.1 & 10073.4 & 733 & 4582 \\ 929 & 7234.7 & 6527.7 & 62945 & 4582 & 69283 \end{bmatrix}^{-1}$$

$b_0 = -4.773$; $b_1 = 0.616$; $b_2 = 0.810$; $b_3 = -0.012$; $b_4 = 0.013$; $b_5 = 0.013$

Hence, the number of deaths caused by an earthquake event can be computed by using the regression equation:

$$\ln y\hat{}_1 = -4.773 + 0.616x_1 + 0.810x_2 - 0.012x_3 + 0.013x_4 + 0.013x_5$$

Table 5. Model Summary

Model	R	R Square	Adjusted R square	Standard error of the estimate
1	0.766	0.587	0.458	2.26762

Table 6. ANOVA

Regression	Sum of Squares	df	mean squares	F	sig.
Regression	117.056	5	23.411	4.553	0.009
Residual	82.273	16	5.142		

Table 7. Model Summary

Model	R	R Square	Adjusted R square	Standard error of the estimate
1	0.790	0.624	0.506	2.04509

Table 8. ANOVA

Regression	Sum of Squares	df	mean squares	F	sig.
Regression	110.968	5	22.194	5.306	0.005
Residual	66.918	16	4.182		
Total	177.887	21			

Table 9. Model Summary

Model	R	R Square	Adjusted R square	Standard error of the estimate
1	0.757	0.572	0.439	2.6748

Table 10. ANOVA

Regression	Sum of Squares	df	mean squares	F	sig.
Regression	153.285	5	30.657	4.285	0.012
Residual	114.475	16	7.155		
Total	267.760	21			

Table 11. Model Summary

Model	R	R Square	Adjusted R square	Standard error of the estimate
1	0.699	0.489	0.329	3.62135

Table 12. ANOVA

Regression	Sum of Squares	df	mean squares	F	sig.
Regression	200.420	5	40.084	3.057	0.040
Residual	209.827	16	13.114		
Total	410.247	21			

2.1.4. SPSS output for multiple regression

SPSS output yields that the coefficient of determination R2 = 0.587 which implied that 58.70% of the variation in the number of death during an earthquake is explained by the regression equation and is significant with p-value of 0.009.

2.1.5. Mathematical model for estimation of injuries

By using the relation

$$b = X'y(XX)^{-1}$$

the following Matrix was obtained:

$$\begin{bmatrix} b_0 \\ b_1 \\ b_2 \\ b_3 \\ b_4 \\ b_5 \end{bmatrix} = \begin{bmatrix} 99.05 \\ 749.88 \\ 694.909 \\ 5531.56 \\ 473.83 \\ 549.69 \end{bmatrix} \begin{bmatrix} 22 & 153.1 & 147.6 & 1903.3 & 109 & 929 \\ 153.1 & 119.65 & 1044.29 & 12733.6 & 733.9 & 7234.7 \\ 147.6 & 1044.29 & 1008.2 & 12651.62 & 736.1 & 6527.7 \\ 1903.4 & 12733.6 & 12651.62 & 362920.36 & 10073.4 & 62945 \\ 109 & 733.7 & 736.1 & 10073.4 & 733 & 4582 \\ 929 & 7234.7 & 6527.7 & 62945 & 4582 & 69283 \end{bmatrix}^{-1}$$

Then the regression coefficients were obtained by using MATLAB

$$b_0 = -3.754;\ b_1 = 0.586;\ b_2 = 0.621;\ b_3 = -0.012;\ b_4 = 0.172;\ b_5 = 0.016$$

Hence the number of injured persons resulting from an earthquake event can be computed by using the regression equation

$$\ln \hat{y}_2 = -3.754 + 0.586x_1 + 0.621x_2 - 0.012x_3 + 0.172x_4 + 0.016x_5$$

2.1.6. SPSS output for multiple regression

SPSS output yields that the coefficient of determination R_2 = 0.624 which implied that 62.40% of the variation in the number of death during an earthquake is explained by the regression equation and is significant with p-values of 0.005.

2.1.7. Mathematical model for estimation of affected families

By using the relation, the following matrix was obtained

$$b = X'y(X'X)^{-1}$$

the following matrix was obtained:

$$\begin{bmatrix} b_0 \\ b_1 \\ b_2 \\ b_3 \\ b_4 \\ b_5 \end{bmatrix} = \begin{bmatrix} 134.08 \\ 1011.739 \\ 933.45 \\ 9296.62 \\ 682.88 \\ 6667.86 \end{bmatrix} \begin{bmatrix} 22 & 153.1 & 147.6 & 1903.3 & 109 & 929 \\ 153.1 & 119.65 & 1044.29 & 12733.6 & 733.9 & 7234.7 \\ 147.6 & 1044.29 & 1008.2 & 12651.62 & 736.1 & 6527.7 \\ 1903.4 & 12733.6 & 12651.62 & 362920.36 & 10073.4 & 62945 \\ 109 & 733.7 & 736.1 & 10073.4 & 733 & 4582 \\ 929 & 7234.7 & 6527.7 & 62945 & 4582 & 69283 \end{bmatrix}^{-1}$$

Then regression coefficient was obtained by using MATLAB

$$b_0 = -8.401; b_1 = 1.595; b_2 = 0.510; b_3 = -0.010; \quad b_4 = 0.318; b_5 = -0.018$$

Hence the number of affected families resulting by an earthquake event can be computed by using the regression equation.

$$\ln y\hat{}_3 = -8.401 + 1.595x_1 + 0.510x_2 - 0.010x_3 + 0.318x_4 - 0.018x_5$$

2.1.8. Mathematical model for estimating total cost of damage

By using the relation

$$b = X\,'y(X'X)^{-1}$$

The following matrix was obtained

$$\begin{bmatrix} b_0 \\ b_1 \\ b_2 \\ b_3 \\ b_4 \\ b_5 \end{bmatrix} = \begin{bmatrix} 384.52 \\ 2760.202 \\ 2617.824 \\ 31826.776 \\ 1974.33 \\ 17619.92 \end{bmatrix} \begin{bmatrix} 22 & 153.1 & 147.6 & 1903.3 & 109 & 929 \\ 153.1 & 119.65 & 1044.29 & 12733.6 & 733.9 & 7234.7 \\ 147.6 & 1044.29 & 1008.2 & 12651.62 & 736.1 & 6527.7 \\ 1903.4 & 12733.6 & 12651\,62 & 362920.36 & 10073.4 & 62945 \\ 109 & 733\,7 & 736\,1 & 10073.4 & 733 & 4582 \\ 929 & 7234.7 & 6527.7 & 62945 & 4582 & 69283 \end{bmatrix}^{-1}$$

Then the regression coefficients were obtained by using MATLAB:

$b_0 = 0.824$; $b_1 = 1.717$; $b_2 = 0.356$; $b_3 = -0.005$; $b_4 = 0.585$; $b_5 = -0.004$

Hence the total cost of damage resulted by an earthquake event can be computed by using the regression equation

$$\ln y\hat{}_4 = 0.824 + 1.717x_1 + 0.356x_2 - 0.005x_3 + 0.585x_4 - 0.004x_5$$

2.1.9. SPSS output for multiple regression

SPSS output yields that the coefficient of determination $R_2 = 0.48$ which implied that 48.90% of the variation in the cost of destruction during an earthquake is explained by the regression equation and is significant with p-values of 0.040.

3. Characteristics of Destructive Earthquakes in Pakistan

Table 13 shows the Mean, Median and standard Deviation of the different independent Variables.

3.1 Intensity

Table 14 shows frequency distribution of intensity for twenty two earthquakes occurred in the Pakistan that has been considered in the present study. As overall 36.4% earthquakes are of intensity 7. Earthquakes of intensity 7 are classified as destructive. Moreover 22.7 % of the considered earthquakes are of intensity 5 while 18.2 % of earthquakes are of intensity 6. And 13.6 % of considered earthquakes are of intensity 10 which are classified as most destructive earthquakes. 4.5 % of the considered earthquakes are of intensity 8 and 9 respectively which are considered as very destructive.

3.2 Magnitude

Table 13 shows that the mean magnitudes of the earthquakes are 6.71 with standard deviation of 0.92. According to Richter scale, seismic activities with magnitude 6 to 7 are strong earthquakes and accompanied by local destructions near the epicenters. First class seismological station can observe these earthquakes wherever occur within the earth.

3.3 Depth of Focus

Table 13 shows that the average depth of considered earthquakes is 86.51 kilometer with standard deviation of 97.16. Shallow earthquakes are those earthquakes whose depth of occurrence ranges from 0 to 70 kilometer. The earthquakes with shallower depths bring more destructions than those which have greater depths.

3.4 Location of Epicenter

Table 15 shows the frequency distributions with respect to the location of epicenter of the considered earthquakes. Table 7 shows that the most of earthquake has epicenter located at Zone

Table 13. Means and standard Deviations of the Independent variables

Variable	Mean	Standard Deviation
Intensity(x1)	6.96	1.61
Magnitude(x2)	6.71	0.92
Depth of Focus (x3)	86.51	97.16
Location of epicenter (x4)	4.95	3.03
interval (x5)	42.22	37.83

Table 14. Distribution of the intensity of the earthquake

Intensity	Mean	Percentage
5	5	22.7 %
6	4	18.2 %
7	8	36.4 %
8	1	4.5 %
9	1	4.5 %
10	3	13.6 %
	n=25	100%

Table 15. Epicenter location of earthquake

Zone	Names	Frequency	%
Zone 2	Kohistan-Kashmir	2	9.1%
Zone 3	Quetta-Sibi	6	9.1%
Zone 4	Southern Baluchistan	2	27.3%
Zone 5	Hindukush	2	9.1%
Zone 6	Makran Coast	2	9.1%
Zone 7	Runn of Kuchch	1	9.1%
Zone 8	Sind-Punjab	1	4.5%
Zone 9	Upper Punnjab-NWFP	1	4.5%
Zone10	Western Baluchistan	2	4.5%
Zone 11	Indian Kashmir	1	9.1%
	Northwestern Afghanistan-Tajikistan	n=25	4.5 %
	Kohistan-Kashmir		100 %

3. The 27.3% earthquake considered in study has epicenter at Southern Baluchistan. This implies that southern Baluchistan is very prone to be stricken by the earthquake or any seismic activity.

3.5 Interval of Earthquakes

The average interval of the earthquake considered in the present study is 42.22 seconds with standard deviation of 37.83 as shown in table 5. Earthquakes with longer time interval bring more destructions than those with shorter one.

3.6 Destructions caused by Earthquakes

Table 16 shows the Mean, Median and standard Deviation of the different Dependent Variables. The mean death owning to earthquake is 7188.3183

Table 16. Mean Medians and Standard Deviation of the Dependent variables

Variable	Mean	Median	Standard Deviation
Death(y1)	7188.3183	29	21963.51653
Injured(y2)	114578.0909	66	38183.36629
Affected Families(y3)	34139.8182	1000	105436.2386

as associated to median 29, which is more lifelike estimate of death. The most number of deaths aroused during the Muzaffarabad earthquake in October 8, 2005 which left 87,371 persons dead. It was an earthquake that resulted in enormous destruction of properties and huge loss of lives.

The mean number of people injured is 114578.0909 while the median is 66. The largest number of injured happened on 26 January 2001 Gujarat earthquake that hit India and some area of southern Pakistan which wounded 166,800 persons. The affected families have a mean of 34139.8182 and median of 1000. The largest families were affected in Muzaffarabad earthquake which was about 3147774. The cost property destruction has a mean of 55518265909 and median of 75000000. The largest cost of destruction occurs in earthquake of October 8, 2005. The earthquake left destruction cost of 3.5 billion $. Also the largest cost of destruction occurred in earthquake of Jan 26, 2001 whose epicenter was about 9 km south-southwest of the village of Chobari in Bhachau Taluka of Kutch District of Gujarat, India. The interpolate earthquake reached 7.7 on the moment magnitude scale and had a maximum felt intensity of X (Extreme) on the Mercalli intensity scale. The total destruction cost in this earthquake was about 7.7 billion$.

4. RESULTS & DISCUSSION

4.1 Characteristics of Earthquakes

36.4 percent of the total considered earthquake event that hit Pakistan from 1909 to 2017 were of intensity 7. These earthquakes classified as destructive. The average magnitudes of the earthquakes that are considered in research are:

- 6.71 With standard deviation of 0.92. According to Richter scale, seismic activities with magnitude 6 to 7 are strong earthquakes and accompanied by local destructions near the epicenters. First class seismological station can observe them wherever they occur within the earth.
- The average depths of considered earthquakes from 1909 to 2017 are 86.51 kilometer with standard deviation of 97.16. Shallow earthquakes are those quakes with depth ranges from 0 to 70 kilometer. The earthquakes with shallower depths bring more destructions than those which have greater depths.
- The 27.3 percent earthquake considered in study has epicenter at Zone 3 and that is in southern Baluchistan. This implies that southern Baluchistan is quit prone to be stricken by the earthquake or any seismic activity.
- The average interval of the earthquake considered in this study is 42.22 seconds with standard deviation of 37.83. Earthquakes with longer time interval bring more destructions than those with shorter time interval.

4.2 Proposed Mathematical Models

$$\ln\hat{y}1 = -4.773 + 0.616x1 + 0.810x2 - 0.012x3 + 0.013x4 + 0.013x5$$

$$\ln\hat{y}2 = -3.754 + 0.586x1 + 0.621x2 - 0.012x3 + 0.172x4 + 0.016x5$$

$$\ln\hat{y}3 = -8.401 + 1.595x1 + 0.510x2 - 0.010x3 + 0.318x4 - 0.018x5$$

$$\ln\hat{y}4 = 0.824 + 1.717x1 + 0.356x2 - 0.005x3 + 0.585x4 - 0.004x5$$

The first model estimate number of deaths and is significant with p-value of 0.009 which has a strong positive linear relationship with correlation coefficient of R=0.766. The second model predicts number of injured persons and is significant with p-values of 0.005 which has a strong positive linear relationship with correlation coefficient of R=0.790. The third model predicts number of affected families and is significant with p-values of 0.012 which has a strong positive linear relationship with correlation coefficient of R=0.757. The fourth

model predicts total cost of destructions and is significant with p-values of 0.040 which has a strong positive linear relationship with correlation coefficient of R=0.699.

5. CONCLUSION

Unlike hurricanes and a few different natural hazards, earthquakes can happen at any time of the year and occur without any warning. The current research has successfully proposed such mathematical models which can estimate the earthquake casualties and destruction costs using multiple linear regression analysis. The multiple linear regression analysis method requires data to be linear whereas our available data was nonlinear so we first used transformation to make it linear and then applied the regression analysis. Thus the resulted mathematical models estimate earthquake casualties and destruction costs more efficiently as compared to the existing model and can be concluded as:

- The most number of deaths provoked during the Muzaffarabad earthquake in October 8, 2005 which left 87,371 persons dead. It was an earthquake that resulted in enormous destruction of properties and huge loss of lives, largest no of families about 3147777 were affected.

- The largest cost of destruction occurs in earthquake of October 8, 2005. The earthquake left destruction cost of 3.5 billion $. Also the largest cost of destruction occurred in earthquake of Jan 26, 2001 and total destruction cost in this earthquake was about 7.7 billion $.

6. REFERENCES

1. Crampin, S., R. Evans., B.K. Atkinson, Earthquake prediction: a new physical basis, *Ceophys, Journal of Royal Astronomy Society,* 76:147-156(1984).
2. Sarwar ,F., S. Iqbal., M. Qaisar., A. Rehman., F. Akhtar., S.M. Raza, Earthquake Statistics and Earthquake Research Studies in Pakistan, *Open journal of earthquake Research,* 5(2):97-105 (2016).
3. Mejia, J., K. Rojas., N. Valeza, & A.R. Villagracia, Earthquake prediction through Kannan-Mathematical-Model Analysis and Dobrovolsky-based clustering Technique, *Conference: DLSU Research Congress,* 3:1-6 (2015).
4. Osborne, J.W, & E. Waters, The Effects of Minimum Values on Data Transformations, *American Education Research Association, New Orleans*, LA 8: 1-5 (2002).
5. Brown, S.H, Multiple Linear Regression Analysis: A Matrix Approach with MATLAB, *Alabama Journal of Mathematics,* 1-3 (2009).
6. Sarwar, F., S. Iqbal, & L.R. Kamal, An analysis of Pakistan's local network catalog of earthquake for the period of 1905-2007, *Science International,* 23(1): 13-17 (2011).
7. Rizwan, S.A., M.A. Khan., S.A. Debaj, Application of probability theory in the earthquake risk assessment and its consequent possible reduction, *12WCEE* 2000: (1948).
8. Urrutia, J.D., L.A. Bautista, & E.D. Baccy, Mathematical models for estimating earthquake casualties and destruction cost through regression analysis using matrices, *Journal of Physics: Conference Series,* 495:1-15 (2014).
9. Nicole, A, & E. Water, Statistical modeling of earth- quake destruction, Honors Program Thesis. *University of Northern Iowa*: 39: (2016).
10. State Disaster Management Authority Muzaffarabad, http://sdma.pk/.
11. National Disaster Management Authority Islamabad (NDMA), *www.ndma.gov.pk/*
12. Pakistan metrology department and NORSAR. Seismic Hazard Analysis and Zonation for Pakistan. *Azad Jammu and Kashmir:* July (2007).
13. Nipp,T.M, University of Tennessee, Knoxville," Development of a Mathematical Model for the Estimation of Required Maintenance for a Homogenous Facilities Portfolio Using Multiple Linear Regression", May 2017.
14. Ye, M.W, Probability and Statistics for Engineers and scientists, Ninth Edition (2014).

Proceedings of the Pakistan Academy of Sciences:
A. Physical and Computational Sciences 56 (2): 29-36 (2019)

ISSN: 2518-4245 (print), 2518-4253 (online)

Pakistan Academy of Sciences

Research Article

Modeling the Relationship between On-Street Parking Characteristics and through Traffic Delay

Nahry[1]*, Heddy R. Agah[1], Antho Thohirin[1], and Nor Hayati Abdul Hamid[2]

[1]Department of Civil Engineering, Faculty of Engineering, Universitas Indonesia
[2]Faculty of Civil Engineering, Universiti Teknologi MARA, Malaysia

Abstract: : In performing regulation concerning the on-street parking prohibition, Jakarta transport authority bases its decision on the Level of Service of link under consideration. It does not make use explicitly of the dynamic of parking, i.e., the variables of parking characteristics whereas in some cases parking is prohibited while indeed the contribution of parking to the traffic jam is not quite significant. The purpose of this study is to examine the effect of on-street parking on the through-traffic by modeling the relationship between the various variables that represent parking characteristics and the variables associated with the traffic flow, with a case study on West Jatinegara Street, Jakarta. Parking variables are represented by parking turnover, parking index, flow-in and flow-out, while the traffic flow is represented by the delay time, i.e. the difference of travel time of with-parking state and the one of without-parking state to pass particular segment before the parking area. The model shows that there is a fairly strong relationship between parking turnover and the delay of vehicles that move toward the parking location, and the volume of the through-traffic also affects such relationship. Local authorities can take advantage of the model as a guideline in performing parking prohibition policy.

Keywords: Parking Characteristics, Parking Turnover, Delay Time, Through Traffic.

1. INTRODUCTION

Parking problems are faced by almost all big cities, including Jakarta, Indonesia. The business district in the city center generally has high on-street parking demand, especially on weekdays. During office hours, half of the vehicles in the downtown streets of big cities are in a condition of cruising for parking [1]. However, due to its interference to the through-traffic flow, on-street parking in many places in the city center is often prohibited by the local administrator. On the other hand, there are still lacks parking space, particularly in the city center. Indeed, office or shop owners in these areas need adequate parking space to provide the best service to their customers, while the road users expect the least possible disturbance on their trip, and the local government is stipulated for the livable and wealthy city.

To satisfy the parking demand, constructing new parking facilities is one of the possible choices. However, construction of new facilities is not always possible due to lack of money, human time, and land resources. Another solution that might be applied to meet the demand for parking is the optimization of parking facility usage. This approach seems to be more efficient since it consumes fewer resources [2]. In this context, parking management has an important role and it is related to the multiple objectives of the inhabitants of the city. Indeed, proper parking management should be able to generate a positive impact on the results of the trade-off between their objectives. The key is to find a method for effective management to maximize opportunities and reduce the difficulties related to the use of on-street parking [3]. Three specific objectives are frequently perceived to conflict parking management, namely the desire to use parking measures as a means of regenerating a specific part of the urban area such as the town center (i.e. providing more parking to attract business); the desire to use parking controls as a means of restraining vehicle traffic and improving

Received: April 2018: Accepted: June 2019
* Corresponding Author: Nahry <nahry@eng.ui.ac.id>

environmental quality or to encourage the use of non-car models; and the need to secure sufficient revenue from the parking operation to cover costs or to make a surplus to fund other activities [4].

In performing parking regulation, especially of on-street parking prohibition, local authorities generally base their decisions by considering the road width, traffic volume, traffic speed, parking vehicle dimensions, parking type and the nature of land use. Jakarta Transport Authority makes use of Level of Service of link under consideration to decide the parking prohibition policy. In contrast, in some cases, the contribution of parking activities to the traffic jam is not quite significant indeed. Usually, the authorities do not make use of the variables of parking characteristics, such as parking turnover, parking index, parking duration, etc. For example, the characteristics of the on-street parking of the retail market are different from the ones of the wholesale market, although their characteristics of traffic and their road geometrics are similar. Parking turnover of the wholesale market may be lower than the rate of the retail market as a result of the process of loading and unloading and also due to the maneuvering of the heavy vehicles of commercial activities.

Consequently, both types of parking generator are likely to have different impacts on traffic flows that pass through it. In order to achieve the best result on parking management, the city government needs to consider the most appropriate conditions carefully to impose parking prohibition, by considering the parameters that describe the parking characteristics, besides the factors related to traffic flow of the through-traffic, and the road geometric. In this case, for two parking areas that have the same conditions of traffic characteristics and road geometric, it is possible to apply different parking policies or parking management. It may be expected to be one of the solutions to the problem of limited parking space in the major cities, including Jakarta.

The purpose of this study is to examine the effect of on-street parking on the through-traffic by modeling the relationship between various variables that represent parking characteristics and variables associated with the traffic flow, with a case study on West Jatinegara Street, Jakarta. It is an old business district in the city center equipped with two-lane one direction road and parallel parking system.

Naseri [5] analyzed the impact of on-street parking on the traffic flow variables in several cities of Iran. Traffic flow variables that were used are the speed, delay time, and traffic volume, while the parking variable was represented by the percentage of use of parking space. This study examined the effect of percentage of parking space usage on the average delay on different road types and V/C ratio. It proposed delay adjustment factor and equation models of the effects of both types of variables. The study showed that the higher the percentage of parking space usage, and the larger the V/C ratio, the higher the delay adjustment coefficient was. It was found that commercial area has the highest delay adjustment coefficient among the one of highway, arterial road and local residential street.

Thirayoot and Sugiarto [6] examined the impact of on-street parking, particularly the impact of road shoulder usage and parking maneuver on the performance of urban artery road in the city of Banda Aceh. The artery road performance was analyzed using dynamic capacity model. It showed that due to the presence of on-street parking, the road capacity was reduced by 10-13% (275-368 vhc/h) and the speed was reduced by 13-19% (3-5 km/h). Simulations were conducted using VISSIM 5:30 program to get the estimated effectiveness measurement by eliminating the on-street parking from the study site. The simulation showed that the absence of on-street parking could make the average delay time reduced by 12 sec/vhc (32%) and the speed can be increased by 5 km/h (24%).

Roza [7] described the characteristics of on-street parking in the area of Petaling Jaya City Council (MBPJ) Malaysia. It made use of some variables, i.e. number of parking lots, parking volume, average number of parking vehicles per hour, maximum parking vehicle per hour, parking turnover, parking duration and parking capacity per hour. The result showed that the differences in the parking characteristics were caused by land use, parking systems, different purpose and behavior of riders.

Portilia [8] examined the effect of on-street parking on the artery road or main road on the

entire traffic flow. The study examined the effect of vehicle maneuver and bad position parking against the average travel time by using queuing model M/M/∞, where the arrival and departure took the form of Poisson distribution. The model was validated using a calibrated micro-simulation through local field measurements taken on the road segments in the city of Santander Cantabria, Spain. Microsimulation was used to calculate the reduction of capacity of road segments for each case study and the addition of the average travel time for each road user. Simulation of the model M/M/∞ showed that the on-street parking maneuver and wrong parking position affected the traffic flow.

Borovskoy and Yakovleva [9] studied parking turnover impact on traffic flow delay. The study method is based on the development of a simulation model depending on the mobility plan; in the course of full-scale studies, using data on the intensity of vehicle movement and the time of vehicle entry to and exit from the parking space. The path of vehicle movement, depending on various positions of the vehicle during parking, was performed with the help of Vehicle Tracking application for AutoCAD. It was noted that the increase in the turnover leads to an increase in delays in traffic flows.

Those previous studies focused more on the influence of parking angle and vehicle maneuvering characteristics to the reduction of road segment capacity, as well as their impact on the traffic delay. Since the measurement of parking characteristics is relatively more comfortable due to the standard procedures in the data collection rather than the measurements of vehicle maneuvers or other variables that are less commonly used in the parking study and traffic study, this research is aimed to see the effect of parking characteristics to the through-traffic, especially in Jakarta. It is intended to take into account the parking characteristics in the justification of parking prohibition regulation in a particular area instead of parking vehicle dimensions, parking type and the nature of land use merely.

2. METHODOLOGY

The flow chart of research methodology is indicated in Fig.1.

2.1 Parking and Traffic Flow Survey

The traffic flow survey was done in two conditions; namely parking and no-parking stated. The 18-hour field surveys of the through-traffic flow for both states use two video cameras which are set on a road segment along the Jatinegara Barat street, i.e. 28 meters and 230 meters toward the starting point of the on-street parking area. This

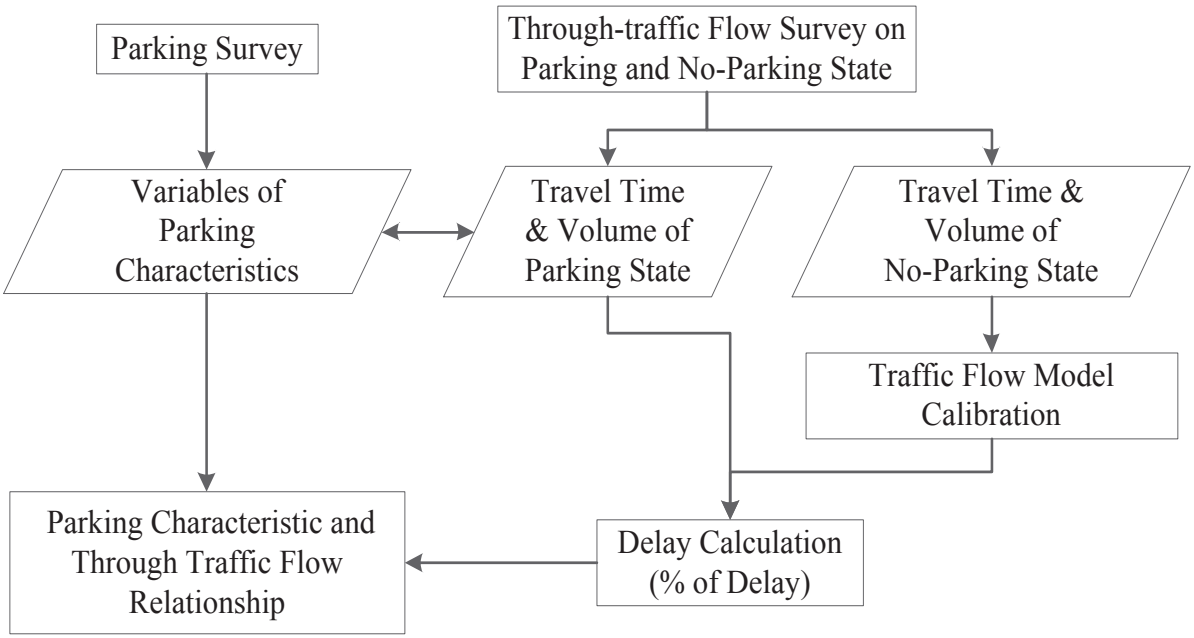

Fig. 1. Research Methodology

segment was located in a parking prohibited area but it was immediately affected by the parked vehicles maneuver on the parking area right after this segment. It was possible to find the traffic data for both states since the on-street parking policy was only performed on the weekend, while parking was prohibited on the weekdays. The 18 hours was divided into 15-minute time increment, so there were 72 data set of traffic flow. In further analysis, the traffic volume of each of 15 minutes' observation was transformed into hourly volume. The speed of each vehicle was calculated from data of travel time to pass the segment of observation. From the data of volume and speed, the traffic density was generated.

For parking survey, parking characteristic data was taken at the same time with the through-traffic data collected, and both types of data were matched for each time increment (i.e 15 minutes) during the observation period. The length of the parking area surveyed was 200 meters with parking capacity as 32 parking space unit (PSU). Primary data of parking activity included parking duration and flow-in and flow-out of the vehicle during a predetermined time of observation. Afterward, the data was processed to obtain a variable that represented the parking characteristics, i.e. parking turnover, parking activity index, parking index, flow-in, and flow-out.

2.2 Delay Calculation

The influence of parking characteristics on the traffic flow is represented by delay time. Delay measurements in this study are slightly different from other studies that generally define the delay through queuing theory or other measurements based on one condition only, namely parking state or using simulation methods [6]. Delay in this study is calculated by comparing the travel time of the through-traffic on a particular road segment right before the parking area under consideration to the travel time on the same segment at the time of no-parking state. Such delay is called absolute delay. Travel time of no-parking state is obtained at the time when the parking is prohibited, vice versa for parking-state. Comparison of travel time of the two states (surely taken at two different times) is allowable since both travel times are associated with the same traffic volume, and it is assumed that the side frictions (such as pedestrian activities and other obstacles) are the same for both states.

Travel time of parking-state and the respective traffic volume for each time of increment are directly found from the observation. Meanwhile, in order to find travel time of no-parking state at any condition of traffic volume, traffic flow model is generated, particularly the model that relates the volume of through-traffic and speed (and the respective travel time). From the calibrated model, the travel time to pass the segment of observation in any condition of traffic volume at the no-parking state could be determined.

Afterward, for each time increment of observation, a final parameter is applied, namely, relative delay. It is a percentage of delay that is expressed in the following equation:

$$\Delta TT = \frac{(TT_1 - TT_2)}{TT_2} x\ 100\% \qquad (1)$$

where:

ΔTT = Percentage of delay (%)
TT_1 = Travel time of on-street parking state
TT_2 = Travel time of no on-street parking state

The parameter of a percentage of delay is intended to see the impact of parking to the through-traffic flow by excluding the internal delay within the traffic flow itself, for example, due to the high volume. By using the percentage of delay, local authorities can decide more judiciously the implementation of parking prohibition policy. For example, in the case of which the effect of on-street parking is not significant, the percentage of delay may be relatively small. It indicates that either the parking is prohibited or not the travel time is still high; accordingly, the travel time difference, as well as the percentage of delay, becomes small. Consequently, even if the travel time toward the parking area is high, parking prohibition is not always the best option to apply for traffic management.

2.3 Calibration Model of the Through Traffic Flow

The calibration model of the through-traffic flow is carried out using 72 data set of observation, namely

volume, speed and density to model the relationship between the travel time (as the complement of speed) and volume of the road segment that represents the traffic flow under uninterrupted condition, i.e. no-parking state. It applies the traffic data at the time when the parking is prohibited. The Green Shields Model, Greenberg Model, and Underwood Model are applied, and one of them is finally chosen as the best model to represent such traffic flow.

2.4 Relationship between the Parking Characteristic and Through Traffic Flow

It is initialized by corresponding the travel time of no-parking state (TT_2) to the travel time of parking state (TT_1) on each time increment of parking state observation. The travel time of no-parking state (TT_2) can be found through the volume and speed relationship of the calibrated traffic flow model by applying the associated traffic volume of parking state to the model to find the speed. The travel time TT_2 comes after the length of observation divided by such speed.

Analysis of the relationship between variables of parking characteristics and through-traffic flow, which is represented by the percentage of delay, is carried out by performing a scatter diagram with the variable of parking characteristics on x-axis and percentage of delay on y-axis. Local authorities can take advantage of the model as a guideline in performing parking prohibition policy. Having the chart and the permitted percentage of delay, the local authority can decide when the parking prohibition should be performed. The decision considers the combination of parking characteristics and one of traffic flow rather than the parking characteristics as a single determinant. As the delay percentage is more than the permitted one, then the parking activity can be prohibited, and vice versa.

3. RESULTS AND DISCUSSION

3.1 Traffic Flow Model for No-Parking State

Based on the Goodness of Fit Test, it is found that the Underwood Model is the best model that represents the uninterrupted flow at the segment of observation with the coefficient of the determination as $R^2 = 0.901$. The relationship among the three variables of traffic flow is shown in Fig. 2 ~ Fig. 4. In our case, Fig. 4 becomes the most critical model since it relates the traffic volume and speed (and the associated travel time). From that figure, the travel time to pass the segment of observation in particular conditions of traffic volume at the no-parking state could be determined.

3.2 Relationships Between Parking Turnover and Delay

Tables 1 shows the result of the traffic flow survey in terms of three parameters, i.e volume, speed and density for parking state and no parking state during 18-hour observation. It can be seen that during period of observation the segment in no-parking state could perform better than the one of parking state by accommodating more vehicles per hour

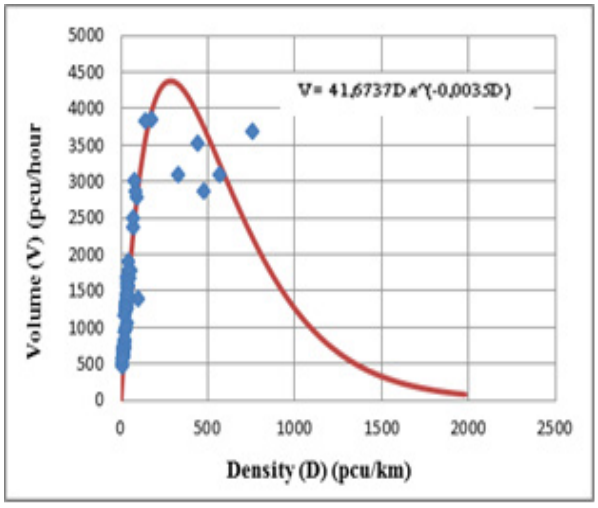

Fig. 2. Relationship of Vloume and Density

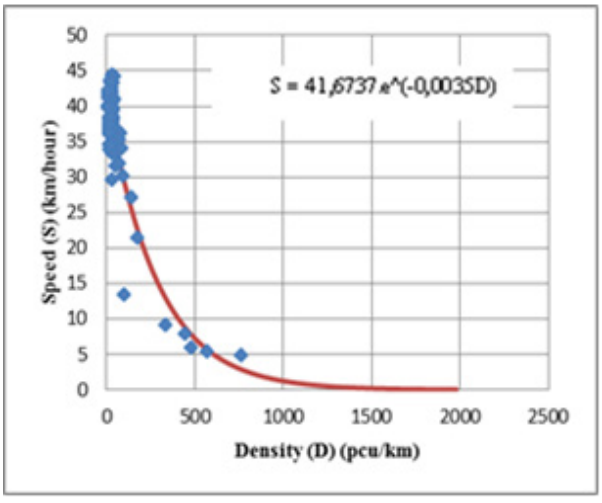

Fig. 3. Relationship of Speed and Density

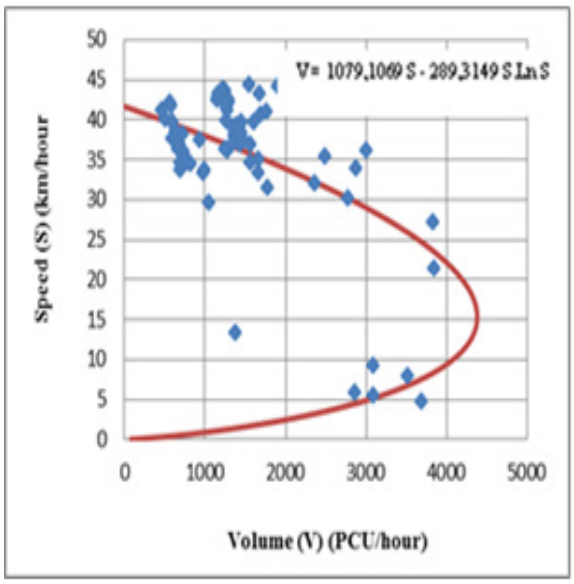

Fig. 4. Relationship of Speed and Volume

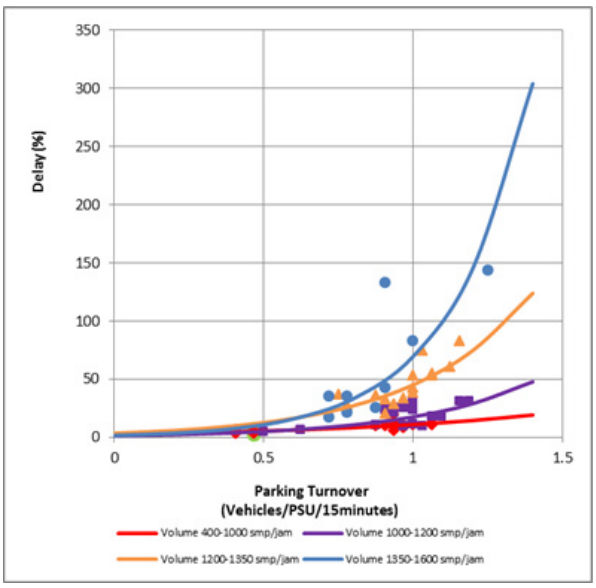

Fig. 5. Relationship between Parking Turnover and Percentage of Delay

(up to 150.78%) and more vehicles per km (up to 395.91%), as well as raising the higher maximum speed (up to 11.74%).

Table 2 shows the result of the parking survey during the 18-hour observation. It can be seen that during the period of observation, the parking system is still in good performance with the average 77.30% of total parking space is occupied, with the level of parking activity is 0.12. The parking turnover is quite low where only 0.36 vehicles occupy one parking space unit per hour. It is relevant to the characteristics of the land use of Jatinegara as a commercial shopping area.

In order to see the relationships between the parking characteristic and percentage of delay, the entire variables of parking characteristics are

Table 1. Traffic Flow Characteristics

No	Traffic Flow Characteristics	Parking State	No-Parking State	% of difference (to parking state)
1	The Lowest Volume	205,60 pcu/hour	458,80 pcu/hour	123.15%
2	The Highest Volume	1533,60 pcu/hour	3846 pcu/hour	150.78%
3	The Lowest Speed	9,98 km/hour	4,84 km/hour	-51.50%
4	The Highest Speed	39,71 km/hour	44,37 km/hour	11.74%
5	The Lowest Density	5,39 pcu/km	11,40 pcu/km	111.50%
6	The Highest Density	153,72 pcu/km	762,31 pcu/km	395.91%

Table 2. Parking Characteristics

No	Parking Characteristics	Value
1	Flow-In Parking Volume	195 vehicles
2	Flow-Out Parking Volume	182 vehicles
3	Average Parking Index	77,30%
4	Parking Turnover	0,36 vehicle/PSU/hour
5	Parking Activity Index	0,12

analyzed (i.e. parking turnover, parking activity index, parking index, flow-in, flow out). It is carried out by conducting Regression Analysis with the percentage of delay as the dependent variable and each of parking variables as the independent variables. The results show that only parking turnover that has good correlation with the percentage of delay. It is relevant to the study done by Borovskoy, A. and Yakovleva, E. [9] that the increase in the turnover leads to an increase in delays in traffic flows. Meanwhile study of Gao and Ozbay [10] on double parking violations of commercial vehicles show that the location, frequency, and duration of the double parking event and overall traffic demand have a certain impact on the average travel time.

Furthermore, since the range of traffic volume is quite big, then the volume is classified into five groups; hence further analysis of the relationship between Parking Turnover and Percentage of Delay becomes more suitable. The classification is as follows:

- Group 1: 0-400 pcu/hour
- Group 2: 400-1000 pcu/hour
- Group 3: 1000-1200 pcu/hour
- Group 4: 1200-1350 pcu/hour
- Group 5: 1350-1600 pcu/hour

Using such classification, the relationship between the parking turnover and percentage of delay is determined and indicated in Fig. 5. From the chart in Fig. 5 it can be explained that:

The relationships between parking turnover (x) and percentage of delay (y) is as follows:

- Group 2 (400-1000 pcu/hour):
  $y = 2{,}802e1{,}381x$, $R^2 = 0{,}660$
- Group 3 (1000-1200 pcu/hour):
  $y = 1{,}497e2{,}476x$, $R^2 = 0{,}476$
- Group 4 (1200-1350 pcu/hour):
  $y = 3{,}646e2{,}519x$, $R^2 = 0{,}559$
- Group 5 (1350-1600 pcu/hour):
  $y = 1{,}760e3{,}680x$, $R^2 = 0{,}629$

From the R^2 values, it can be concluded that for the entire group of volume, parking turnover has a strong influence on vehicle delay. The higher the parking turnover, the higher the additional travel time of the vehicles approaching the parking area. At low volume, this condition is not quite sensitive, but as the volume increased the contribution of parking activity to increase the travel time becomes more significant. The delay change indicates it as the parking turnover changed from 0 to 1:

- For group 2: delay changed at 8.35%
- For Group 3: delay changed at 16.31%
- For Group 4: delay changed at 41.62%
- For Group 5: delay changed at 68.02%

For all groups of volume, as the parking turnover is zero, i.e. a condition in which there are no flow-in and flow-out vehicles at the parking area (where the parking volume is not always zero), the delay of through-traffic still occurs. It may occur since when a driver sees the road segment in front of him is occupied by parking vehicles, he may tend to move away from his lane and shift to the next lane while approaching the bottleneck (the initial point of parking area). Hence, such movement may mess up the traffic and affects the travel time of other vehicles.

The model shown in Fig. 5 could be used to see the borderline at which the authority is allowed to prohibit the parking operation. It can be done simply by defining the maximum allowable percentage of delay. Then by using the observed maximum volume of the segment, we can find the maximum parking turnover allowed. This number could be used to justify the parking prohibition policy. Using this number, the effect or contribution of parking to the traffic jam could be justified more accurately.

As the local authority only takes into account the land use type or vehicle dimension without considering the parking characteristics before the application of parking prohibition, the regulation may not be successful in practice. For example, one wholesale business district has a low parking turn over, while the other is a retail business district whose parking turnover is quite high. Both districts have similar characteristics of traffic flow. When the parking regulation only considers their types of land use (as a business district) and the traffic flow, regardless of their parking turn over, both districts may be treated as on-street parking prohibition areas. In contrast, as their parking turnover is different, they may result in different disturbances

on through-traffic indeed.

4. CONCLUSIONS

For the area under consideration, e.g. 2 lanes one direction road with parallel on-street parking in the business district, there is a reasonably strong relationship between parking turnover and the delay of through traffic flow that move toward to the parking location, and the volume of the through-traffic also affects such relationship. The higher the volume and the parking turnover, the higher the delay will be. At low volumes, the relationship is less sensitive, while as the traffic volume increased the impact of parking to the delay becomes greater.

Local authority can take advantage of the model that relates the parking turn over and the delay as a guideline in performing parking prohibition policy. Having the relationship, the local authority can decide when the parking prohibition should be performed. In this case, the decision considers the combination of characteristics of both parking and through-traffic flow rather than the parking characteristics as a single determinant. Due to the limited space for movement and parking, especially in the downtown area, all road users compete for the space. Hence, the local authority needs rigorous exercise before the implementation of parking regulation.

As a preliminary study, the proposed model still needs further improvement on model calibration by using more data, as well as its validation.

5. REFERENCES

1 Arnott, R. & E. Inci, An Integrated Model of Down Town Parking and Traffic Congestion. *Journal of Urban Economics* 60: 418-442 (2006).

2 Voa, T.T.A., P.V. Waerden, & G. Wetsc, Micro-Simulation of Car Drivers' Movements at Parking Lots. *Procedia Engineering* 142 :100-107 (2016).

3 Cerreño, A.L.C. *The Dynamics of On-Street Parking in Large Central Cities*. Rudin Center for Transportation Policy and Management, New York. University Robert F. Wagner Graduate School of Public Service (2002).

4 Marsden, G. The evidence base for parking policies—a review. *Transport Policy* 13: 447–457 (2006).

5 Naseri, A. A Method for Estimating Average Delay Time due On-Street Parking. *Australian Journal of Basic and Applied Sciences*.7(8): 767-774 (2013).

6 Thirayoot, L, & Sugiarto. Impact of On-street Parking on Urban Arterial Performance: A Quantitative Study on Travel Speed and Capacity Deterioration. *Aceh International Journal of Science and Technology*. 2(2): 63-69 (2013).

7 Angelalia, R. On Street Parking Maneuvers and Their Effects on Design. *Journal of Society for Transportation and Traffic Studies* (JSTS). Vol 4, N1 (2010).

8 Portilia I.A., Using M/M/∞ Queueing in On- Street Parking Maneuvers. *ITE Journal. Washington DC*. (2009).

9 Borovskoy, A. & E. Yakovleva, Simulation Model of Parking Spaces Through the Example of the Belgorod *Agglomeration. Transportation Research Procedia* 20: 80 – 86 (2017).

10 Gao, J. & K. Ozbay, Modeling Double Parking Impacts on Urban Street. *Transportation Research Board's 95th Annual Meeting*, Washington, D.C. (2016).

Proceedings of the Pakistan Academy of Sciences:
A. Physical and Computational Sciences 56 (2): 37-47 (2019)

ISSN: 2518-4245 (print), 2518-4253 (online)

Pakistan Academy of Sciences

Research Article

Exploring the Factors Influence the Usage of Private Transport at Ayer Keroh, Melaka

Heoy Shin Loo*, Boon Cheong Chew, and Yu Xin Ou Yang

Faculty of Technology Management and Technopreneurship,
Universiti Teknikal Malaysia Melaka (UTeM), Malaysia

Abstract: Local authority's council, Majlis Perbandaran Hang Tuah Jaya (MPHTJ), Melaka is aiming to reduce the traffic congestion and reduce Green House Gases (GHG) emission from private transport in Ayer Keroh. Ayer Keroh is selected as the research location because it consists of residential, industrial, commercial, state government administrative centre and tourist spot which cause it to be crowded with vehicles such as private cars, motorcycle, lorry and busses. Thus, the high usage of private transportation leads to serious traffic congestion and high emission of GHG in Ayer Keroh. Although effort to promote green transportation to reduce usage of private transport and GHG emission, most of the public in Melaka still prefer the usage of private transportation. Hence, the problems of traffic congestion and emission of GHG could not be reduced significantly. Therefore, this study aims to examine the factors influence the public to use private land transport in the area. The research design for this research is exploratory and mixed method (qualitative data and quantitative data source).Since the novelty of the research and MPHTJ does not implement any sustainable transport system in Ayer Keroh. The factors are lastly arranged based on the significant level by comparing the result from qualitative data and quantitative data: vehicle ownership, mobility substitute, vehicle cost, local neighborhood retail and service quality, walking and cycling conditions and health and environmental concerns. The data is further use for determination of strategies that change the public behavior in transport usage and proposing the sustainable transport planning.

Keywords: Green House Gases (GHG), Private Transport, Sustainable Transport Planning.

1. INTRODUCTION

Melaka Green City Action Plan (GCAP) that produced on 22nd April 2014, it has listed six thematic areas which help in further enhanced the planning for green development in Melaka [1]. One of the focus areas is green transportation and in this field the main goal is to increase the opportunities for alternative modes of transportation and reduce Greenhouse Gases (GHG) emissions resulting from vehicular use. Melaka had taken a big step in improving the transport system for public transport. Two electric buses have start operating around Melaka since August 2016 and there are the first electric buses used in Melaka for public. Looking at the large state transport system, it is not adequate if public transport implements eco-friendly technology, but private transport is put aside. Hence, it is important to consider the private transport system to achieve the overall sustainable transport system in Melaka.

Ayer Keroh, Melaka is located 13 km away from the main entry point through North-South Expressway. It is accommodated with residential, industrial, commercial and tourist spots. Since Ayer Keroh is the most developed township in Melaka, hence it is important for the town act as role to other township in the implementation of sustainable transport system. The local authority, Hang Tuah Jaya Municipal Council (MPHTJ) has created the vision as "to make Hang Tuah Jaya a world-class smart city with the concept of green technology".

In line with the vision of MPHTJ, the local authority also starts to enhance the transport system in the area. This paper focuses on the private transport usage at Ayer Keroh, Melaka. Before

Received: April 2018; Accepted: June 2019
* Corresponding Author: Heoy Shin Loo < heoyshin_loo@outlook.com>

changing the behavioral on transport usage for community, the factors of influencing the private transport usage are identified. After the finding process, the researchers start to rank the factors based on the significantly. The factors are used for further strategies implementation.

Generally, sustainable is the presence of the system and developments [2]. Sustainable transport can explain as the transport system that have the ability to meet the needs of society to move freely, gain access, communicate, trade and establish relationships without sacrificing other essential human or ecological values today or future [3]. For every country that implements the sustainable transport, there will have the common sustainable transport objectives to fulfill. There are four general objectives that listed [4]: improved transport system diversity, smart growth land use development, energy conservation and emission reductions and efficient transport pricing.

To fulfill the objectives on achieving sustainable transport, it is needed to identify the factors that influencing the usage of private transport. The factors are categories into four groups [5]:

i. Vehicle Cost

Vehicle cost is referred to the monetary cost for the consumer and it is the critical factor that affects the travel behavior. The higher vehicle cost for a type of vehicles will lead to lower consumption and shift to substitute choice of transport. Based on the summarization, several of price charges can have different effect on travel behavior [6].Consumer will tend to reduce the number of vehicles they own or change the type of vehicles own.

ii. Walking and Cycling Conditions

Walking and cycling known as non-motorized transport as well as active transport. The quality of the active transport influences the travel activity in several ways. Improving of the condition for the active transport able to raise the non motorized travel, transit travel and reduce automobile travel. Other than that, if ever there are walk way provided around the bus stop, the transit travel will also increase [7]. In addition, improvement for sidewalks and make it as a completed network in typical town will increase the average daily per-capita non-motorized travel.

iii. Mobility Substitute

Telecommunication and internet provided a wide range of possibilities for community to carry out any activity virtually without travelling [8]. There are four types of effects possible to occur due to the ICT on activitites: substitution, modification, generation and neutrality. Based on the comparison, internet usage for any purpose is easily to adopt and utilise by youngsters rather than older people [9].

iv. Local Neighborhood Retail and Service Quality

The built environmental affects the price or generalized cost of travel through short-term impact on travel time and influence the consumption of travel [10]. In long term manner, built environment able to influence the location choices of households and business and therefore affect the travel mode choices. It is crucial to take a balance point between jobs and housing in a location as can lead to reduce the distance and time of commuting.

v. Vehicle Ownership

Department for Transport (DfT) in Great Britain had shown that there are increasing in car ownership trend since year 1960 to year 2010. The transforming of the status from non-car owning to car-owning has two crucial impacts on travel behavior. First impact that brought by this issue is the total distance travel each year by the resident. The second impact is that

Table 1. Factors that influence the usage of private transport [15]

Groups	Factors
Economic factors of productivity, incomes and price	Vehicle cost
Quality of available transport options	Walking and cycling conditions Mobility substitute
Land use factors	Local neighbourhood retail and service quality
Emerging social patterns and preferences	Vehicle ownership Health and environmental concern

the increasing in car ownership lead to reducing in depending on other transport modes.

vi. Health and Environmental Concerns

Transport pattern contributes to a wide range of environmental diseases, economic inefficient, health and safety issue and social inequalities [11]. The increasing number of private cars usage in urban area generates more obvious effect on the environment as well as on human health. The intentions to behave in environmental response are highly related to the environment, car and hazard of traffic. Pro-environmental behaviors are the comprehensive model that develops in varies aspect: risk perception, subjective knowledge or attitudes.

2. MATERIALS AND METHODS

The researcher discussed the materials and methods in two different parts: data collection and data analysis. Data collection is the justification on qualitative data collection and data analysis is the description of analysis for qualitative data.

2.1. Data Collection

Research design is the general plan that guides the researcher to answer the research questions [12]. The research design that has been used in this research start with exploratory. Exploratory is used when the researcher wish to clarify the understanding of an issue, problem and phenomena. This research aiming for long term planning on the sustainable land transport system implementation at Ayer Keroh, Melaka. Hence, it is crucial for the researcher to find out the factor and design a set of strategy to overcome the transport usage issues. Deep understanding is gained during data collection process and new insight able to create in order to help in the creation of sustainable land transport system.

Qualitative research method was adopted in this research project. Qualitative research is highly associated with an interpretive philosophy because researchers are required to get on of the subjective and socially constructed meanings explicit about the phenomenon being studied. Qualitative research method was chosen in this research project because the researcher required to obtain in depth understanding on the relationship of factor that influence utilisation of private transport with sustainable transport.

The qualitative data collection method that used in this research is open-ended questionnaires through semi-structure interview. Semi-structured interviews is where there will be a themes and possible key questions that will cover. Semi-structured interview was carried out and the respondent involved the staff of HTJMC as well and the community respresentatives. The respondents from the HTJMC were selected randomly out from 15 staff as all of them were invovled in the project. However, the community representatives were selected based on the areas the respondents stay and the frequency of usage for private transport at Ayer Keroh. The number of respondents that from HTJMC was targeted for half of the staff that involved in this project which 7 respondents while the community respresentatives were set to have 8 respondents to avoid overload of data.

The researcher could easily arranged an interview session with the HTJMC's staff because they had the idea of the research. Moreover, they also understood that the purpose of the interview session conducted was to ask deeply for the opinion on the implementation of sustainable transport system (private or public). On the other hand, it was required to understand the topic and each of the technical term that would be used during conducting the interview session so that it could be easily to explain to the community respresentative. The questionnaire was prepare and the order of the questions rely to the flow of the conversation and additional questions is require to probe the research questions and objectives. The respendents is freely to give their opinions and ideas based on the questions asked. All the voice was required to be recorded as further reference. Digital recorder is used throughout the interview process so that the data interpretation able to dosmoothly. The research also used the memo to write down the important keyword and generate for probe questions during interview session.

The data collection is mainly for the purpose of planning on sustainable private transport planning at Ayer Keroh, Melaka. Hence, the respondents

focused on the local authorities member and community representatives from the area. Local authorities' member refers to the staff that worked for green development department for MPHTJ. The community representatives are selected as the respondent as they are the individual that close to the local community and able to voice out the needs of them. The data that obtained from the local authorities member and community representatives are used for data triangulation purpose. The information and perspective from different field of respondent help in formation of a better sustainable transport system implementation.

By taking the population at Ayer Keroh is 38,00 residents, the respondents that required in this research is around 381 respondents (SurveyMonkey, 2016). The researcher set the margin of error to be 5 % and the confidence level as 95 %. This figure indicated that to obtain the accurate of the data, the researcher required to find at least 381 respondents to complete the questionnaire. However, the more of the respondents involve in this research, the high the accuracy of the result could be obtained. Two methods that the researcher used to publish the survey form: distribute face-to-face and require the respondents to complete the questionnaire on the spot where the other methods was to upload the questionaire to the website and spread the link to the respondents that involved. The researcher need to keep updating the result after get the feedback from the respondent to ensure the validity and reliability of the data.

2.2. Location of the Research

Ayer Keroh is situated on the outskirt of Melaka, about 15 km east from the city center. Ayer Keroh, Melaka is selected as the location because it is the most developed township among the cities in Melaka. The city is well accommodated with residential, tourist spot, administration centre and industry area. Fig. 1 shows the location maps for this research where the red ink boundary is Ayer Keroh. Even the research's location only focuses on Ayer Keroh, but other area around also need to consider in this research because the transport and road connectivity is linked. The areas that involve are Durian Tunggal, Batu Berendam, Bukit Beruang and Bukit Katil (marked with red ink).

2.3. Data Analysis

Research strategy is a plan action to achieve a goal; therefore it is often defined as a method of how a researcher will go about answering the research questions [12]. The researcher chooses action research as the research strategy because this research is the collaboration with the municipal council Melaka (MPHTJ) to solve problem that generated by land transport system. Action research help to generates improvements for the relevant practices and gaining in-depth knowledge on the problem faced.

There are three concurrent sub-processes for the purpose of Data Display and Analysis approach

Fig. 1. Location of the Research [16]

for qualitative data, which are: data reduction, data display and verifying conclusions [13]. Data reduction is the process of simpllifying and concluding the data collected from primary and secondary data sources. The data were organised accordingly based on the theory listed to ensure the precision of the data. Data display refer to structure and categorise the data into summary diagram or visual displays. The analysis can only complete when the verification for the conclusion examination is done. This research focus on triangulation of data where the variation between the feedback from the staff of MPHTJ and community representative is made. The information is important be interpreted to identify and justify for future actions in planning and improvements.

3. ANALYSIS AND DISCUSSION

This chapter will list all the respondents that involve in this study. Six factors that will influence the public to utilize the private transport are been discussed.

3.1. Respondents List

There are 15 respondents in this study where 8 respondents from the staff of local authorities centre and 7 respondents from the community representatives. Their designation and the location they administrated are listed in the Table 2.

3.2. Factors that Influence the Usage of Private Transport at Ayer Keroh, Melaka.

Based on the factors that listed by Litman (2015), the researcher select the particular factors that suit to the culture of Ayer Keroh, Melaka. The data analysis is discussed based on the factors that listed.

3.2.1 Economic Factors of Productivity, Incomes and Price

Under this factor, the vehicle cost is believed that cause the public to utilize the usage of private transport. The higher the vehicle cost for type of vehicles, the lower the consumption of the usage of vehicles. Different type of vehicles also brings the impact for fuel pricing adjusting where the motorist tends to choose those fuel-efficient vehicles such as electricity or hybrid generated.

Staff 6, Staff 7 and Representative 2 commented that the cost for Hybrid and Electric Vehicle (EV) are higher due to technology applied. The installation of battery and fuel cell are required to operate for these vehicles. Higher vehicle cost also due to the low production volume. The demand

Table 2. Respondents List [17]

MPHTJ Staff	**Department**
Staff 1	Penilaian dan Pengurusan Harta
Staff 2	Undang-Undang
Staff 3	Pusat Setempat
Staff 4	Korporat, Pembangunan Ekonomi dan Masyarakat
Staff 5	Korporat, Pembangunan Ekonomi dan Masyarakat
Staff 6	Penguatkuasaan
Staff 7	Pelesenan dan Kesihatan Awam
Staff 8	Perancang Bandar dan Desa
Community Representative	**Location**
Representative 1	Taman Bayam, Durian Tunggal
Representative 2	Taman Merdeka
Representative 3	Durian Tunggal
Representative 4	Bukit Katil
Representative 5	Ayer Molek
Representative 6	Taman Tasik Utama
Representative 7	Bukit Beruang

for Hybrid and EV are not as high as conventional vehicles. Hence, Representative 5 strongly agreed that the higher vehicle cost cause only minority of people affordable to pay and own for it.

On the other hand, Representative 7 emphasized that the fuel pricing does not bring any impact to the user. "Budgeting is important to overcome the fuel fluctuation every week." The statement is strongly agreed by Representative 6:

"Own budget is very important. We couldn't avoid fuel consumption when we use vehicles to travel. Therefore, the increasing of petrol price able help to reduce the usage of private vehicles. If over budget for transportation cost, unnecessary trip can be reduced or avoided to cut down the expenses."

Based on the above discussion, it showed that vehicle cost does not stop the community to own private transport. Most of the community nowadays prefers to own lower cost vehicles as long as they able to travel for daily usage. The researcher believes that the fluctuation trend of fuel pricing in Malaysia will not affect the people to change the transport mode choice but it able to reduce the travel distance.

3.2.2 Quality of Available Transport Options

Two factors that discussed under this group: walking and cycling conditions and mobility substitute.

i. Walking and Cycling Conditions

The quality of the active transport affects the travel activity in a few ways. The improvement of the condition for the active transport helps to raise the non-motorized travel, transit travel and reduce automobile travel. The average daily per-capita non-motorized travel will increase if the improvements for sidewalks and make it as a completed network in typical town.

The infrastructure has provided help to encourage the public to utilize the active transport. Staff 8 explained that condition on road and infrastructure available influence public not to utilize active transport. She mentions that there is needed to provide a special lane for the pedestrian and bicycle rider to ensure their safety. Staff 1 further claims that the travel behavior of the cars and heavy vehicles cause put the active transport on risk. They overtake the wrong side of road because neglecting the existence of those riders which always lead to serious accidents. Travels distance also one of the considerations for transport mode choice. From the justification of Staff 5 and Representative 5, longer distance cause the public relying on own car.

Weather is one of the considerations that the community not to use other transport choices especially active transport (walking and cycling). Staff 2 and Representative 7 emphasize that weather is the main concern on public prefer to use car due to avoid from the exposure of weather uncertainty (hot weather or raining). Based on the explanation form WordTravels (2017), there is no four seasons in Malaysia. The weather uncertainty due to Malaysia has a tropical climate which hot and humid all the year.

The researcher agrees that the walking and cycling condition able to affect the community transport mode choice. In Melaka, the weather is hot and humid along the year due to the geographical location near to Strait of Melaka. Unexpected weather causes the community to depend on motorized vehicle for daily routine. The condition for the community to use bicycle is when the distance is short to reduce the risk. Besides, the infrastructure also causes the community do not know how to start to walk and cycle. There is no special lane for pedestrian and bicycle to ensure their safety. In line with the statement from Staff 8, there are needed to separate the traffic lane for pedestrian and bicycle. A well management and proper designed infrastructure believe help to increase the usage of walking and cycling.

ii. Mobility Substitute

Telecommunication and internet have provided a wide range of possibilities for community to carry out any activity virtually without travelling. There are four types of effects that possible to occur due to the usage of ICT on daily activitites: substitution, modification, generation and neutrality. Internet usage for any purpose is easily to adopt and utilise by youngsters rather than older people.

There are several platforms that offered for online purchase: Zalora, Lazada, Lelong, Amazon and 11street start to appear in the market. Besides online purchase, bill payments also can be done through online payment especially the house utilities, telecommunication bill and quit rent. However, Representative 1 doubted that mobility substitute does help in reducing the transport usage and travel mode choice. "Internet helps only 50% to reduce transportation usage. Even though most of the payment can be done through online, there are people that still want to human-touch when they do payment." In addition, Representative 7 emphasized that:

"Normally purchasing through internet able to help to reduce the transportation usage. However, some of them surf the online purchase platform just to compare the price and will still visit to supermarket to compare the price as well where the usage of vehicle occurs. After the comparison, the buyer will choose to buy the one with the cheapest price."

Staff 4 added that "every community are looking forward for improvement of new technology. The community want to become modern. No one choose to look backward. Even the elder people, we need to encourage them to enjoy this technology era. As long as they willing to learn, there will no gap for them to adapt to the ICT world."

Based on the discussion, the researcher agrees that mobility substitute is helpful in reducing the usage of private transport. The creation of online purchase and payment help to bring a lot of convenient for the community to do any transaction through online. This is because through online purchasing, it can reduce the travel distance of the buyers and the usage of vehicle that eventually helps to reduce traffic congestion. Besides time and cost saving, internet also help to provide a purchasing platform that offer a wide range of product which allow the buyers to search for the interested products without leaving the house. In addition, online payment service able to display a systematic transaction of the payer for checking purpose; thus, it able to save time and cost because the payers do not need to queue for payment purposes. The researcher believes that this situation able to bloom the economy of the city that cause by the introducing and utilize the ICT.

3.2.3 Land Use Factors

Local neighborhood retail is discussed under land use factors. Retailing refer to the local business that for the benefit of neighborhood. People tend to more active if the areas are compacted with mixed-use communities or retail. For short term impact, retailing able to affect the generalized travel cost while for long term impact, the location choices and households is believing that will affect the travel mode choices.

The appearance of amenities that situated in the housing area is one of the considerations when choosing for home's location. Staff 8 commented that a good housing area is the place that accommodate with school, grocery shops, food center and clinic. It is easy for the local community to reach the shop because the location is within walking and cycling distance. This help to reduce the transport usage of the community.

Based on the explanation of Staff 8, Representative 2 agreed that the local neighborhood retail able to encourage people to walk and bicycle as the distance between destinations is shorter. Furthermore, Representative 2 claimed that the place that always congested with vehicles is usually caused by the community from outside of the area but not the one stay within the area.

The researcher agrees that local neighborhood retail is the one of the aspects that will influence the transport mode choices. This is due to the short distance travel to reach the destinations and convenient that brought to the local community. the convenient that brought by local neighborhood retail leads to the adjustment of timing for outing. Unless go for leisure, the local community can have their daily necessities through local retail with non-motorized transport such as walking or cycling.

3.2.4 Emerging Social Patterns and Preferences

Two factors that discussed under this group: vehicle ownership and health and environmental concerns.

i. Vehicle Ownership

Based on the research, many developing countries start to consider the restriction vehicle ownership to

reduce traffic congestion. Car ownership and utilize it playing an important role in modifying the human life quality [14]. The main reason for the increasing number of car ownership due to the creation of identity, tranquility and easy access for the owners.

Referring to the statistics generated by The Nielsen Global Survey of Automotive Demand, the car ownership in South-East Asian (SEA) market is relatively lower among global. Surprisingly, Malaysia is the only country from SEA to buck the trend and posting in third place for car ownership globally (93%). Staff 6 acknowledged that there is no rule that mention on the limitation of vehicle ownership in Malaysia cause the number of vehicles increasing. Staff 3 described that the increasing of vehicles ownership in Malaysia due to the existing of the local automotive manufacturer in Malaysia which is Proton and Perodua.

Furthermore, Representative 3 supported that the ownership of motor vehicles increasing due to the affordable installment. The improvement of life quality cause the community able to own vehicles due to stable income. Based on the comment of Staff 8, the owning power of the community will increase if they are placing in higher position and identity. Different routine purpose will cause different type of transport mode choice.

All the respondents above agreed that vehicle ownership help to increase the tendency for the community to own transport. The researcher justified that the choices mostly is due to the lower interest rate from bank and the easy procedure to apply for loan. When the community have the vehicle ownership, they are not willing to change their transport mode choice. The community prefer to use car which it has become a trend. From the aspect of image, the people that with high position in their job, they prefer to have vehicle ownership due to their ability to own a transport.

ii. Health and Environmental Concerns

Transport pattern can contribute to a wide range of environmental diseases, economic inefficient, health and safety issue and social inequalities. The increasing number of using private cars in urban area generates more obvious effect on the environment and human health. Staff 1 clearly explained that electric car contributes to green environment.

"EV is fully operated by the electricity that stored in the battery pack. When the electricity is running low, the battery is needed to recharge from charging units. Since the operation is not by gasoline, EV can consider as zero emissions vehicle which do not emits tailpipe pollutants."

Besides EV, Representative 2 also emphasized that walking and cycling are the other transport modes that do not bring any negative environmental impact. This is because there is no any complicated manufacturing process involves and the operation is easy. On the other hand, health issue also one of the consideration for travel behavior.

Staff 8, Representative 3 and Representative 4 strongly agreed that cycling is a good exercise as it help to encourage better physical and mental health. It helps to reduce the risk on experiencing various type of health problem such as obesity, cardiovascular, arthritis and stress. Staff 8 further described that combination of regular exercise such as walking and cycling with daily routine provide a most-time efficient method.

Other than air pollution, the researcher claims that noise pollution also one of the environmental impacts that bring by the transport usage. According to the Department of Statistics Malaysia (2016), noise pollution is recorded approximately 70% of the emission is from the land transportation field (20% from air transport and 10% from rail transport). The researcher concludes that utilising of convention vehicles (vehicles that using internal combustion engine for propulsion) cause the serious environmental especially air pollution and noise pollution. EV, walking and cycling is the zero emission transport mode and the usage of these transport mode is believe able to protect environment and improve health.

3.3. Quantitative Data Analysis

Another form of data source obtains from survey that distributed to the community stay in the location involved. 700 respondents involve in this survey and the data is analyzed using SPSS with multiple regression analysis. The results obtained are displayed as Descriptive Statistics, Model Summary, ANOVA and coefficients.

Table 3. Descriptive Statistics [18]

	Mean	Std. Dev.
Frequency of Usage	4.6314	1.97875
Vehicle Cost	3.6929	1.13405
Mobility Substitute	3.8029	1.20490
Walking & Cyling	3.2814	1.22303
Local Retail	3.5700	1.17409
Vehicle Ownership	3.7414	1.14487
Environmental and Health	3.6171	1.15184

Table 4. Model Summary [19]

Model	R	R Square	Adjusted R Square	Std. Error of the Estimate
1	.824a	.680	.676	1.12631

Table 5. ANOVA [20]

Model	Sum of Squares	df	Mean Square	F	Sig.
Regression	1860.326	8	232.541	183.309	.000b
Residual	876.583	691	1.269		
Total	2736.909	699			

a. Dependent Variable: Frequency of Usage

b. Predictors: (Constant), Health and Environment Concerns, Mobility Substitute, Car Sharing and Carpooling Options, Vehicle Cost, Demographic, Vehicle Ownership, Local Neighborhood Retail and Service Quality, Land Use Development Patterns

Table 6. Coefficients [21]

Model	Unstandardized Coefficients		Standardized Coefficients
	B	Std. Error	Beta
1 (Constant)	-1.593	.170	
Vehicle Cost	.168	.058	.096
Mobility Substitute	.171	.052	.104
Walking & Cycling	.129	.049	.080
Local Retail	.140	.061	.083
Vehicle Ownership	.147	.063	.085
Environ &Health	.099	.070	.057

a. Redictors: (Constant), Health and Environment Concerns, Mobility Substitute, Car Sharing and Carpooling Options, Vehicle Cost, Demographic, Vehicle Ownership, Local Neighborhood Retail and Service Quality, Land Use Development Patterns

b. Dependent Variable: Frequency of Usage

From Table 4, R square of the factors that affect the public in utilizing the private transport is .680. It indicates that near to 1.0 and hence it has strong prediction between two dependent variables and independent variables. Besides that, the value of .68 also means that the model explains 68% of the variance in usage of private transportations.

The statistical significance of the result can be observed in Table 5. Statistically significance refer

to the relationship between two or more variables that caused by something other than multiple R in the population equals 0 where this study reaches statistical significance (Sig.=.000; p<.0005). With the p value of .0005, it refers to that the confidence level used in this research is 95% and less than .0005 indicate the significant results between each of the factors with the frequency of usage.

The Beta value under Standardized Coefficients in Table 6 is to compare the contribution of each independent variable; whereas, the un standardized coefficients listed as B is used to construct a regression equation. Regression equation formed using the un standardized coefficient, B value. The largest beta value in the Beta column shows the strongest unique contribution to explaining the dependent variable. In conclusion, the factors that have strongest contribution in affecting the transport usage is Mobility Substitute, Vehicle Cost, Vehicle Ownership, Local Neighborhood Retail and Service Quality, Walking and Cycling Options and lastly the least contribution in transport usage is Health and Environment Concerns.

4. CONCLUSIONS

In line with the vision of local authorities Ayer Keroh, Melaka, this township is aiming move toward green smart city. To achieve this transformation, one of the fields is to implement sustainable transport system planning. Sustainable transport is important to maximize the economy wealth of the city. Besides, it also leads to the creation of health environment and harmonious socialization. Before review on the Sustainable Transport Planning from other country, it is needed to identify the factors that the public utilizing private transport for daily routine. There are four main fields of the factors that been categorized: Economic factors of productivity, incomes and price, Quality of available transport options, Land use factors and Emerging social patterns and preferences. Six factors that the authors discussed in this paper. Based on the feedback and the information that collected from the primary and secondary data, the authors arrange the factors that influence the usage of private transport according to their significant level. The arrangement of the factors is from the most significant to the least significant: vehicle ownership, mobility substitute, vehicle cost, local neighborhood retail and service quality, walking and cycling conditions and health and environmental concerns. The factors that listed are used to generate the strategies to overcome the problem that public utilizing private transport for further study. The researchers wish the officer can contribute to lead the successful of this planning. with the successful of the implementation, this planning believes able to implement in other state of Malaysia and even for other developing countries.

5. ACKNOWLEDGEMENTS

The authors are very grateful to the entire staff of HTJMC for their generous time in taking part in interviews. We also thank the Universiti Teknikal Malaysia Melaka (UTeM) and Knowledge Transfer Programme (KTP) for their financial support under grant KTP GLuar/ KTP/2/2015/FPTT/FK/G00040.

6. REFERENCES

1. Asian Development Bank. *Green City Action Plan: A Framwork for Green Actions,* Melaka: Asian Development Bank (2014).
2. United Nations. *Sustainable Transport.* November2.https://sustainabledevelopment.un.org/topics/sustainabletransport (2016).
3. William, R.B. Sustainable Transport: Definitions and Responses. *Baltimore: Symposium on Sustainable Transportation* (2016).
4. Todd, L, *Well Measured: Developing Indicators for Sustainable and Livable Transport Planning.* Victoria Transport Policy Institute (2016).
5. Todd. L, *The Future Isn't What It Used to be: Changing Trends and Their Implications for Transport Planning.* Victoria Transport Policy Institute (2015).
6. Todd, L. *Understanding the Transport Demands and Elasticities,* Victoria Transport Policy Institute (2011).
7. Ryan, Sherry, and Lawrence F Frank. Pedestrian Environments and Transit Ridership, *Journal of Public Transportation*, 39-57 (2009).
8. Zwerts, E., J. Davy, & W. Geert, *The Impacts of Virtual Mobility on Travel Behavior: An Overview* (2004).
9. Bert van. W., K. Geurs, & C. Chorus, Information, Communication, Travel Behavior and Accessibility, *The Journal of Transport and Land Use*, 1-6 (2013).
10. Boarnet, M. G, & R. Crane, The Influence of Land Use on Travel Behavior: Specification and

Estimation Strategies, *Transportation Research Part A: Policy and Practice,* 823-845 (2001).

11. Belzer, D, & G. Autler, Countering Sprawl with Transit-Oriented Development, *Issues in Science and Enchnology*, 51-58 (2002).
12. Saunders. M., P. Lewis, & A. Thornhill, *Research Methods for Business Students.* England: Pearson (2012).
13. Miles, M.B., A.M. Huberman, & J. Saldana, *Qualitative Data Analysis: A Methods Sourcebook,* London : Sage (2014).
14. Shaygan, M., M. Amirreza, & M. Houshmand, Car Ownership Models in Iran, A Review of Methods and Determinants.*Transport and Telecommunication*, 45-49 (2017).

Proceedings of the Pakistan Academy of Sciences:
A. Physical and Computational Sciences 56 (2): 49–54 (2019)

ISSN: 2518-4245 (print), 2518-4253 (online)

Pakistan Academy of Sciences

Research Article

Design and Analysis of Microstrip Line and Lumped Element Based 3dB Equal-Ripple Low Pass Filter for C- Band

Waseem Abbas*, Jawad Yousaf, and Zubair Mehmood

Department of Electrical and Computer Engineering, Sungkyunkwan University, Suwon, Republic of Korea

Abstract: This work presents design, study and comparable circuit modelling of an equal ripple Microstrip transmission line (MLIN) based low pass filter (LPF) for C-band. A 5th order LPF is considered for corner frequency of 4GHz with 3dB attenuation using ideal lumped elements and MLIN based structure with FR4 substrate. Advanced Design System (ADS) software tool is used for design and simulation of LPF.The comparison of results confirms that MLIN based designed filter has excellent stop and pass band characteristics around the intended break frequency of 4 GHz and can be utilized in extensive choice of C-band microwave implementations due to its simple design and easy manufacturing compared to lumped elements based filter.

Keywords: 3dB Equal Ripple, C-band, Low Pass Filter, Lumped Elements, Microstrip transmission line, Advanced Design System.

1. INTRODUCTION

Low pass filters (LPF) are normally used for frequency selection application in satellite, radar and wireless communication systems. The LPFs are critical to reject harmonic components which are not required for the system under observation [1]. High and low impedance Microstrip transmission line (MLINs) are utilized for the designing of LPFs [1, 2]. Typical MLIN are manufactured using printed circuit board (PCB) technology and are mainly used for the filter application with quasi-TEM propagation mode [3, 4]. MLIN based microwave circuit designs are preferred because of smaller size, lesser cost, lighter weight and compact structure comfort [1, 4, 5, 6]. MLIN based LPFs works as an important functional block in numerousRF and microwave systems for the passing of desired frequency signals to the connecting microwave blocks [3, 5, 6].

In this work, a5th order 3dB equal ripple microstrip-line LPF was designed for the 0 to 4 GHz frequency range. The designed filter can be used for wide range of application in C-band like in weather radar systems, cordless telephones and Wi-Fi device [1, 2, 4]. ADS software is used for filer design and simulation [7]. An equivalent lumped element-based filter is also designed; the results are compared with MLIN based filter which shows very good agreement. The LPF can be used for removal of high frequency noise from desired signal, it can also be used with the amplifier circuits for limitation of input frequency.

The rest of the paper is organized as follows: Section 2 demonstrates the filter design theory. Section 3 describes the specifications of the designed LPF. The comparison of the designed filter results for MLIN and lumped elements based structure isfocused in Section 4. Section 5 accomplishes the conclusion.

2. FILTER DESIGN THEORY

The common examples of MLIN are filter application based on planner transmission lines. Fig. 1 shows a simple typical structure of MLIN. The width *(W)*, length *(L)* and thickness *(t)* of the metal strip along with substrate properties controls

Received: June 2018; Accepted: June 2019
* Corresponding Author: Waseem Abbass <engr.waseemabbas1694@gmail.com> ; <waseem1694@skku.edu>

the characteristics impedance of a MLIN. In Fig.1, the thickness of the FR4 substrate is represented by *'h'*. The relative permittivity of the used FR4 substrate is denoted by ε_r.

2.1 Procedure For Designing Low Pass Filter

The designed LPF used 3dB equal ripple estimation with maximally flat response in the pass band. The 1Ω is used for source impedance tonormalize LPF calculation method [1, 4]. Fig. 2 illustrate the variation in the attenuation characteristics of a nominal filter with various orders (N) with regard to normalized frequency.

The cut of frequency and stop band attenuation of the designed filter are 4 GHz and -35 dB respectively. The considered target attenuation is more than -35 dB at stop band frequency. The stop band reflecting the transition from cut off to stop band is at 6 GHz. The information of Fig. 2 is used for the determination of the order of the filter.

The design procedure for LPF has been well thought-out as a low pass model (i.e., 3dB equal ripple approximation) with a 5th order *(N=5)*. The LPF element values are x_i *i.e.,* x_0, x_1, x_2, x_3, x_4, x_5, and x_6. The normalized element values i.e., x_0,x_1, x_2, x_3, x_4, x_5, and $x_6$are then changed to lumped elements for the required corner frequency of f_c= 4 GHz. Normally 50Ω source impedance is used for MLIN-based filter [4].

The FR4 substrate is used with $\boldsymbol{\varepsilon}_r$ of 2.6 and thickness of 0.5 mm. The load and source impedances are considered as unity. A stepladder

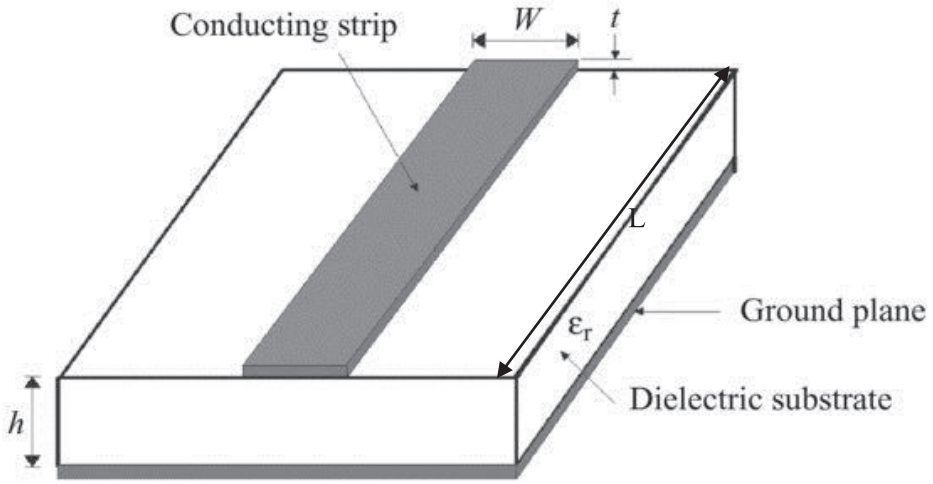

Fig. 1. Microstrip transmission line (MLIN)

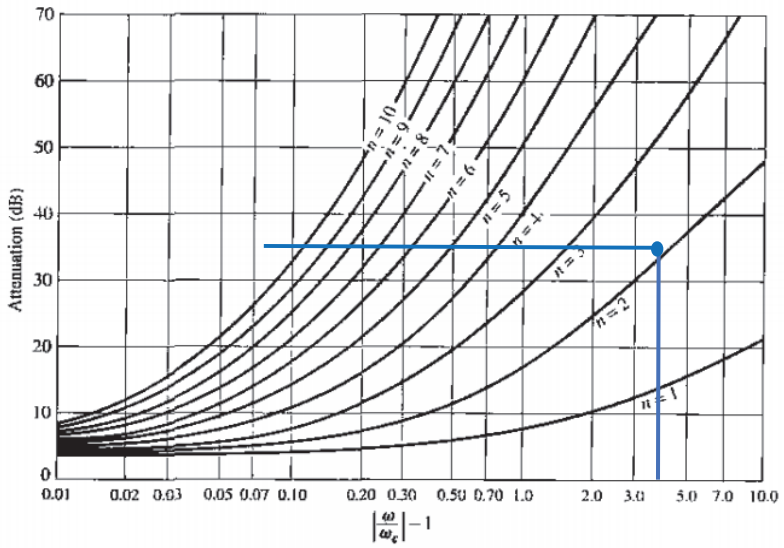

Fig. 2. Attenuation versus normalized frequency for 3dB equal-ripple filter prototypes [4]

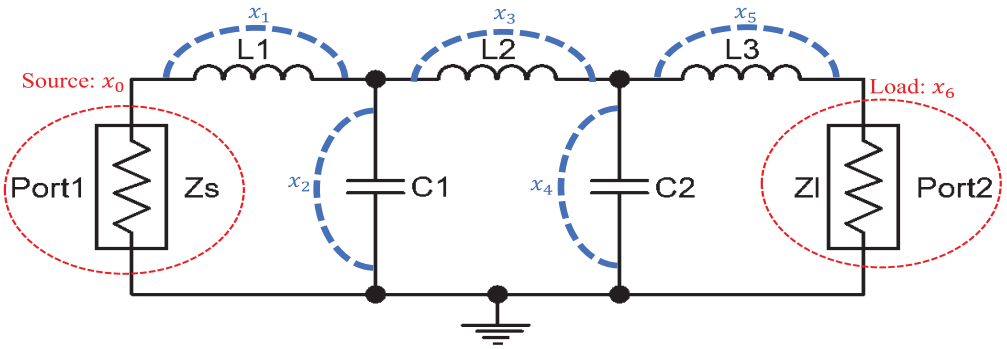

Fig. 3. Designed 5th order low pass filter based on lumped element (see Table 1 for component values)

circuit that initiated with cascaded elements of x_1, x_3 and x_5 are inductors and x_2, $x_4$are capacitors as revealed in Fig.3

The L and C of different components can be obtained from the equations (1) and (2) correspondingly from the regularized values [4].

$$L_{k+1} = \frac{Z_0 x_{k+1}}{2\pi f_c} \qquad (1)$$

$$C_k = \frac{x_k}{Z_0 2\pi f_c} \qquad (2)$$

In equations (1) and (2), L_{k+1} and C_k represents the inductances and capacitances of the MLIN respectively. Z_o is the source and load impedance, and f_c is the corner frequency [4]. The capacitor and inductor's width for low pass microwave filter are considered using the below mentioned formulations [1, 4]:

Below equation (5) is used for the calculation of the ε_e (effective dielectric constant).

$$\text{For } \frac{w}{h} \leq 2, \qquad (3)$$

$$\frac{w}{h} = \frac{8e^A}{e^{2A-2}} \qquad (4)$$

$$A = \frac{Z_0}{60}\sqrt{\frac{1+\varepsilon_r}{2}} + \left(\frac{-1+\varepsilon_r}{1+\varepsilon_r}\right)\left(0.23 + \left(\frac{0.11}{\varepsilon_r}\right)\right)$$

$$\varepsilon_e = \frac{1+\varepsilon_r}{2} + \frac{\left(\frac{-1+\varepsilon_r}{2}\right)}{\sqrt{1+12\left(\frac{h}{w}\right)}} \qquad (5)$$

3. LOW PASS FILTER DESIGN SPECIFICATIONS

The designed LPF has 50 Ω characteristics impedance with 4 GHz cut off frequency. The highest and lowest designed impedances are 100 Ω and 25Ω respectively. The designed filter constitutes of capacitive and inductive transmission lines segments. Equations (6) and (7) are used for the determination of the electrical length (l) of those capacitive and inductive segments [4].

Where phase constantis β and l is representing the transmission line's physical length, Z_o is the source and load impedance which is 50 Ohm. The inductive and capacitive impedance of the transmission lines are represented by Z_{high} and Z_{low} respectively [3].

The designed LPF schematic illustration is shown in Fig. 4. In Fig. 4, the open stub length is most sensitive because it grounds the undesired signal and thus have an impact on the attenuation characteristics of the filter.

$$\beta l = \frac{Z_0 L}{Z_{high}} \qquad (6)$$

$$\beta l = \frac{C Z_{low}}{Z_0} \qquad (7)$$

Table 1. Lumped elementparameters for Fig. 3

Component	Values
Z_s (Ω)	50
Zl (Ω)	50
L1 (nH)	6.92
L2 (nH)	9.02
L3 (nH)	6.92
C1 (fF)	606
C2 (fF)	606

The width and length of the different sections of the designed filter of Fig. 4 are determined using the designed equations of (3), (6) and (7). A Matlab code for the calculations of the different parameters of the designed filter is written and is shown in Appendix.

The layout design is revealed in Fig. 5. The Fig. 5(a) displays the 2D layout and Fig. 5(b) depicts the 3D layout of designed filter.

4. COMPARISON OF LUMPED ELEMENT & MLIN BASED LOW PASS FILTER

This section presents the comparison between two types of designed LPFs i.e. one is MLIN based LPF and other one is lumped element based LPF. The scattering parameters are obtained using ADS software for comparison results. Fig. 6 shows the simulation results of designed low pass filters and Fig. 7 depicts the comparison between both filter types.

The S-parameter simulation results clearly depict that S_{11} is -3.730 dB at 4GHz in case of MLIN based structure and S_{11} is -3.094 dB in case of lumped element based structure, so it is clear from the comparison that results are similar and MLIN is preferable because of its simple design and real time fabrication. Also S_{21} for MLIN filter is -3.041dB and -2.928 dB for the lumped element based filter. The flat response after 4GHz is also similar for both cases however the response of MLIN based LPF is sharper compared with lumped elements based LPF. In Fig. 7. The stopband ripples are less in lumped elements based LPF as compared to MLIN based LPF, but it does not affect the performance of filter and this is not required because of out of intended band of frequency.

Although results of both designs are similar but the lumped element based design is not preferred for real time applications due to the non-ideal characteristics of the actual lumped elements which can have adverse impact on the performance of the filter and hence can deteriorate the desired performance of the microwave system.

Table 2. MLIN dimensions for Fig. 4

Tee Section		
	W_1=W_2(mm)	**W_3(mm)**
Tee1	1.2	13.3
Tee2	1.2	13.3
TL Section		
	W(mm)	**L(mm)**
TL1	1.2	16.4576
TL2	1.2	18.1160
TL3	1.2	16.4576
TL4	13.3	3.0676
TL5	13.3	3.0676

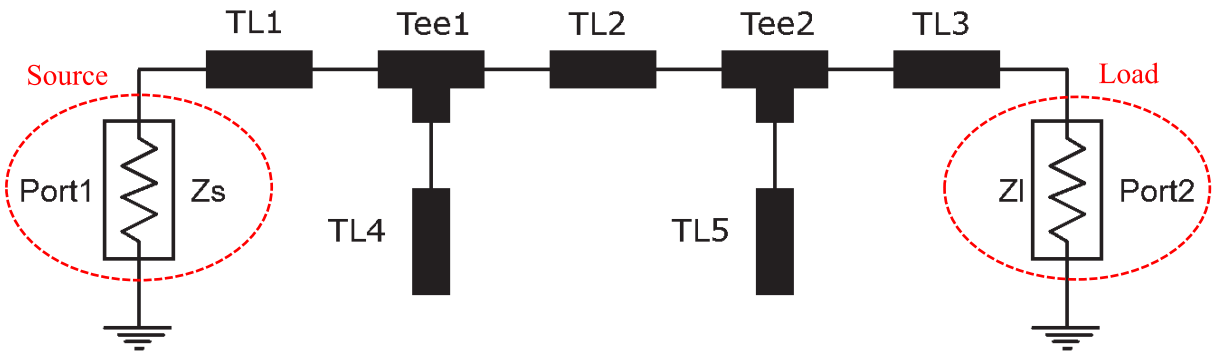

Fig. 4. Designed low pass filter based on MLIN (see Table 2 for transmission lines dimensions)

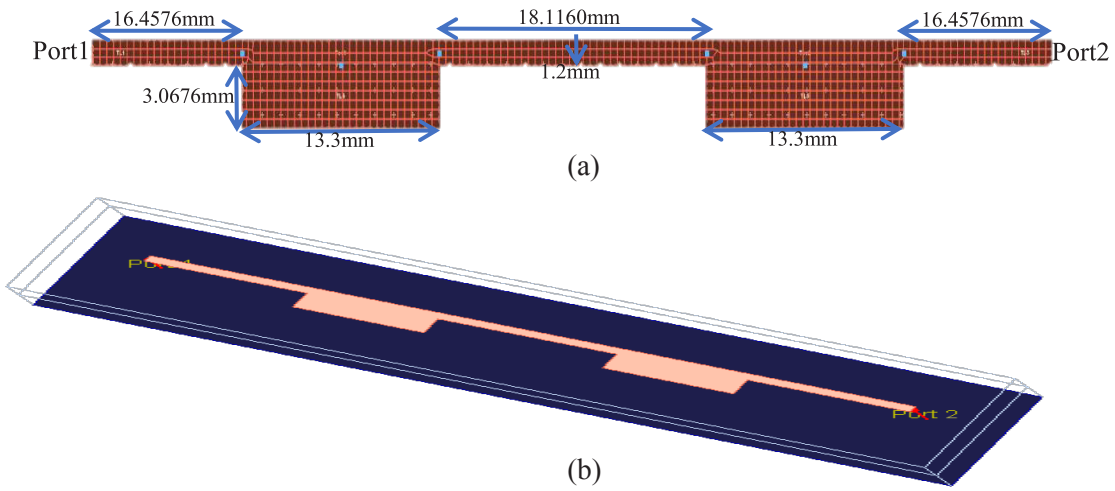

Fig. 5. (a) Microstrip LPF layout (b) 3D view of microstrip LPF layout

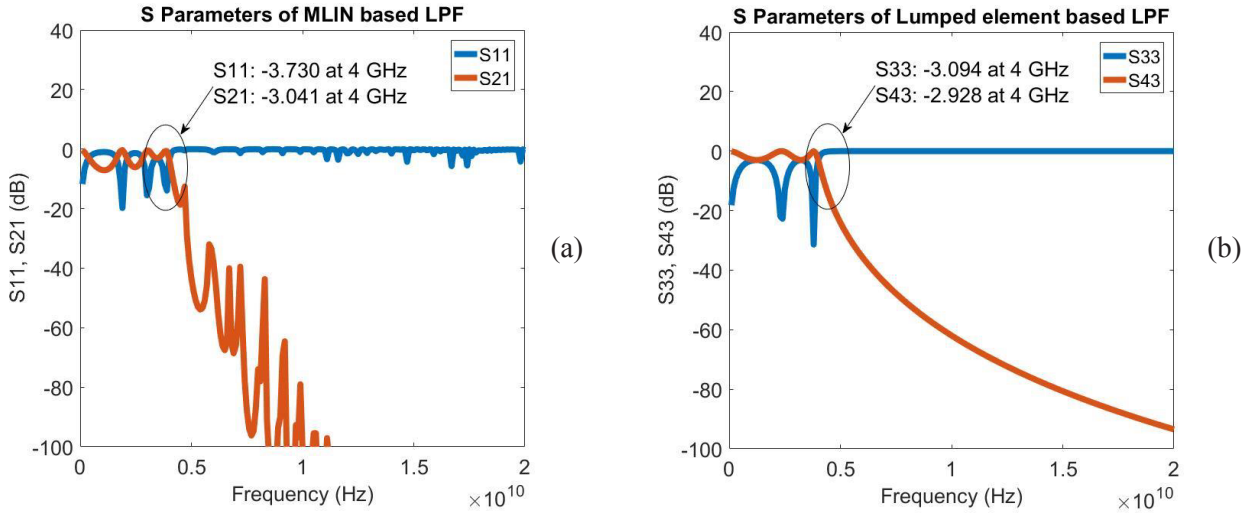

Fig. 6. S-parameters: (a) MLIN based S_{11} and S_{21} (b) Lumped element based S_{11} and S_{21}

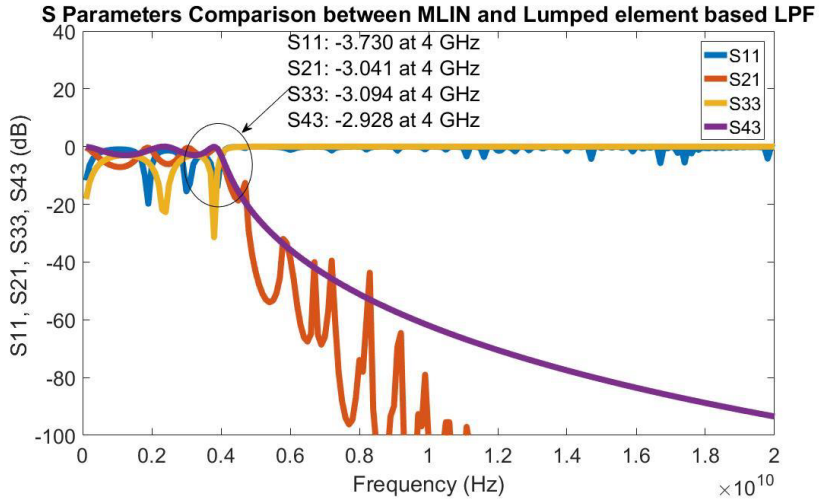

Fig. 7. Comparison between MLIN based (solid) and lumped element based (dashed) S_{11} and S_{21} (Port 1 and 2 are for MLIN filter and port 3 and 4 are for lumped element-based filter)

5. CONCLUSION

This study presents a comparison between MLIN and lumped element based low pass filters for C-band. The comparison shows that MLIN based LPF shows similar performance as ideal lumped elements based filter but the first one is more compact, simple and smaller. There is no need of surface mount elements and circuit is compressed in MLIN based LPF which add advantage for its easy manufacturing in real time applications.

6. REFERENCES

1. Worapishet A., K. Srisathit, & W. Surakamponton, Stepped imepdance coupled resonators for implementation of parallel coupled microstrip filters with spurious band suppersion. *IEEE Trans Microwave Theory and Technique,* 60: 585-591 (2012).
2. Levy R., R.V. Snyder, & G. Matthaei. Design of microwave filters, *IEEE Trans Microwave Theory and Technique*, 50: 783-793 (2002).
3. Yousaf J., M. Amin, S. Iqbal, & H. Durrani, Analysis of conducted emission measurements of dc-dc converter with load for proper filter design, *International Journal of Microwave and Optical Technology*, 10(6):464–470 (2015).
4. Pozar M., *Microwave Engineering*,4th Edition. Wiley Sons Edition, pp. 388-422.
5. Yousaf J., H. Jung., K. Kim, & W. Nah, Design, analysis, and equivalent circuit modeling of dual band pifa using a stub for performance enhancement, *Journal of Electromagnetic Engineering And Science,* 16(3):169–181 (2016).
6. Yousaf J., Z. Mehmood., W. Abbass, & K. Shehzad, Design of broadband matching network for complex reactive load using L-matching. *Proceedings of the Pakistan Academy of Sciences: A. Physical and Computational Sciences,* 54(3):243-255 (2017).
7. *Advanced Design System (ADS)*. KEYSIGHT Technologies (2017) http://literature.cdn.keysight.com/ litweb/pdf/ 5988-3326EN.pdf?id=921864.

Proceedings of the Pakistan Academy of Sciences:
A. Physical and Computational Sciences 56 (2): 55–65 (2019)

ISSN: 2518-4245 (print), 2518-4253 (online)

Pakistan Academy of Sciences

Research Article

Path Loss Model for Future Terahertz (THz) Wireless Communication Systems

Sabir Shah[1], Majid Ashraf [1], Nasir Saeed[2], Tariqullah Jan[1*], Ruhulamin Khalil[1], M. Inayatullah Babar[1], Gulzar Ahmad[1], and Syed Waqar Shah[1]

[1]Department of Electrical Engineering, University of Engineering and Technology, Peshawar, Pakistan
[2]Department of Electrical Engineering, King Abdullah University of Science and Technology, Thuwal, Makkah, Saudi Arabia

Abstract: Terahertz (THz) band is visualized to alleviate the capacity limitation and spectrum scarcity of the current wireless communication system. One of the major constraints for the realization of THz wireless communication is the high path loss. Terahertz band wireless communication have a very high molecular absorptions well as molecular noise generated by water vapor in response to attenuation of electromagnetic radiation that have a very high path loss propagation. Besides molecular losses communication in the terahertz spectrum has also spreading losses like reflection and scattering losses. Taking into account all these peculiarities of the terahertz radiation a proposed channel model based on ray approach is designed that accounts for terahertz wave propagation. An equivalent path loss model for terahertz multipath propagation based on ray tracing approach is developed and corroborated with the existing experimental results.

Keywords: THz, Multipath propagation, Ray-tracing, Transfer function, Cosine law, Refractive index.

1. INTRODUCTION

Data traffic of wireless communication is excessively increasing from the last few years because of far-flung use in society creates, consume and share of information. Now a day customers regularly demanding broader bandwidth and high data rate applications with the rapid growth of mobile and wireless networks [1]. The rapid increasing demand for mobile data rates and large transmission capacity for wireless communication stimulates the needs for high data rates and lager spectrum transmission technologies in future [2]. wireless capacity and data rates has seen increasing doubled every 18 months, leads to a distinct decision that 15-Gbps wireless data rate will be required in future after 10 years. Furthermore, wireless nomadic traffic and data rate capacities will be approaching that of communication in wire line systems [3, 4]. Terahertz (THz) spectroscopy becomes the most promising and emerging technique to study organic and bio-molecules [5]. The current systems and upcoming emerging systems including WLANs and UWB systems use bandwidths ranges from few MHz to several GHz. But unfortunately, these systems cannot be sufficient to provide enough larger bandwidth and very high data rates to satisfy the future need.

The large spectrum offered by the terahertz band unlocks gate to many applications that demands very high data-rates. Due to distinctive nature of THz band, the emerging applications supported by THz technology offered viable opportunities to many scientists and researchers working in different fields on a large range of subjects [6]. Some of the visualized applications at terahertz band are predicted already and with technology enhancement other will be arise very soon. The terahertz band will provide base for upcoming 5G

Received: June 2018; Accepted: June 2019
* Corresponding Author: Tariqullah Jan < tariqullahjan@uetpeshawar.edu.pk>

cellular networks in next generation small cells [6]. Terahertz wireless communication will enable ultra-high-speed interconnection of different links. For example, optical fiber links with tablets and laptop like devices enabling high definition video conferencing and wireless distribution of huge data in data centers [7, 8]. In defense and military fields terahertz band will provide secure communication. Terahertz technology could be used in health monitoring system to gather meaningful data about patient's health [9].

Terahertz technologies are quickly advancing and the novel development of antennas and architecture of new transceivers in THz Band communication are bringing THz spectrum closer to the reality [10]. Larger-bandwidth and short-range terahertz wireless communications have been proposed for indoor communication along their standardization within the WPAN (Wireless Personal Area network) interest group EEE 802.15 [11]. There are several efficient design and development challenges in the realization of terahertz wireless communication and networks communication perspective. THz signal path loss is the major constraints for the realization of the terahertz wireless communications [9]. Materials characterization in terahertz frequency band is becoming progressively more important due to a vast variety of applications [12]. Due to absorption attenuation of oxygen molecules and water vapors in the air, THz signal experience harsh path losses that restrict the wireless communication to few meters. Wireless communication in THz band has very high molecular absorptions as well as molecular noise generated by water vapors in response to attenuation of electromagnetic radiation. Besides molecular absorption THz signals may suffer reflection and scattering losses in multipath propagation [13].

In order to realize the wireless networks in the terahertz spectrum, it is necessary to design an equivalent model that characterizes precisely the terahertz band peculiarities, requirements and constraints to be disserted for the design and analysis of terahertz band channel. Due to high spreading and molecular absorption loss in the terahertz band the pre-existing models designed for low frequency band cannot be used for terahertz spectrum because they do not attain the behavior of terahertz band [14]. The estimation of terahertz signal path loss can be determined from the particular terahertz channel transfer function. Terahertz signal short range applications already available like body scanner and medical imaging devices operating in terahertz band are applicable up to few meters. Therefore, it is necessary to design an indoor channel path loss model for future terahertz wireless propagation.Based on ray tracing technique several channel models have been verified for mm-wave frequencies through measurements to provide accurate simulation results [15].Therefore, the main focus of the paper is to design an equivalent multi-ray model for the signal path loss measurement for wireless propagation in terahertz spectrum. Terahertz signal path loss has been anticipated on the basis of different propagation scenario.

2. TECHNIQUE AND SYSTEM DESIGN

Communication in THz band can provide an extreme increase in the bandwidth but it experiences harsh path loss, thus limiting the range of THz communications. A great amount of research has been done in the past to overcome this problem by modeling the peculiarities of THz channel. In [16], a path loss model is presented for a nano-sensors network that explains the behavior of a propagating terahertz signal over plant foliage. Channel analysis, ray-tracing simulations and different propagation scenario modules are presented in [17] for THz communications. Channel model for ultra MIMO terahertz communication systems is also anticipated in [18]. Consequently, a THz channel path loss model presented in [19] for intra-body nano scale communications. In [20] the propagation channels have been characterized for different propagation scenarios. The propagation channel key components are anticipated via direct and reflected paths. All of the literature agrees that the THz communication is highly affected by the composition of medium and the distance between the transmitter and receiver. All of the above work consider high-resolution transmission molecular absorption (HITRAN) database for molecular absorption loss. As a consequence, the modeling of a THz link and to provide appropriate tools and design guidelines is a challenging task.

Provoked by the abovementioned challenges, we present a mathematical model for Terahertz signal communication link which takes into

account the major peculiarities such as spreading, absorption, scattering and reflection. The equivalent path loss model for THz signal propagation is designed and simulated for line of sight scenario. We have used Friis formula and analyzed the impact of spreading loss and molecular absorption on the path loss. Reflection coefficient for smooth surfaces is characterized by Kirchhoff's scattering theory and Rayleigh roughness factor. Similarly scattering from rough surfaces are characterized by modified Beckmann-Kirchhoff's scattering theory.

For validation of our proposed model for signal path loss, the experimental measurements conducted in an office of *5.2m ×2.75m × 2.25m* walls dimensions [21] are used. All walls and ceiling are made of concrete and covered by plaster. The transmitter T_x is located just beneath the ceiling and the receiver R_x is placed in the middle of the office. For short range communication, ray tracing is the efficient technique for computing LoS, reflection and scattering components in multipath signal propagation. Case-1 is considered when there is only line of sight propagation between transmitter T_x and receiver R_x as given below in Fig. 1.

Case-2 consider terahertz signal reflection scenario in non-line of sight propagation. THz signal reflection from wall and table are considered as shown in Fig. 2.

In case-3 scenario no line of sight propagation available between T_x and R_x as shown in Fig-2. Terahertz signal scattering from rough surface of wall made of plaster and both scattering and reflection from smooth and rough surfaces of table and wall are also considered in Fig. 3.

3. LINE OF SIGHT PROPOAGATION

The channel transfer function CTF of a fixed channel when an electromagnetic signal in terahertz band travel over distance r between stationary transmitter and receiver, when there is direct path or line-of-sight communication can be represented in equation (1) as

$$H^{L.Sight}(f) = H(f).e^{-j2\pi ftL.sight} \quad (1)$$

In equation (1), f is frequency, $t^{L.sight}$ is the arrival time of terahertz signal when there is line of sight propagation at distance d between transmitter and receiver, and is given as:

where c is the light speed $c=3x10^8$ m/s the transfer function H(f) of the channel for terahertz signal line of sight propagation can be defined as the addition of both signal spreading losses

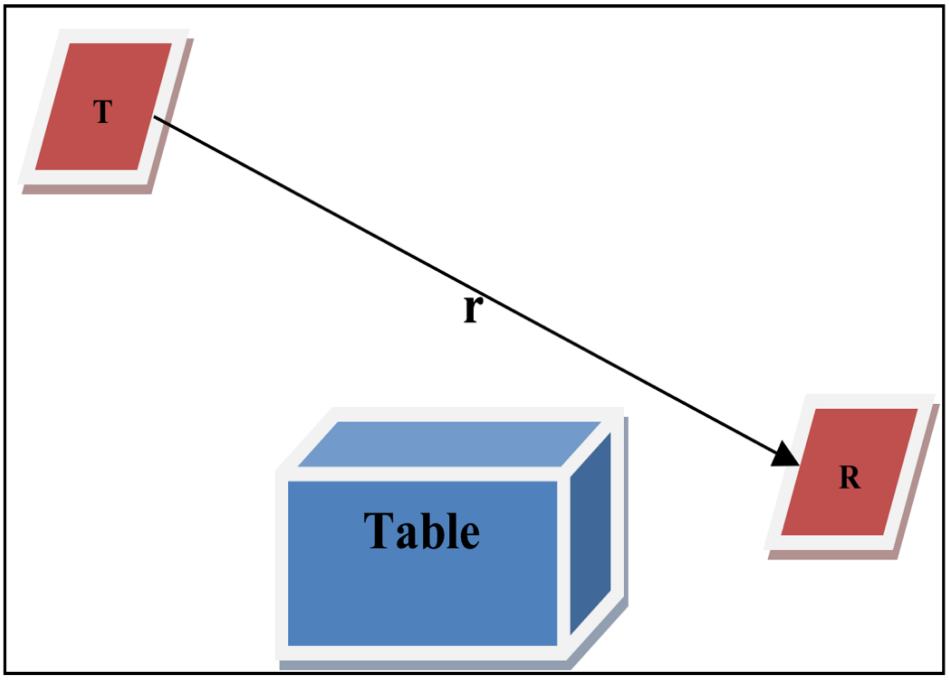

Fig. 1. THz Signal LoS Propagation Scenario

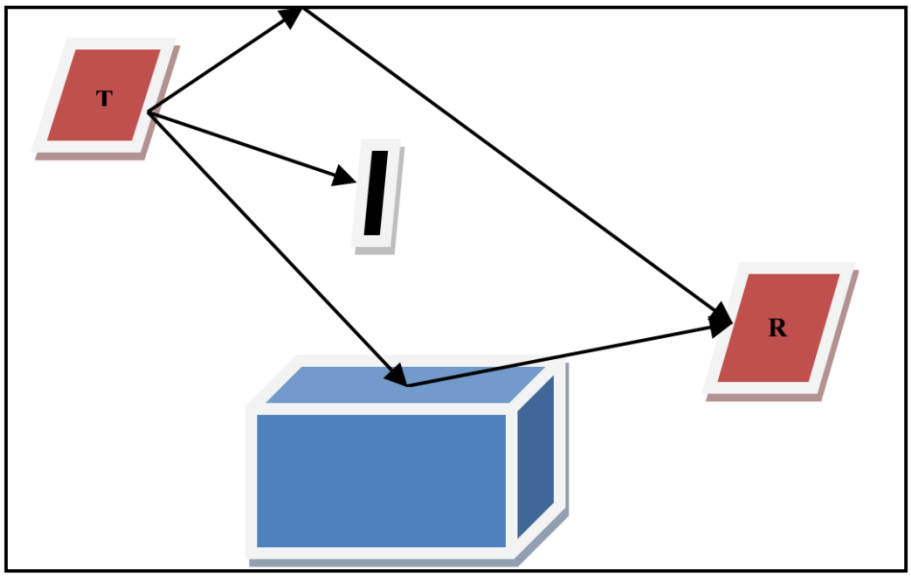

Fig. 2. THz Signal Reflection Scenario

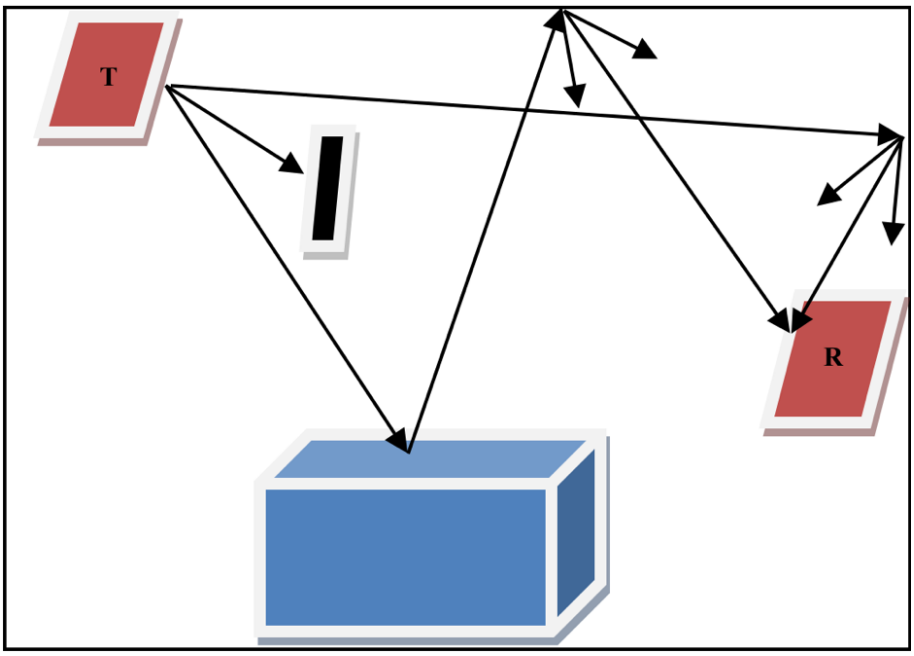

Fig. 3. THz Signal Scattering and Reflection Scenario

and atmospheric absorption losses represented in equation (2) as:

$$H(f) = H^{spread}(f).H^{abs}(f) \quad (2)$$

where $$H^{spread}(f) = \frac{c}{4\pi.f.d} \quad (3)$$

and $$H^{abs}(f) = e^{\beta(f_s)d} \quad (4)$$

Where ß is the molecular and atmospheric absorption coefficient at frequency f_s. The atmospheric loss of terahertz signal based on medium transmittance ψ can be determined with the help of Beer-Lambert law as

$$\psi(d, f_s) = \frac{P_i}{P} = e^{\beta(f_s)d} \quad (5)$$

The atmospheric attenuation coefficient ß depends upon the composition of mixture of medium gasses. Assuming office air as standard that is mainly composed of nitrogen 78%, oxygen 21% dust particles and water vapors 1%, the atmospheric attenuation coefficient ß can be determined as

$$\beta(f_S) = \sum_g \beta^g(f_S) = \beta^{NO_2}(f_S) + \beta^{O_2}(f_S) + \beta^{H_2O}(f_S) \quad (6)$$

The molecular absorption coefficient of a medium for transmitting signal having frequency f_s depends upon temperature, pressure and medium composition of the molecules. Molecular absorption coefficient can also be represented as

$$\beta(f_S) = N\eth^a(f_S) \tag{7}$$

Where ð is the absorbing species cross sectional area and N represents the number these species. An indoor medium absorbing molecules normal abundance can be predicted in high resolution transmission molecular absorption database HITRAN [22]. Dry air integrant natural abundances should be investigated by using water vapors volume mixing ratio. The water vapors volume mixing ratio is calculated with saturated water vapor partial pressure p^w as

$$p^w = 6.1121(1.0007 + 3.46 \times 10^{-6}p).\exp\left(\frac{17.502T}{240.97+T}\right) \tag{8}$$

So, water vapor volume mixing ratio in presence of relative humidity is given by

$$\mu_{water} = \frac{\omega}{100}.\frac{p^w}{p} \tag{9}$$

The saturated water air Atmospheric attenuation coefficient because of these gases, dust particles and water vapors in the air can be found in detail in [23]. Also, the channel transfer function for terahertz signal molecular absorption loss in equation (2) can be determined by

$$H^{abs}(f) = e^{\beta(f_S)} \tag{10}$$

4. REFLECTING SIGNAL

Terahertz Band Electromagnetic waves suffer reflection losses when reflected from rough surfaces. These reflection losses are dependent upon the shape; roughness and surface material on that electromagnetic signal have been reflected. The transfer function of the frequency dependent reflected Terahertz signal with reflected coefficient R(f) is defined in equation as:

$$H_{Ref} = R(f).A^{Abs}(f)$$

$$H_{Ref} = \frac{c}{4\pi.f.(r_1+r_2)}.e^{\beta(f_S)d}.R(f).e^{-j2\pi f\tau_{Ref}} \tag{11}$$

Here in equation (11), r_1 and r_2 is the incident and reflected path length between transceivers, and τ_{Ref} represents terahertz signal arrival time from transmitter to receiver and can be determined as:

$$\tau_{Ref} = \tau_{LoS} + \frac{(r_1+r_2-d)}{S} \tag{12}$$

For a smooth surface the reflection coefficient R(f) can be calculated by Kirchhoff's scattering theory as:

$$R(f) = ¥(f).\rho(f) \tag{13}$$

Here ρ(f) the Rayleigh roughness factor can be calculated as follow as in [24]

$$\rho(f) = e^{-\frac{\epsilon}{2}} \tag{14}$$

Also $$\epsilon = \left(\frac{4\pi.f.\sigma.cos\theta_i}{c}\right)^2 \tag{15}$$

So, equation (14) now becomes

$$\rho(f) = e^{\frac{8\pi^2.f^2.\varphi^2.cos^2(\theta_i)}{c^2}} \tag{16}$$

In equation (16),θ_i is the incident wave angle, φ is the surface height standard deviation, ƛ denotes the speed of light and f is the terahertz signal frequency.

Table 1. Terahertz Signal Arrival at 0.3THz Frequency

S.No	Signal Type	Path Gain(dB)	Delay(ns)
1	LoS	-104.6	8.94
2	1st reflected ray	-112.1	9.14
3	2nd reflected ray	-113.4	9.77
4	3rd reflected ray	-116.7	10.01
5	1st scattered ray	-125.8	9.80
6	2nd scattered ray	-144.2	10.27
7	3rd scattered ray	-141.7	11.08

The surface reflection coefficient ¥(f)for incident terahertz signal reflection polarized with incident terahertz signal electric field perpendicular to the plan can be derived from Fresnel reflection equation ¥(f) can be derived by using reflection law

$$\theta_i = \theta_r \tag{17}$$

According to Snell's law

$$n_1 \sin(\theta_i) = n_2 \sin(\theta_2) \tag{18}$$

The reflectance for incident terahertz signal polarized with electric field becomes

$$¥(f) = \left|\frac{n_1 \cos(\theta_i) - n_2 \cos(\theta_t)}{n_1 \cos(\theta_i) + n_2 \cos(\theta_t)}\right|^2$$

$$= \left|\frac{\cos(\theta_i) - n_t\sqrt{1 - (\frac{1}{n_t}\sin(\theta_i)^2}}{\cos(\theta_i) - n_t\sqrt{1 - (\frac{1}{n_t}\sin(\theta_i)^2}}\right|$$

$$\approx \frac{\sqrt{1 - (\frac{n_1}{n_2}\cos(\theta_t)^2}}{n_1 \cos(\theta_i) - n_2\sqrt{1 - (\frac{n_1}{n_2}\cos(\theta_t)^2}}$$

$$\approx -(1 + \frac{-2\cos(\theta_i)}{\cos(\theta_i) + \sqrt{n^2 - sin^2(\theta_i)}}$$

$$\approx -\left(1 + \frac{-2\cos(\theta_i)}{\sqrt{n^2 - 1}}\right)$$

$$\cong -e^{-(\frac{2\cos(\theta_i)}{\sqrt{n^2-1}})}$$

So

$$¥(f) = -e^{-\frac{2\cos(\theta_i)}{\sqrt{n^2-1}}} \tag{19}$$

Here in equation (19),θ_i is the terahertz signal incident angle to a rough surface, can be derived from cosine law and distance between transmitter, rough surface and receiver given by

$$\theta_i = \frac{1}{2}cos^{-1}\left(\frac{r_1^2 + r_2^2 - r^2}{2r_1 r_2}\right) \tag{20}$$

5. SCATTERING SIGNAL

Electromagnetic signal in Terahertz Band suffers diffuse scattering because of their shorter wavelengths. The scattering effect increases with the roughness level. The transfer function of the channel because of scattering effect can be expressed as: Here s1 is the separation distance between receiver and scattering point, s2 denotes the distance between scattering point and receiver. τ_scatis the scattered signal arrival time at the receiver and can be mathematically defined as:

$$H^{scat}(f) = \frac{c}{4\pi.f.(s_1 + s_2)}.e^{(-j2\pi f\tau_{scat})}.S(f).e^{\beta(f_S)} \tag{21}$$

Here s_1 is the separation distance between receiver and scattering point, s_2 denotes the distance between scattering point and receiver. τ_{scat} is the scattered signal arrival time at the receiver and can be mathematically defined as:

$$\tau_{scat} = \tau_{LoS} + \frac{(s_1 + s_2 - d)}{c} \tag{22}$$

Here τ_{LoS} is line-of-sight signal arrival time from sender to receiver and d denotes separation distance between signal transmitting point and receiver. The coefficient of scattering S(f) at large angles of incident for rough surfaces is determined by the Beckmann-Kirchhoff modified theory [25] and is given in equation (23) below as:

$$S(f) = \rho_{rough}.Y(f) \tag{23}$$

In equation (23),Y(f) represents Fresnel coefficient for scattered signal. The effective roughness coefficient causing scattering losses derived from [26] for rough surfaces ρ_{rough} can be determined in equation (24) as

$$\rho_{rough} = \rho_{smooth}.e^{-2k_n\varphi sin\theta_1^2} \tag{24}$$

$$\rho_{rough} = e^{\frac{8\pi^2.f^2.\varphi^2.cos^2(\theta_i)}{c^2}}.e^{-2k_n\varphi sin\theta_1^2} \tag{25}$$

In equation (25), ρ_{smooth} is known as Raleigh roughness derived from [23], $k_n = \frac{2\pi}{\lambda}$ represents wave number and φ is the standard deviation of the surface. From equation (23) the Fresnel scattering coefficient Y(f) is given by

$$Y(f) = -e^{-\frac{2\cos(\theta_i)}{\sqrt{n^2-1}}} \tag{26}$$

Where θ_i is the incident angle and is can be calculated from cosine law, by known distance between signal transmitting and receiving point and scattering point, and expressed in equation (27) as below

$$\theta_i = \frac{1}{2}cos^{-1}\left(\frac{s_1^2 + s_2^2 - d^2}{2s_1.s_2}\right) \tag{27}$$

Considering both reflection and scattering in non-line of sight propagation of terahertz signal through the channel, the transfer function becomes

$$H(f) = H^{scat}(f).H^{ref}(f) \tag{28}$$

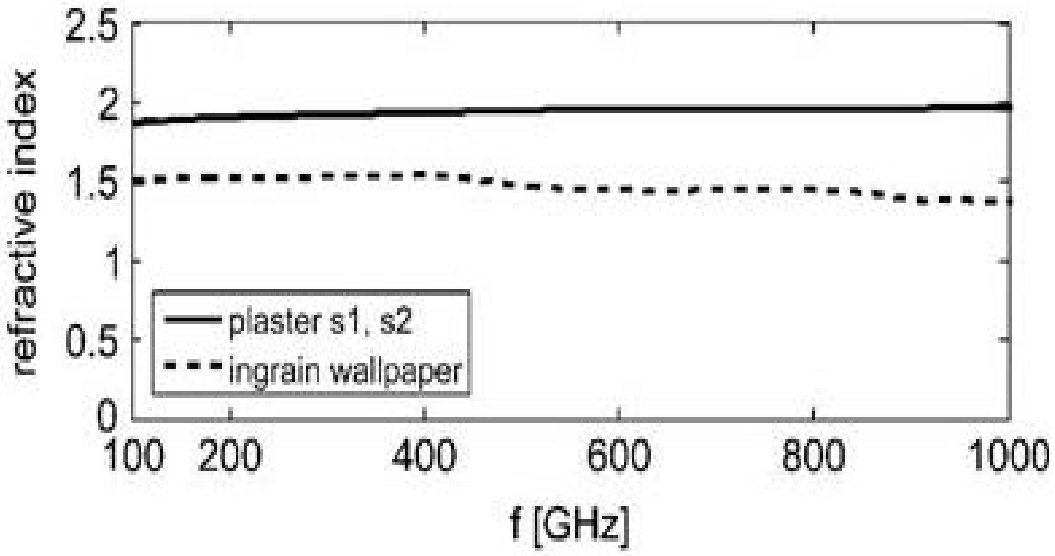

Fig. 4. Material Refractive index at THz signal

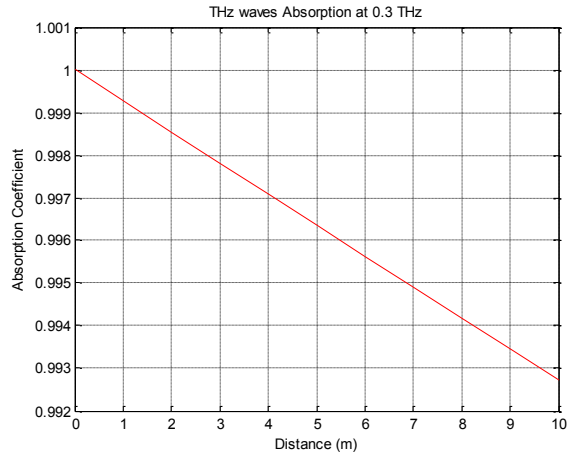

Fig. 5. Terahertz Waves Absorption Coefficient

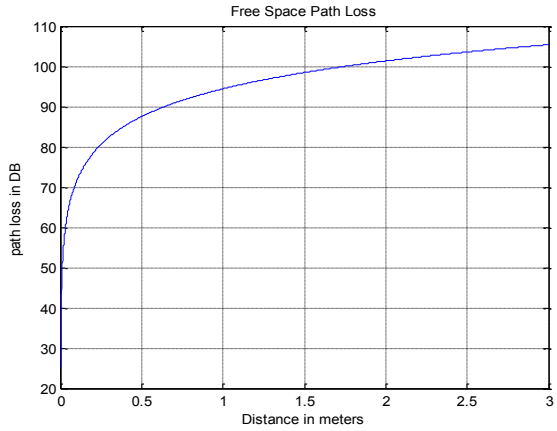

Fig. 6. Free space Path Loss in LOS Propagation

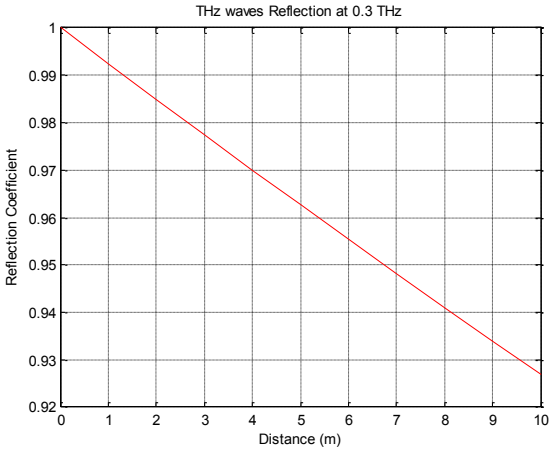

Fig. 7. THz waves reflection Coefficient

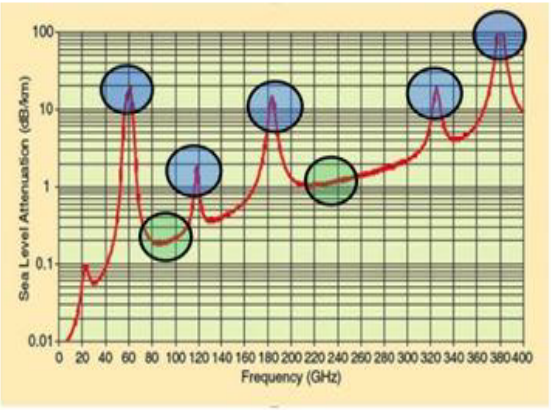

Fig. 8. Electromagnetic waves Absorption Attenuation

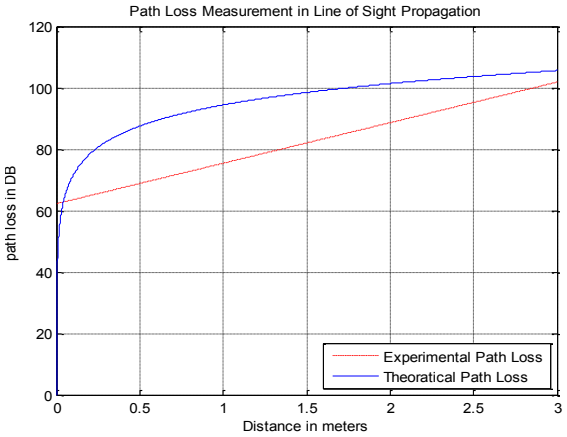

Fig. 9. THz signal LOS Path Loss Measurement

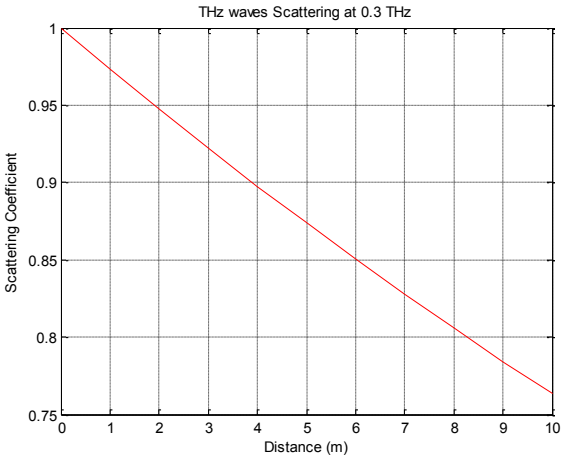

Fig. 10. THz waves scattering coefficient from rough surface

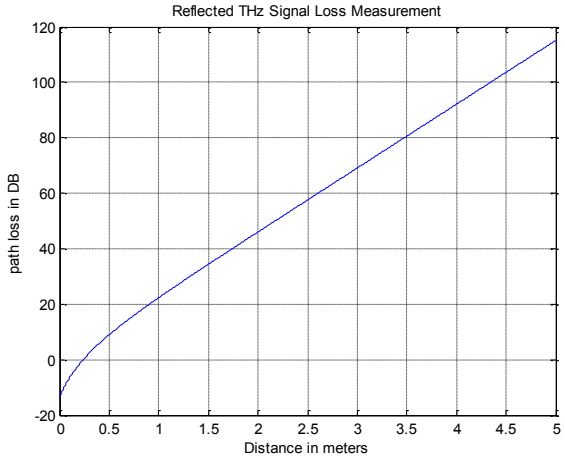

(a) Reflection loss

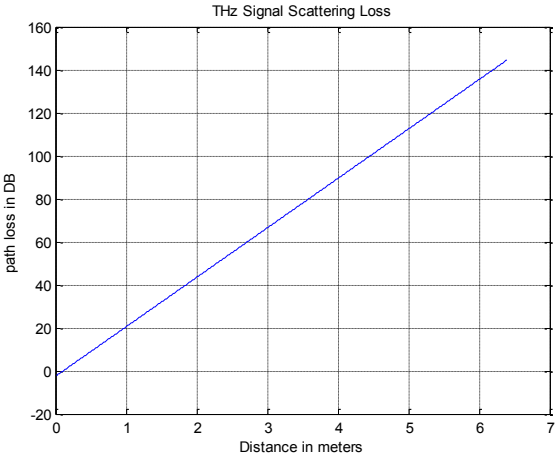

(b) Scattering loss

Fig. 11. THz Signal NLOS Path Loss Measurement

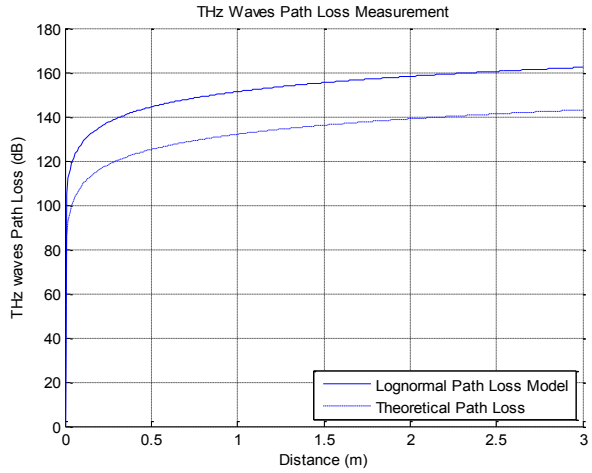

Fig. 12. Scattered THz Signal Path Loss Measurement

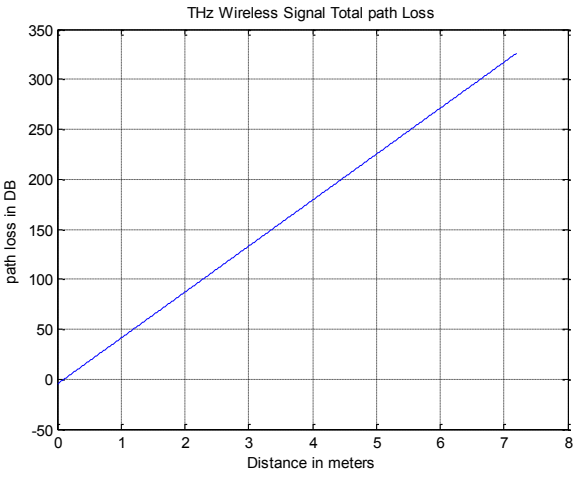

Fig. 13. THz signal Reflection and Scattering Loss

6. EQUIVALENT PATH LOSS MODEL

Now the propagation channel path loss model based on ray tracing approach that combine all the measurements of signal spreading losses, losses due to atmospheric absorption and water vapors in the atmosphere, losses due to signal scattering and reflection through different smooth and rough surfaces of table and wall as well as both scattering and reflection losses of electromagnetic signal in the Terahertz Band is proposed. Combining all the designed models about atmospheric molecular absorption losses, scattering losses and reflecting losses, a multi ray model for the ith-frequency sub-band is developed in (29) that addresses the peculiarities of the Terahertz Band.

$$H^{Eq}(f) = H^{L.sight}(f) + H^{sca}(f) + H^{ref}(f) \qquad (29)$$

7. VALIDATION OF THE PATH LOSS MODELS

Our proposed multi ray model for the measurement of terahertz signal path loss is demonstrated with the existing simulated experimental results. The experimental results simulated in [27] including type of terahertz signal at 0.3 THz arrival path, delay and path gain are outlined in Table 1. Experiment-1 is conducted for direct or line-of-sight transmission path between transmitter Tx and receiver R_x at 3m distance. While in experiment-2 no Line-of-Sight propagation between transmitter T_x and receiver R_x or terahertz signal multiple arrival paths are considered

8. RESULTS AND DISCUSSION

Terahertz signal spreading occurs by signal scattering due to collision of incident terahertz signal from smooth and rough surfaces of table and walls of indoor office channel. The free space path losses due to THz signal spreading are simulated for 3m distance between transmitter and the receiver. The absorption coefficient for THz waves propagating in the atmospheric medium are at 0.35 THz frequency at 10 m distance are simulated and is shown in Fig. 5. The distance between transmitter and reflection point is r_1 = 3.3m, reflection point and receiver distance is taken 1.7m for simulating reflection losses. Since walls and ceiling are made up bricks covered with plaster. The refractive index of plaster for 1THz colliding signal is measured 1.9 and for wood is 1.4 in [24]. The surface roughness σ which is the Rayleigh factor exponent is estimated 0.05mm for plaster and 0.12mm for wood by Gaussian distribution. An average refractive index for a medium can be approximated 1.6 at frequency f nearly equals mineral dust at frequencies of visible light [28]. Reflection coefficient for THz waves propagation at distance of 10 m and 0.3 THz frequencies are simulated and is depicted in Fig. 7. The scattering coefficient for scattered terahertz signal at 0.3THz frequency is measured where THz transmitter is fixed at incident angle $\theta_i=30^0$ to the signal scattering surface. The THz receiver sweep for angle range $\theta_2=0^0\ldots.90^0$. For all measurements for terahertz scattering as function of θ_2 , θ_3 is taken 0^0[3]. The distance between Terahertz signal transmitter T_x and surface scattering point s_1 = 3.8m, the scattering point and receiver Rx s_2 = 2.6m. The refractive index is dependent on frequencies and the medium material is assumed n = 2.1 and the surface height standard deviation φ is 0.088mm [29]. Terahertz signal free space path loss for 3m separation distance between transmitter and receiver is in Fig. 6. The atmospheric absorption at sea level causes additional losses to free space path loss of electromagnetic waves [30]. Terahertz signal free space path loss measurements including atmospheric attenuation given in Fig. 9 for line of sight propagation are very much equal to experimental measurement results performed in [31].

The scattering coefficient for THz wave propagation at 10 m distance and 0.3 THz frequencies are shown in Fig. 10. Terahertz signal reflection and scattering losses for non-line of sight propagation in indoor environment are shown in Fig. 11 (a) and (b) from smooth and rough surfaces of table and wall of office. The proposed theoretical model for scattering THz signal path loss is also compared with lognormal path loss model presented in [32] and is shown in Fig. 12. Terahertz Signal scattering and reflection or double reflection and scattering losses from smooth and rough surfaces is given in Fig. 13.

9. CONCLUSIONS

In this paper, the main constraints to wireless communications in the Terahertz spectrum are studied. We examined the line of sight free space path loss including attenuation losses, non-line of

sight reflection and scattering losses impact to the wireless propagation of terahertz signal. Taking into consideration these peculiarities of the terahertz wireless communication a complete channel model based on ray tracing technique is derived. We have validated our proposed channel model through simulations in MATLAB. The simulation results show that our proposed channel path loss model is more practical and useful for interference and link budget calculations in the design of indoor wireless applications at terahertz band.

10. REFERENCES

1. Nagatsuma, T. (2015, August). Terahertz communications: Past, present and future.,*40th IEEE International Conference on Infrared, Millimeter, and Terahertz waves (IRMMW-THz),* pp. 1-2 (2015).
2. Forecast, C.V., Cisco visual networking index: Global mobile data traffic forecast update 2009-2014, *Cisco Public Information*, 9 (2010).
3. Piesiewicz, R., T. Kleine-Ostmann., N. Krumbholz., D. Mittleman., M. Koch., J. Schoebei, & T. Kurner,, Short-range ultra-broadband terahertz communications: Concepts and perspectives., *IEEE Antennas and Propagation Magazine,* 49(6): 24-39 (2007).
4. Cherry, S., Edholm's law of bandwidth., *IEEE Spectrum,* 41(7): 58-60 (2004).
5. Weihao, Z., F. Lan., J. Xuan., P. Mazumder., M. Aghadjani., Z. Yang, & L. Men, Ultrasensitive dual-band terahertz sensing with metamaterial perfect absorber, In *Advanced Materials and Processes for RF and THz Applications (IMWS-AMP), 2017 IEEE MTT-S International Microwave Workshop Series on*, 1-3. IEEE, (2017).
6. Adnan. Z., K. Yang., H. Heidari., C. Li, M.A. Imran., A. Alomainy, & Q.H. Abbasi, Terahertz characterisation of living plant leaves for quality of life assessment applications, *In 2018 Baltic URSI Symposium (URSI)*. IEEE, (2018).
7. Akyildiz, I. F., D.M. Gutierrez-Estevez., R. Balakrishnan, & E. Chavarria-Reyes, LTE-Advanced and the evolution to Beyond 4G (B4G) systems, *Physical Communication*, 10: 31-60 (2014).
8. Wu. K., J. Xiao, & L.M. Ni, Rethinking the architecture design of data center networks, Frontiers of Computer Science, 6(5): 596-603 (2012).
9. Katayama. Y., K. Takano., Y. Kohda., N. Ohba, & D. Nakano, Wireless data center networking with steered-beam mmwave links, *IEEE Wireless Communications and Networking Conference (WCNC)*, 2179-2184 (2011).
10. Akyildiz, I.F., J.M. Jornet, & C. Han, Terahertz band: Next frontier for wireless communications., *Physical Communication*, 12: 16-32 (2014).
11. Kleine-Ostmann, T., & T. Nagatsuma, A review on terahertz communications research., *Journal of Infrared, Millimeter, and Terahertz Waves*, 32(2): 143-171 (2011).
12. Konrad, G, & Y. Yashchyshyn, Broadband characterization of dielectrics in sub-THz range, In *2018 22nd International Microwave and Radar Conference (MIKON)*. IEEE, (2018).
13. Moldovan, A., S. Kisseleff., I.F. Akyildiz, & W.H. Gerstacker, Data rate maximization for terahertz communication systems using finite alphabets, *IEEE International Conference on Communications (ICC)*,1-7 (2016).
14. Danping, H., K. Guan, A. Fricke., B. Ai., R. He, Z. Zhong, A. Kasamatsu., I. Hosako, & T. Kürner. Stochastic channel modeling for kiosk applications in the terahertz band, *IEEE Transactions on Terahertz Science and Technology* 7(5):502-513 (2017).
15. Priebe, S., M. Jacob., C. Jansen, & T. Kürner, Non-specular scattering modeling for THz propagation simulations, *Proceedings of the 5th IEEE European Conference on Antennas and Propagation (EUCAP)*, 1-5 (2011).
16. Priebe, S., M. Kannicht., M. Jacob., & T. Kürner, Ultra-broadband indoor channel measurements and calibrated ray tracing propagation modeling at THz frequencies, *Journal of Communications and Networks*, 15(6): 547-558 (2013).
17. Armita, A., A. Davy., B. Jennings, & C. Brennan, An initial path-loss model within vegetation in the THz band, In *Antennas and Propagation (EuCAP), 2015 9th European Conference on*. IEEE pp, (2015).
18. Ke. G., B. Ai., B. Peng., D. He., X. Lin, L. Wang., Z. Zhong, & T. Kürner, Scenario modules, ray-tracing simulations and analysis of millimetre wave and terahertz channels for smart rail mobility, *IET Microwaves, Antennas & Propagation,* 12(4): 501-508 (2017).
19. Chong, H., J.M. Jornet, & I. Akyildiz, Ultra-Massive MIMO Channel Modeling for Graphene-Enabled Terahertz-Band Communications, *In 2018 IEEE 87th Vehicular Technology Conference (VTC Spring)*, 1-5. IEEE, (2018).

20. Hadeel, E., M.R. Shubair., J.M. Jornet, & P. Johari, Terahertz channel model and link budget analysis for intrabody nanoscale communication, *IEEE transactions on nanobioscience* 16 (6) 491-503: (2017).
21. Piesiewicz, R., C. Jansen., D. Mittleman., T. Kleine-Ostmann., M. Koch, & T. Kurner, Scattering analysis for the modeling of THz communication systems, *IEEE Transactions on Antennas and Propagation*, 55(11): 3002-3009 (2007).
22. Jansen, C., S. Priebe., C. Moller., M. Jacob., H. Dierke., M. Koch, & T. Kurner, Diffuse scattering from rough surfaces in THz communication channels., *IEEE Transactions on Terahertz Science and Technology*, 1(2): 462-472.
23. Rothman, L.S., I.E. Gordon., A. Barbe., D.C. Benner., P.F. Bernath., M. Birk, & K. Chance, The HITRAN 2008 molecular spectroscopic database., *Journal of Quantitative Spectroscopy and Radiative Transfer,* 110(9-10): 533-572 (2009).
24. Beckmann, P, & A. Spizzichino, The scattering of electromagnetic waves from rough surfaces., *Norwood, MA, Artech House, Inc*., 511 (1987).
25. Vernold, C.L, & J.E. Harvey, Modified Beckmann-Kirchoff scattering theory for nonparaxial angles., *International Society for Optics and Photonics: Scattering and Surface Roughness II*, 3426: 51-57 (1998).
26. Piesiewicz, R., C. Jansen., D. Mittleman., T. Kleine-Ostmann., M. Koch, & T. Kurner, Scattering analysis for the modeling of THz communication systems, *IEEE Transactions on Antennas and Propagation*, 55(11): 3002-3009 (2007).
27. Molisch, A. F., Wireless communications., John Wiley & Sons., 34 (2012).
28. Marinier, P., G.Y. Delisle, & L. Talbi, A coverage prediction technique for indoor wireless millimeter waves system, *Wireless Personal Communications*, 3(3): 257-271 (1996).
29. Kandler, K., N. Benker., U. Bundke., E. Cuevas., M. Ebert., P. Knippertz, & S. Weinbruch, S, Chemical composition and complex refractive index of Saharan Mineral Dust at Izana, Tenerife (Spain) derived by electron microscopy, *Atmospheric Environment*, 41(37): 8058-8074 (2007).
30. Rappaport, T.S., J.N. Murdock, & F. Gutierrez, State of the art in 60-GHz integrated circuits and systems for wireless communications., *Proceedings of the IEEE*, 99(8): 1390-1436 (2011).
31. Sawada, H., K. Fujii., A. Kasamatsu, H. Ogawa., K. Ishizu, & F. Kojima, Path loss model at 300 GHz for indoor mobile service applications, *IEICE Communications Express*, 5(11): 424-428 (2016).
32. Afsharinejad, A. A. Davy, B. Jennings, S. Rasmann, & C. Brennan. "A path-loss model incorporating shadowing for THz band propagation in vegetation." *In Global Communications Conference (GLOBECOM), 2015 IEEE*, pp. 1-6. IEEE, (2015).

Proceedings of the Pakistan Academy of Sciences:
A. Physical and Computational Sciences 56 (2): 67-75 (2019)

ISSN: 2518-4245 (print), 2518-4253 (online)

Pakistan Academy of Sciences

Research Article

Optimization of Process Parameters using Full Factorial Design in Injection Molding of Polypropylene

Shakir Azim*, Sahar Noor, Rehman Akhtar , Tufail Habib, and Mubashir Hayat

Department of Industrial Engineering, University of Engineering and Technology, Peshawar

Abstract: Injection molding process is widely used in industry for manufacturing of various kinds of products made of plastics. It is a fundamental polymer processing practice in plastic industry. In this process various optimization techniques are used to improve the product quality. Process parameters play a vital role in injection molding and have an effect on the worth of the product made up of different plastics. Along with molding conditions,plastic properties have a significant impact on the quality of plastic products in injection molding and optimised parameters enhance the quality of product and shrink the cycle time. In this research paper, the optimization of process parameters is implemented for polypropylene to manufacture a pharmaceutical cup. The technique applied for optimizing molding parameters is full factorial design. Analysis of Variance (ANOVA) technique is applied in Minitab software to find the significance of each parameter. Selected parameters like total time, injection pressure, injection temperature and mould's temperature are taken and analyzed during experimentation and best applicable combination of these parameters is set to get the desired results. The results obtained after performing experiments suggest that total time and mould temperature are significant factors in shaping the product's quality.

Keywords: Polypropylene, Injection Molding Process, Parameters Optimization, Surface Roughness, Full Factorial Design.

1. INTRODUCTION

Due to the global competition, industry is striving to produce high quality products to end customers. Industries are using different approaches to fulfil the market demands. Injection molding is one such industry that is using injection molding process to manufacture quality products. Industrialists use plastic injection molding machines with various kinds of plastics such as polyethylene, polyvinyl chloride, polypropylene, high-density polyethylene, polystyrene, and other engineering plastics etc. The foremost advantage of injection molding is its ability to mass production and once the setup cost is being paid then manufacturing in injection molding per unit is extremely low. Scrape rates in injection molding is very less as compared to traditional machining like CNC machining cut large amount of extra material which is wasted. In injection molding repetitiveness is a big advantage in which identical parts can be produced in large numbers. To smooth the progress of molding process, components to be injection moulded are very watchfully designed. And for this, material of mould, material of parts, desired features and shapes of components and characteristics of moulding machine needs to be considered. The versatility and usefulness of injection molding is enhanced by design considerations. Apart from material characteristics, the optimization of process parameters is a key to high quality products in this industry.

2. LITERATURE REVEIW

Several researchers worked on injection molding machine and proposed different methods to optimize its parameters for different products made up of different materials. M. V. Kavade and S. D. Kadam [1] deployed Taguchi method for optimization of parameters of injection molding machine for polypropylene and considered barrel temperature, holding time, injection speed, coolant flow rate, injection pressure, cooling time, and

Received: October 2018; Accepted: June 2019
* Corresponding Author: Shakir Azim <Shakirazim3070@gmail.com>

holding pressure as input variables for response variable that is productivity. Hyoungjun Moon et al. [2] studied parameters of injection molding of display front panel by using Taguchi method and analyzed packing pressure and cooling pattern to solve deflection problem in panels. Subodh Tomar et al, [3] performed research on parametric process of injection molding using a H200mk Grade of polypropylene. Molding parameters considered and analyzed by these researchers were injection temperature, holding pressure, injection speed, injection pressure, cooling time, holding time and polypropylene tensile property was considered as a response variable.

Likewise, Hasan Oktemand and co-researchers [4] used Taguchi optimization method for a thin-shell part in unearthing plastic injection molding process parameters. Different parameters were tried to reduce the warpage problem. This problem is linked to shrinkage variation dependent of unlike parameters during manufacturing of thin-shell plastic tools. Rajalingam et al, [5] determined best possible molding parameters by deploying two level factorial design with center points. They considered injection speed, mould temperature, injection pressure that significantly effects asking price of production, demand of production, quality, and productivity in injection molding industry.

Babur [6] in plastic injection molding helped in determining the influence of two parameters such as mould materials and shot parameters on mechanical characteristics of Acrylonitrile-butadiene-styrene (ABS). Factors taken into consideration were melt temperature, injection pressureand cooling time. And for mechanical properties of ABS, Taguchi method was deployed to estimate the signal to noise ratio. The result of parameters on mechanical properties was established using Analysis of variance. Kuo Ming et al, [7] did work on the effects of processing parameters on lenses optical quality at some stage in injection molding process. And they revealed that the key process parameters that ha an impact on the waviness of surface is a temperature called melt temperature, followed by injection pressure, mould temperature and packing pressure.

Wei Guo et al. [8] did research on the influence of processing factors on molding process in microcellular injection molding. And for decreasing advance dimensional accuracy and weight of plastic goods, temperature, time and gas controlling were considered. Alireza and Mohammad [9] carried out research on optimization in plastic injection molding process with the help of IWO algorithm and statistical methods. They were successful in finding the impacts of different process parameters or treatments in the form of packing time, melting temperature, and pressure on polystyrene (PS) and polypropylene(PP). Mustafa Kurt et al, [10] did experimental analysis of plastic molding, in which the they investigated the effect of mould temperature and the pressure inside cavity on quality of end products. Full factorial design is a common experimental designs which was used for warpage values consequent to training data [11]. Similarly, various researchers have researched on the process parameters of injection molding machine for different materials and used new techniques.

Till date, significant research work has been carried in the area of injection molding process. However, research studies on specific plastic materials are scarce. Local manufacturers in Peshawar (Pakistan) were facing surface roughness issue in products of polypropylene and there was no optimization technique applied on it to resolve the issue. Polypropylene is a thermoplastic polymer and is widely used in packaging and labelling, plastic parts, textile and reusable containers of different types and automotive components. It is unusually resistant to many acids and bases. In this research, parametric optimization of injection molding machine is done for polypropylene. For this material, four input variables such as, injection temperature, total time, mould temperature, and injection pressure are used to find the response variable. In the factorial design, best feasible grouping of the four parameters is obtained for a product fabricated of polypropylene having superior surface smoothness that can be utilized in local industry for better quality products.

The rest of the paper is ordered as follows: Section 3 depicts the proposed method while section 4 presents the design and manufacturing of mould. Section 5 illustrates the experimental setup in this study. Section 6 presents the results obtained from the experiments and section 7 discusses the significance of the approach and the interpretation

of the results obtained. In the end, Section 8 and 9 sum up and concludes the paper.

3. MATERIALS AND METHODS

In this study full factorial design is used to study the effects of several factors that must have a certain response. During experiments, varying levels of factors and their interactions are used at the same time to get the results.

3.1. Selected Parameters

In this research, four parameters are selected in our analysis. Those four parameters are injection temperature, injection pressure, mould's temperature and total time. Next, three levels of each variable are considered, which resulted in eighty one (81) runs (number of experiments). Surface roughness acted as a response or reaction variable. And for selected input variables and a response variable, Analysis of Variance (ANOVA) technique is deployed for testing. ANOVA is being applied in Minitab specifically to find the significance of each parameter and its relationship with other parameters.

Cutting tool speed and feed of the cutting tool are not considered as process parameters in the ANOVA because they are used in the manufacturing of mould design and not used in the production of plastic products.

3.2. Multilevel Factorial Design

Full factorial design technique is used to get the required experiments that are being performed and is shown in Table 1.

In Table 1, the factors 4 means that there are four factors and the experiments are run for 81 times. Replicates 1 propose that every experiment or test will be done only once and for each parameter, numbers of levels taken into consideration are three. Four factors and levels of each factor is shown in Table 2.

The required determined experiments using full factorial design were executed on vertical plastic injection molding machine. Surface roughness tests were carried out on a device called surface roughness tester. Appendix 1 provides the details regarding input variables and surface roughness. After getting surface roughness values from products using surface roughness tester for conducted experiments, Analysis of Variance is applied in Minitab software to determine significant factors from the above declared four factors i.e. injection temperature, total time, mould temperature and injection pressure. On the basis of generated results from Minitab, best feasible combination of parameters/treatments is selected for this material i.e. polypropylene.

3.3. Mould Modeling & Fabrication

Mould is used when large numbers of parts are to be produced. To fulfil complete product development, mould has also been modelled and fabricated. Modeling of a mould has been done using CREO software. The objective of modelling a mould is to learn the basics of mould making, creation of mould models and to assemble the work pieces into the mould.

Table 1. MINITAB results using full factorial design

Sr. No	Full factorial design	
1	Factors: 4	Number of levels: 3
2	Total runs: 81	Replicates: 1

Table 2. Factors and selected levels

Sr. No		Level 1	Level 2	Level 3
1	Injection Pressure	45	50	55
2	Injection Temperature	190	200	210
3	Mould temperature	50	65	80
4	Total Time	40	45	50

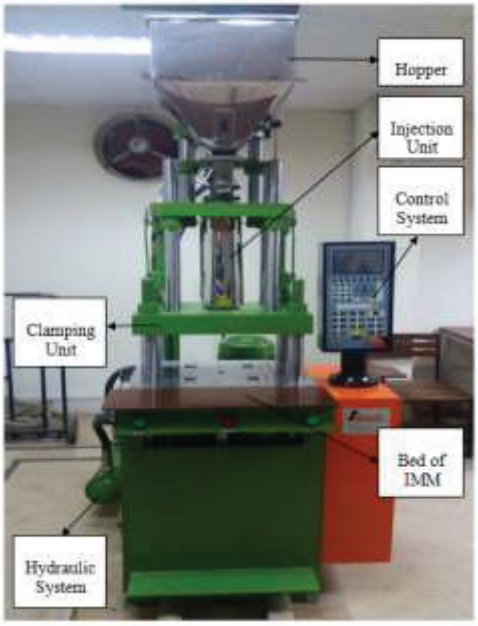

Fig. 1. Vertical plastic injection molding machine

Keeping in view the specifications and bed of injection molding machine, models of different plates are generated and then drawing of each plate is developed in CREO. The same drawings are then interacted with CNC five-axis machine through programs already generated from the drawings. Manufacturing of a mould in itself on CNC machine is a very difficult job. After programs communication with CNC five-axis machine, different process parameters are selected. Cutter diameter is taken as 20 mm while two process parameters are specifically paid attention. Cutting tool's speed is taken as 800 rpm while feed of cutting tool is taken as 100 mm/min as shown in Table 3. During removal of additional material, speed and feed of cutting tool is maintained constant as variations in speed and feed causes vibrations in various parts of a machine. The material of manufactured mould is mild steel which is generally used in market and the reason of selecting mild steel is the feasibility of this particular material in the market. Different views or phases of a mould in injection molding process can be seen in Fig. 2.

Table 3. Two process parameters and their values

Sr. No			
1	Parameter 1	Speed	800 rpm
2	Parameter 2	Feed	100 mm/min

3.4. Experimental Setup

The equipment on which parametric study is carried out is plastic injection molding machine (vertical) shown in Fig. 1. Each and every part of a machine has been labelled.

Injection molding process cycle is completed in four stages namely clamping, injection, cooling and ejection. Three stages of injection molding process have been shown in Fig. 2.

After performing experiments, picture of one of the product (Pharmaceutical cup) and surface roughness measuring tool used for measuring surface roughness of each and every product has been shown in Fig. 3.

Surface roughness taken over here is basically the arithmetic mean of the absolute values of the profile divergences or deviations from the mean bar, and it is represented by Ra.

Fig. 2. Different Phases of Injection Molding Process

Fig. 3. Surface Roughness Tester and Final Product (Pharmaceutical Cup)

4. RESULTS

The concluding results that are achieved from ANOVA using Minitab software by getting rid of all the insignificant process parameters are given in Table 4.

Referring to p-values given in Table 4 of analysis of variance, it is clear that these values are below 0.05. Hence, it is obvious that with more than 95% of confidence we can litigate that C_3 and C_4 (Mould Temperature and Total Time) are the significant factors and response variable (surface roughness) changes with these two factors. Hence, we reject the null hypothesis. The reason behind the insignificance of injection pressure and injection temperature (C_1 and C_2) is that the range between the first and the last level is very less and if injection pressure and injection temperature is taken less than the first level or greater than the final level, it will affect the response variable greatly and there will be chances of their significance.

Graph is drawn (Fig. 4) for all experiments and their corresponding surface roughness depicted in Appendix 1. It can be seen that random variation of combination of all the above mentioned parameters causes a general trend in surface roughness. Hence, increase or decrease of surface roughness of a product is random.

The maximum and minimum surface roughness that has been measured is 21.5 µm and 0.12 µm respectively and is obtained from experiment 5 and

Table 4. ANOVA Results

Analysis of Variance	
Source	P-Value
C_3 (Mould Temperature)	0.018
C_4 (Total Time)	0.012

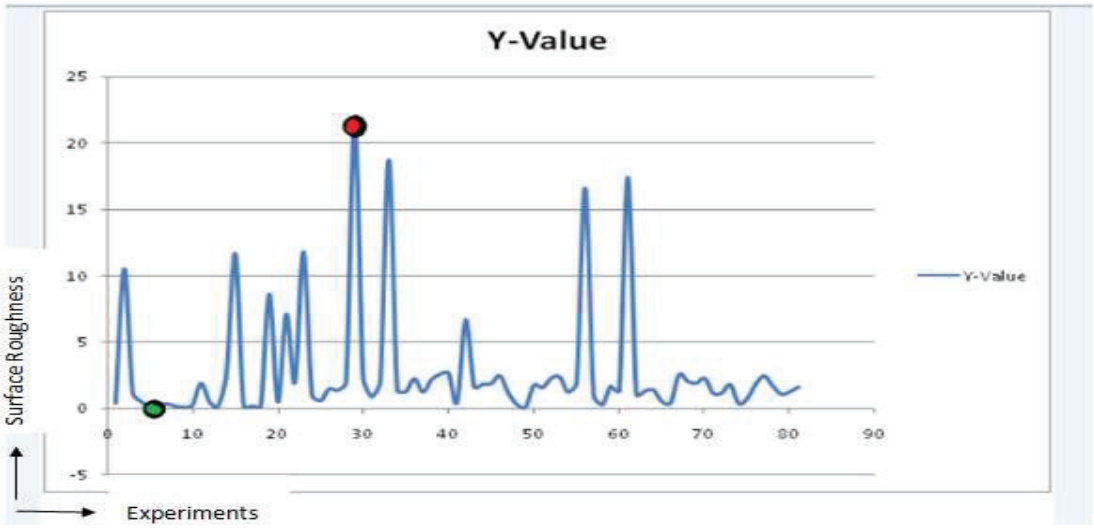

Fig. 4. Surface Roughness for the entire experiments

Table 5. The Best and worst case of process parameters and responses for polypropylene

Sr. No	Factor 1	Factor 2	Factor 3	Factor 4	Response
	Pressure (Bar)	Temperature (Ċ)	Mould Temperature (Ċ)	Total Time (Sec)	Surface Roughness (μm)
Exp 5	45	190	65	40	0.12
Exp 29	50	210	80	45	21.5

experiment 29 as shown in table 5. These values are also represented by red and green dots in Fig. 4.

Table 5 shows the best and worst cases of combination of process parameters and the resulting response variable. It is also evident from the best and worst cases that the difference between the surface roughness values is very large. Hence research can also be carried out on effect of mould material and mould surface roughness. In this case the mould used was made of mild steel which is largely used in local industry.

5. DISCUSSION

Injection molding has always been a challenging and demanding process to produce good quality products with low cost. With stiff competition in injection molding business, deploying the trial and error approach to establish the optimal process parametersis not good enough. Local manufacturer's in plastic injection molding (PIM) industry was facing problems of surface roughness and no design process and optimization techniques was applied to address the issue. As a consequence, product waste percentage was very high and final products quality was not up to the mark.

Setting of process variables and their optimization is very vital to enhance the worth of the moulded products. However, optimization of input parameters is not a simple task, because it usually depends on various factors, such as product design, mould surface finish, the molding machine and molding material etc [12]. Minute modifications of molding conditions may enhance a considerable jolt to the plastic's features. Several experimental research works were carried out to study the impact of the injection molding process parameters on the features of moulded products and their respective defects [13].

In this study or research paper, four parameters are selected for the analysis while surface roughness acted as a response variable. The experiments were performed on injection molding machine(vertical machine). After getting surface roughness values for each and every experiment, analysis of variance is applied in Minitab software to determine significant factors from the four selected input factors i.e. Temperature, time, pressure, and mould temperature. After interpretation of results obtained from Minitab, best feasible blend of input parameters is chosen for polypropylene. While performing the required number of experiments best and worst cases of surface roughness were achieved (as shown in Table 4). Furthermore, it can be observed that the surface roughness varied with the variation of these parameters and mould temperature and total time are the significant process parameters during experimentation.

Local industry making plastic products will benefit from the product and process development using latest tools employed in this project. It is an observation that the local industry is not using the scientific tools for their products made by injection molding process. Mould material would certainly have an impact on the mechanical properties of the products. Different mould materials behave differently during fabrication and if the quality of the mould cavity is not good enogh during manufacturing, it would certainly leed to quality problems during production of plastic products.

6. CONCLUSIONS

This research work has been conducted that aims to optimize the process parameters and position the best viable integration of selected process parameters. From the results in ANOVA , it has been observed that mould temperature and total time are the significant process parameters (shown in Table 4) and the minimum surface roughness value that has been measured for these parameters is 0.12 (shown in Table 5). Results showthat the best likely combination of parameters for polypropylene's with better surface smoothness is 45 bar, 190 Ċ, 65 Ċ, 40

sec for pressure, temperature, mould temperature and total time respectively (Experiment 5).

As most of the moulds used locally are imported from different countries which increase the final cost of plastic products, that's why mould designed and manufactured locally will benefit local customers, suppliers and manufacturers with minimum cost. So reducing the burden on foreign exchange by indigenous product development locally.

7. FUTURE PROSPECTS

Till date, a number of researchers worked on injection molding machine and large number of parameters were optimized to obtain a product with good quality and reasonable cost. Furthermore, future research work can be carried out by changing the mould material and its impact on surface finish of final product using injection molding machine. A comparative analysis of using other mould materials , its design and manufacturing process can be carried out for optimized results.

Likewise, material of plastic products might also be changed to find the impact of optimization on the parameters of the molding machine. Research can be taken into consideration in future related to bio-degradable polypropylene as it can be bio-degradable, if enhance bio decompositions (EBD).

8. ACKNOWLEDGMENT

This research work was supported by University of Engineering and Technology Pewshawar, Pakistan.

9. REFERENCES

1. Kavade. M, & S. Kadam. Parameter Optimization of Injection Molding of Polypropylene by using Taguchi Methodology, *IOSR Journal of Mechanical and Civil Engineering (IOSR-JMCE),* 4(4): 49-58 (2012).
2. Moon, H. Application of Taguchi Method in Parametric Study of Injection Molding of Display Front Panel, *Journal of Materials Science and Engineering,* 1(1A): 123 (2011).
3. Tomar. S. S., A. K. Sinha, & A. Shrivastava. Parametric Study of Injection Moulding Using Polypropylene H200mk Grade, *International Journal of Science*, 2(3): (2016).
4. Oktem. H., T. Erzurumlu, & I. Uzman .Application of Taguchi optimization technique in determining plastic injection molding process parameters for a thin-shell part, *Materials & design,* 28(4): 1271-1278 (2007).
5. Sokkalingam, R. Determining Optimal Moulding Process Parameters by Two Level Factorial Design with Center Points. in *Institute of Applied Statistics, Sri Lanka. Institute of Applied Statistics. Sri Lanka* (2011).
6. Ozcelik. B., A. Ozbay, & E. Demirbas. Influence of injection parameters and mold materials on mechanical properties of ABS in plastic injection molding, *International Communications in Heat and Mass Transfer,* 37(9):1359-1365 (2010).
7. Tsai, K. M., C.Y. Hsieh, & W.C. Lo. A study of the effects of process parameters for injection molding on surface quality of optical lenses*, Journal of materials processing technology,* (7): 3469-3477 (2009).
8. Guo. W., H. Mao., B. Li, & X. Guo. Influence of Processing Parameters on Molding Process in Microcellular Injection Molding, *Procedia Engineering,* 81: 670-675 (2014).
9. Akbarzadeh. A, & M. Sadeghi. Parameter study in plastic injection molding process using statistical methods and IWO algorithm, *International Journal of Modeling and Optimization,* 1(2): 141 (2011).
10. Kurt. M., O. Saban., Y. Kayanak, & G. Atakok. Experimental investigation of plastic injection molding: Assessment of the effects of cavity pressure and mold temperature on the quality of the final products, *Materials & Design,* 30(8): 3217-3224 (2009).
11. Ozcelik. B. & T. Erzurumlu, Comparison of the warpage optimization in the plastic injection molding using ANOVA, neural network model and genetic algorithm*. Journal of materials processing* technology, 171(3): 437-445 (2006).
12. Shen. C., l. Wang, & Q. Li. Optimization of injection molding process parameters using combination of artificial neural network and genetic algorithm method, *Journal of Materials Processing Technology,* 183: 412– 418 (2007a).
13. Tang, S.H., Y.J, Tan., S.M, Sapuan., S, Sulaiman, & N. Ismail. The use of Taguchi method in the design of plastic injection mould for reducing warpage, *Journal of Materials Processing Technology,* 182: 418-426 (2007).

Supplementary Data

APPENDIX 1. Combination of four process parameters and response variable(surface roughness)

Sr. No	Variable 1	Variable 2	Variable 3	Variable 4	Response Variable
	Injection Pressure (Bar)	Injection Temperature (Ċ)	Mould's Temperature (Ċ)	Total Time (Sec)	Surface Roughness (μm)
1	50	200	50	45	0.45
2	50	190	50	45	10.52
3	55	190	65	45	1.23
4	45	190	80	40	0.545
5	45	190	65	40	0.12
6	55	200	50	40	0.225
7	55	210	50	50	0.38
8	50	210	65	45	0.2
9	45	210	80	45	0.13
10	50	210	65	40	0.285
11	45	210	50	45	1.91
12	55	190	65	50	0.52
13	45	210	65	45	0.21
14	55	190	50	50	2.74
15	50	200	50	50	11.675
16	55	190	80	50	0.23
17	45	210	50	50	0.22
18	55	200	65	50	0.238
19	55	200	65	45	8.62
20	55	200	65	40	0.52
21	55	190	80	45	7.125
22	55	210	50	45	1.97
23	55	210	65	45	11.79
24	45	190	50	50	1.04
25	55	200	80	40	0.6
26	45	210	80	50	1.5
27	50	210	50	40	1.4
28	55	210	80	45	2
29	50	210	50	45	21.5
30	55	210	65	40	2.37
31	45	200	80	40	0.9
32	50	190	80	40	2.09
33	50	200	50	40	18.693
34	50	190	80	45	1.39
35	45	210	65	40	1.29
36	50	190	50	40	2.27
37	50	190	50	50	1.27
38	50	210	80	50	2.2
39	55	200	80	50	2.6

40	55	200	50	50	2.67
41	45	190	65	50	0.5
42	45	200	50	45	6.71
43	55	210	80	40	1.65
44	45	190	80	45	1.85
45	55	200	80	45	1.89
46	50	200	65	40	2.49
47	45	200	80	50	1.19
48	55	210	65	50	0.34
49	50	210	65	50	0.14
50	50	190	65	40	1.77
51	50	190	80	50	1.59
52	55	190	65	50	2.29
53	50	190	80	40	2.4
54	50	190	50	45	1.25
55	50	190	65	45	1.95
56	55	190	50	45	16.574
57	45	200	65	50	1
58	50	210	50	50	0.3
59	50	200	65	45	1.7
60	45	190	50	40	1.35
61	50	200	50	45	17.39
62	50	210	50	45	1.071
63	50	210	65	40	1.34
64	50	200	80	45	1.42
65	50	210	50	50	0.54
66	50	200	80	50	0.44
67	45	190	80	40	2.57
68	45	190	50	45	2.072
69	45	190	50	40	1.932
70	45	200	65	45	2.3
71	50	200	80	50	1.17
72	45	210	80	45	1.2
73	45	210	65	40	1.81
74	55	210	80	50	0.4
75	55	190	80	40	0.8
76	50	210	80	40	1.874
77	55	190	65	40	2.48
78	45	200	50	50	1.693
79	50	190	65	50	1.1
80	50	190	65	50	1.3
81	45	200	80	40	1.654

Proceedings of the Pakistan Academy of Sciences:
A. Physical and Computational Sciences 56 (2): 77 (2019)

ISSN: 2518-4245 (print), 2518-4253 (online)

Pakistan Academy of Sciences

Obituary

Prof. Dr. M. Ajmal Khan (1953–2019)

Vice President, Pakistan Academy of Sciences, (PAS)
&
Vice Chancellor, University of Karachi, Karachi

It is with profound grief to inform all colleagues, friends, associates and well-wishers that Prof. Dr. M. Ajmal Khan *(S.I)*, a versatile Botanist of Pakistan, Vice President, Pakistan Academy of Sciences and Vice Chancellor, University of Karachi, Karachi breathed his last on May 04, 2019 at Karachi. As one of the most highly rewarded academician and scientist of Pakistan, Prof. Dr. M. Ajmal Khan has left behind a rich harvest of sweet memories and achievements as inspiration for all those who know him.

Prof. Dr. M. Ajmal Khan joined Pakistan Academy of Sciences as Fellow in 2001. He served the Academy as Secretary: PAS Karachi Chapter from 2004-2007 as well as Vice President, PAS from 2018- May 2019.

Prof. Dr. Ajmal Khan had a distinguished career in the field of Botany. His specific research interests included Seed Dormancy, Salt Tolerance, Demography of Salt Marsh and Salt Desert Species and Evaluation of Cash-crop Halophytes. In recognition of his outstanding contributions in the field of Botany, Ecological Management of Inter-tidal, Coastal and Inland Saline Ecosystems. Prof. Dr. M. Ajmal received prestigious civil awards, including: Sitara-i-Imtiaz (2007) and Presidential Award of Pride of Performance, (2001). His others awards include Life Time Achievement Award by Pakistan Botanical Society, 2016; Distinguished Scientist of the Year, Pakistan Academy of Sciences, 2008; Gold Medal, Pakistan Academy of Sciences, 1999; 1st Position in M.Sc., University of Karachi, Pakistan.

Prof. Dr. M. Ajmal Khan was also honored with membership of various outstanding national and international bodies, including The Islamic World Academy of Sciences (IAS), The World Academy of Sciences (TWAS), Fulbright Research Fellowship, German Academy Exchange Services (DAAD), Germany, Member: Botanical Society of America, International Ecological Society (INTECOL), Life Member, Pakistan Botanical Society, Sigma Xi, USA; National Curriculum Committee, University Grants Commission.

Throughout his scientific career, Prof. Dr. M. Ajmal Khan remained a strong source of encouragement and support for his students and associated scientific community. There are no words to describe how much he will be missed. Our thoughts and heartfelt condolences go out to the family, friends and colleagues.

May ALLAH Almighty bless his soul in peace in heavens; Aameen.

Proceedings of the Pakistan Academy of Sciences:
A. Physical and Computational Sciences 56 (2): 79 (2019)

ISSN: 2518-4245 (print), 2518-4253 (online)

Pakistan Academy of Sciences

Obituary

Engr. Dr. M. Yousaf Hasan Bangash (1932–2019)

Foreign Fellow, Pakistan Academy of Sciences

Engr. Dr. M. Yousaf Hasan Bangash, a Foreign Fellow of the Pakistan Academy of Sciences breathed his last on June 10, 2019 in London, UK. While working abroad as one of the most highly rewarded and versatile engineer of Pakistan, Dr. Yousaf Hasan Bangash has left behind a rich harvest of memories and professional achievements as inspiration for all those who know him.

Dr. Bangash was born in British India on April 1st, 1932. He received his B.Sc. and B.Sc. Engg. Degree from University of Peshawar in 1953, M.Sc. Engg. Degree from California Institute of respectively. He was well recognized for his distinguished contributions in the field of Aerospace Engineering, Software Development in Engineering Sciences, Explosion Dynamics. In recognition of his outstanding contributions, he received eleven Gold Medals including the 1999 Dr. F. L. Rahmam Medal from Chicago Consultants Inc.

Throughout his professional career, Dr. Bangash held important positions including Defense Consultant, Aerospace-Naval Structures, UK Defense Department, London, 1991-1993; Professor of Aerospace Structures, Middlesex University, London, 1980-91; Group Consulting Engineer, Atomic Power Construction Ltd., Surrey, 1973-80; Consultant UKAEA, 1966; Consultant, Nuclear Aerospace Structures, British Aerospace, Surrey, 1966-1969; Reader, Aerospace Structures, Imperial College, London, 1966-73; Senior Lecturer, Aerospace Structures, University of Greenwich, London, 1963-65; Senior Manager, Nuclear Construction, General Atomic Inc., San Diego, California, 1962-64; Senior Group Engineer, Lockheed International Inc., California, 1960-1962; Senior Lecturer in Structural Engineering, College of Engineering, University of Peshawar, 1957-59; Structural Design Engineer, US Core of Engineers, Kharian,1954-56.

Dr. Bangash was also honored with membership of various outstanding bodies, including FeACE, Struct. E. of UK; Member: Nuclear Inst., British Standards (BSI) and International Standards (ISO); Cited in American WHO's WHO, New York and in Federal Emergency Agency (FEMA) Report, Washington, D.C.; Structural Board of American Institute of Aeronautics and Astronautics, 2004; Governor of the Union of Muslim Organizations (UMD), UK.

Dr. M. Yousaf Hasan Bangash will always be missed by all the Academy Fellows. Our thoughts and heartfelt condolences go out to the family, friends and colleagues.

May ALLAH Almight bless his soul in peace in heaven; Aameen.

Proceedings of the Pakistan Academy of Sciences
Instructions for Authors

Aims and Scope: *Proceedings of the Pakistan Academy of Sciences* is official journal of the Academy, published quarterly, in English. This open access journal publishes research papers in *Engineering Sciences & Technology, Life Sciences, Medical Sciences, and Physical Sciences*. State-of-the-art reviews (~20 pages, supported by recent references) summarizing R&D in a particular area of science, especially in the context of Pakistan, and suggesting further R&D are also considered. Manuscripts undergo double-blind review. Authors are not required to be Fellows or Members of the *Pakistan Academy of Sciences* or citizens of Pakistan.

Manuscript Format

Manuscript may contain **Abstract, Keywords, INTRODUCTION, MATERIALS AND METHODS, RESULTS, DISCUSSION (or RESULTS AND DISCUSSION), CONCLUSIONS, ACKNOWLEDGEMENTS and REFERENCES** *and any other information that the author(s) may consider necessary.* The Manuscript sections must be numbered, i.e., **1. INTRODUCTION, 2. MATERIALS AND METHODS,** and so on.

Manuscripts, in *Times New Roman*, 1.5-spaced (but single-space the Tables), with line numbering and one-inch margins on all sides on A-4 size paper, should not exceed 20 pages including Tables and Figures. Number manuscript pages throughout. The text (in **Font Size 11,** except for the sections mentioned in **Font Size 10)** must be typed in a single column across the paper width. All Tables and Figures must be placed after the text, i.e., after REFERENCES section.

(a) **Title** of the article **(**Capitalize initial letter of each main word; font size 16; **bold**), max 160 characters (no abbreviations or acronyms), depicting article's contents; (b) Author' first name, middle initial and last name (font size 12, **bold**), and professional affiliation (i.e., each author's Department, Institution, Mailing address and Email; but no position titles) (font size 12); (c) Indicate the corresponding author with *; (d) **Short running title**, max 50 characters (font size 10).The **next Page** should start with **Title** of the Article, followed by entire manuscript. **Headings and Subheadings** (font size 11): All flush left

LEVEL-1: **ALL CAPITAL LETTERS; bold**

Level-2: **Capitalize each main word; bold**

Level-3: Capitalize each main word; Bold, Italic

Level-4: *Run-in head*; *Italics*, *in the normal paragraph position. Capitalize the initial word only and end in a colon (i.e., :)*

Abstract (font size 10; max 250 words)**:** Must be self-explanatory**,** stating rationale, objective(s), methodology, main results and conclusions of the study. Abbreviations, if used, must be defined on first mention in the Abstract as well as in the main text. Abstract of review articles may have variable format.

Keywords (font size 10)**:** Three to eight keywords**,** depicting the article.

INTRODUCTION: Provide a clear and concise statement of the problem, citing relevant recent literature, and objectives of the investigation.

MATERIALS AND METHODS: Provide an adequate account of the procedures or experimental details, including statistical tests (if any), in a concise manner but sufficient enough to replicate the study.

RESULTS: Be clear and concise with the help of appropriate Tables, Figures and other illustrations. Data should not be repeated in Tables and Figures, but must be supported with statistics.

DISCUSSION: Provide interpretation of the RESULTS in the light of previous relevant studies, citing published references.

ACKNOWLEDGEMENTS (font size 10)**:** In a brief statement, acknowledge financial support and other assistance.

REFERENCES (font size 10)**:** Cite references in the text **by number only** in **square brackets**, e.g. "Brown et al [2] reported ..." or "... as previously described [3, 6–8]", and list them in REFERENCES section, in the order of citation in the text, Tables and Figures (not alphabetically). Only published (and accepted for publication) journal articles, books, and book chapters qualify for REFERENCES.

List of REFERENCES must be prepared as under:

a. **Journal Articles** *(Name of journals must be stated in full)*

1. Golding, I. Real time kinetics of gene activity in individual bacteria. *Cell* 123**:** 1025–1036 (2005).
2. Bialek, W. & S. Setayeshgar. Cooperative sensitivity and noise in biochemical signaling. *Physical Review Letters* 100**:** 258–263 (2008).
3. Kay, R.R. & C.R.L. Thompson. Forming patterns in development without morphogen gradients: differentiation and sorting. *Cold Spring Harbor Perspectives in Biology* 1: doi: 10.1101/cshperspect.a001503 (2009).

b. **Books**

4. Luellen, W.R. *Fine-Tuning Your Writing*. Wise Owl Publishing Company, Madison, WI, USA (2001).
5. Alon, U. & D.N. Wegner (Ed.). *An Introduction to Systems Biology: Design Principles of Biological Circuits*. Chapman & Hall/CRC, Boca Raton, FL, USA (2006).

c. **Book Chapters**

6. Sarnthein, M.S. & J.D. Stanford. Basal sauropodomorpha: historical and recent phylogenetic developments. In: *The Northern North Atlantic: A Changing Environment.* Schafer, P.R. & W. Schluter (Ed.), Springer, Berlin, Germany, p. 365–410 (2000).
7. Smolen, J.E. & L.A. Boxer. Functions of Europhiles. In: *Hematology, 4th ed*. Williams, W.J., E. Butler & M.A. Litchman (Ed.), McGraw Hill, New York, USA, p. 103–101 (1991).

Tables, with concise but self-explanatory headings must be numbered according to the order of citation (like **Table 1**, **Table 2**). Round off data to the nearest three significant digits. Provide essential explanatory footnotes, with superscript letters or symbols keyed to the data. Do not use vertical or horizontal lines, except for separating column heads from the data and at end of the Table.

Figures may be printed in two sizes: column width of 8.0 cm or page width of 16.5 cm; number them as **Fig. 1**, **Fig. 2**, … in the order of citation in the text. Captions to Figures must be concise but self-explanatory. Laser printed line drawings are acceptable. Do not use lettering smaller than 9 points or unnecessarily large. Photographs must be of high quality. A scale bar should be provided on all photomicrographs.

Declaration: Provide a declaration that: (i) the results are original; (ii) the same material is neither published nor under consideration elsewhere; (iii) approval of all authors has been obtained; and, (iv) in case the article is accepted for publication, its copyright will be assigned to *Pakistan Academy of Sciences*. Authors must obtain permission to reproduce, where needed, copyrighted material from other sources and ensure that no copyrights are infringed upon.

Reviewers: Authors may suggest four relevant reviewers, two local and two from scientifically advanced countries.

Manuscripts must be submitted in Microsoft Word (.doc or .docx format; **pdf** files not acceptable). Figures can be submitted in Word format, TIFF, GIF, JPEG, EPS, PPT.

Manuscripts may be submitted as email attachment at the following email address. In case of any difficulty while submitting your manuscript, please get in touch with:

Editor
Pakistan Academy of Sciences
3-Constitution Avenue, G-5/2, Islamabad, Pakistan
Email: editor@paspk.org
Tel: +92-51-920 7140
Website: www.paspk.org

PROCEEDINGS
OF THE PAKISTAN ACADEMY OF SCIENCES:
A. Physical and Computational Sciences

CONTENTS

Volume 56, No. 2, June 2019 **Page**

Research Articles

Obituaries

PAKISTAN ACADEMY OF SCIENCES, ISLAMABAD, PAKISTAN

HEC Recognized, Category Y; PM&DC Recognized

Website: www.paspk.org